Investigation into Shrinkage of High-Performance Concrete Used for Iowa Bridge Decks and Overlays – Phase II Shrinkage Control and Field Investigation

Final Report | April 2019

IOWA STATE UNIVERSITY
Institute for Transportation

Sponsored by
Iowa Highway Research Board
(IHRB Project TR-690)
Iowa Department of Transportation
(InTrans Project 15-540)

About the Institute for Transportation

The mission of the Institute for Transportation (InTrans) at Iowa State University is to develop and implement innovative methods, materials, and technologies for improving transportation efficiency, safety, reliability, and sustainability while improving the learning environment of students, faculty, and staff in transportation-related fields.

Disclaimer Notice

The contents of this report reflect the views of the authors, who are responsible for the facts and the accuracy of the information presented herein. The opinions, findings and conclusions expressed in this publication are those of the authors and not necessarily those of the sponsors.

The sponsors assume no liability for the contents or use of the information contained in this document. This report does not constitute a standard, specification, or regulation.

The sponsors do not endorse products or manufacturers. Trademarks or manufacturers' names appear in this report only because they are considered essential to the objective of the document.

Non-Discrimination Statement

Iowa State University does not discriminate on the basis of race, color, age, ethnicity, religion, national origin, pregnancy, sexual orientation, gender identity, genetic information, sex, marital status, disability, or status as a U.S. veteran. Inquiries regarding non-discrimination policies may be directed to Office of Equal Opportunity, Title IX/ADA Coordinator, and Affirmative Action Officer, 3350 Beardshear Hall, Ames, Iowa 50011, 515-294-7612, email eooffice@iastate.edu.

Iowa Department of Transportation Statements

Federal and state laws prohibit employment and/or public accommodation discrimination on the basis of age, color, creed, disability, gender identity, national origin, pregnancy, race, religion, sex, sexual orientation or veteran's status. If you believe you have been discriminated against, please contact the Iowa Civil Rights Commission at 800-457-4416 or the Iowa Department of Transportation affirmative action officer. If you need accommodations because of a disability to access the Iowa Department of Transportation's services, contact the agency's affirmative action officer at 800-262-0003.

The preparation of this report was financed in part through funds provided by the Iowa Department of Transportation through its "Second Revised Agreement for the Management of Research Conducted by Iowa State University for the Iowa Department of Transportation" and its amendments.

The opinions, findings, and conclusions expressed in this publication are those of the authors and not necessarily those of the Iowa Department of Transportation.

Technical Report Documentation Page

1. Report No.	2. Government Accession No.	3. Recipient's Catalog No.	
IHRB Project TR-690			
4. Title and Subtitle Investigation into Shrinkage of High-Performance Concrete Used for Iowa Bridge Decks and Overlays – Phase II Shrinkage Control and Field Investigation		**5. Report Date** April 2019 6. Performing Organization Code	
7. Author(s) Kejin Wang (orcid.org/0000-0002-7466-3451), Yifeng Ling (orcid.org/0000-0002-8846-0524), Gilson Lomboy (orcid.org/0000-0002-2399-1156), and Sri Sritharan (orcid.org/0000-0001-9941-8156)		**8. Performing Organization Report No.** InTrans Project 15-540	
9. Performing Organization Name and Address Institute for Transportation Iowa State University 2711 South Loop Drive, Suite 4700 Ames, IA 50010-8664		**10. Work Unit No. (TRAIS)** **11. Contract or Grant No.**	
12. Sponsoring Organization Name and Address Iowa Highway Research Board Iowa Department of Transportation 800 Lincoln Way Ames, IA 50010		**13. Type of Report and Period Covered** Final Report **14. Sponsoring Agency Code**	
15. Supplementary Notes Visit www.intrans.iastate.edu for color pdfs of this and other research reports.			

16. Abstract

This Phase II research project on the shrinkage behavior of high-performance concrete (HPC) used in Iowa bridge decks and overlays evaluated several concrete mixes, building off or modifying mixes developed in Phase I. Based on shrinkage behavior and mechanical properties, the mixes studied in Phase I were characterized as having either high, medium, or low cracking potential. In the Phase II study, three concrete mixes (Mixes 6, 8, and 2, characterized in Phase I as having high, medium, and low cracking potential, respectively) were selected for further investigation. The selected mixes were modified using three shrinkage control technologies: shrinkage-reducing admixtures (SRAs), cementitious materials (CM), and internal curing (IC) agents, respectively. The modification methods were first studied in a laboratory until the optimal shrinkage behavior of each concrete mix was achieved. Two pairs of the tested concrete mixes (Mixes 6 and 8 with and without modification) were then used in a field investigation on the US 20 over I-35 dual bridge. The mixes were placed side by side for the bridge overlays, which were monitored for about one year with strain gages, temperature and moisture sensors, and regular visual examinations.

The laboratory investigation confirmed positive effects for the concrete shrinkage control technologies used. The laboratory test results also provided specific details for the concrete mix modifications, ensuring optimal concrete performance and shrinkage control. The modifications included the addition of 1.0/1.25 gal/yd^3 of SRA in Mix 6, the use of 10% CM reduction for Mix 8, and the use of lightweight fine aggregate as an IC material in Mix 2. The results of the field investigation suggest that environmental conditions on the casting day and the first few days of curing play an important role in the development of concrete properties. Future studies could benefit from a comprehensive stress analysis to better understand the long-term effects of the shrinkage control technologies, as well as further field tests and an extended monitoring time.

17. Key Words	18. Distribution Statement		
bridge decks—cementitious material (CM)—concrete overlays—high-performance concrete (HPC)—internal curing (IC) agents—shrinkage-reducing admixtures (SRAs)	No restrictions.		
19. Security Classification (of this report)	**20. Security Classification (of this page)**	**21. No. of Pages**	**22. Price**
Unclassified.	Unclassified.	148	NA

Form DOT F 1700.7 (8-72) **Reproduction of completed page authorized**

INVESTIGATION INTO SHRINKAGE OF HIGH-PERFORMANCE CONCRETE USED FOR IOWA BRIDGE DECKS AND OVERLAYS – PHASE II SHRINKAGE CONTROL AND FIELD INVESTIGATION

Final Report
April 2019

Principal Investigator
Kejin Wang, Professor
Civil, Construction, and Environmental Engineering, Iowa State University

Co-Principal Investigators
Scott M. Schlorholtz, Scientist
Office of Biotechnology, Iowa State University

Sri Sritharan, Professor
Civil, Construction, and Environmental Engineering, Iowa State University

Research Assistants
Gilson Lomboy and Yifeng Ling

Authors
Kejin Wang, Yifeng Ling, Gilson Lomboy, and Sri Sritharan

Sponsored by
Iowa Department of Transportation and Iowa Highway Research Board
(IHRB Project TR-690)

Preparation of this report was financed in part
through funds provided by the Iowa Department of Transportation
through its Research Management Agreement with the
Institute for Transportation
(InTrans Project 15-540)

A report from
Institute for Transportation
Iowa State University
2711 South Loop Drive, Suite 4700
Ames, IA 50010-8664
Phone: 515-294-8103 / Fax: 515-294-0467
www.intrans.iastate.edu

TABLE OF CONTENTS

ACKNOWLEDGMENTS xi

EXECUTIVE SUMMARY xiii

Laboratory and Field Investigation xiii
Results, Observations, and Conclusions xiv
Recommendations xvi

1. INTRODUCTION 1

1.1 Summary of Phase I Study 1
1.2 Objectives of Phase II Study 3
1.3 Scope and Tasks 4

2. LITERATURE REVIEW 5

2.1 Effects of Cementitious Materials 5
2.2 Effects of Shrinkage-Reducing Admixtures 10
2.3 Shrinkage Compensating Admixture (SCA) 14
2.4 Effects of Internal Curing 17

3. LABORATORY INVESTIGATION 22

3.1 Materials 22
3.2 Mixture Proportions 26
3.3 Tests and Methods 27

4. LABORATORY TESTS RESULTS AND DISCUSSION 34

4.1 Shrinkage Behavior of Mixes with and without Modifications 34
4.2 Fresh Concrete Properties 48
4.3 Mechanical Properties 49
4.4 Surface Resistivity and F-T Durability 57

5. FIELD INVESTIGATION 64

5.1 Field Preparation 64
5.2 Crack Survey 67
5.3 Sensor Installation 70
5.4 Field Construction and Sample Preparations 82
5.5 Field Sample Tests and Results 88
5.6 Field Sensor Monitoring and Data Analysis 92

6. SUMMARY, CONCLUSIONS, AND RECOMMENDATIONS 103

6.1 Research Activities 103
6.2 Results and Observations from Laboratory Investigation 103
6.3 Results and Observations from the Field Investigation 110
6.4 Major Findings 115
6.5 Recommendations 118

REFERENCES 121

APPENDIX A: SHRINKAGE TEST RESULTS OF CONCRETE (MIX 2) HAVING SUPERABSORPTENCE POLYMER (SAP) AS AN INTERNAL CURING AGENT 125

APPENDIX B: STRAIN MEASUREMENT OF GAUGES ON THE TOP/BOTTOM SURFACES OF DECKS AND WEBS OF GIRDERS 129

LIST OF FIGURES

Figure 2.1. Influence of cement type on autogenous shrinkage 6
Figure 2.2. Shrinkage of OPC and expansive cements concrete 6
Figure 2.3. Creep (a) and drying shrinkage (b) strains of HPC 7
Figure 2.4. Autogenous shrinkage (a) and drying shrinkage (b) of concrete with fly ash.....7
Figure 2.5. Development of restraint stress 8
Figure 2.6. Effect of curing and w/c ratio on drying shrinkage of silica fume concrete 8
Figure 2.7. Effect of metakaolin on (a) early age shrinkage (less than 24 hrs) and (b) after 24 hrs 9
Figure 2.8. Effect of metakaolin on (a) total shrinkage and (b) pure drying shrinkage of concrete 9
Figure 2.9. Effect of nano- and micro-limestone on (a) drying shrinkage and (b) mass loss.....10
Figure 2.10. Internal RH and autogenous shrinkage of cement pastes with and without SRA 10
Figure 2.11. Drying shrinkage of HPC with and without SRA 11
Figure 2.12. Shrinkage strain of (a) NSC and (b) HSC with 0-2% SRA.....12
Figure 2.13. Shrinkage and capillary suction of samples with 0–2% SRA 12
Figure 2.14. Free expansion test 13
Figure 2.15. Plastic shrinkage of concretes with and without SRA.....14
Figure 2.16. Expansion of cement pastes containing 8% MEA with various hydration reactivities calcined under different temperatures for 1 hr (cured in 40°C water).....15
Figure 2.17. Effect of MSA composition on the autogenous length change of mortar 15
Figure 2.18. Effects of CaO-based SCA and SRA on concrete length change 16
Figure 2.19. Combined effects of EX, SRA, and FA on mortar length change 17
Figure 2.20. Effect of SAP on autogenous deformation of mortars 18
Figure 2.21. Kinetics of swelling of dry SAP and de-swelling of water-swollen SAP upon immersion in artificial pore solution and cement paste filtrate.....19
Figure 3.1. Coarse aggregate gradation 25
Figure 3.2. Fine aggregate gradation 25
Figure 3.3. Specimen mold and comparator for concrete autogenous shrinkage measurement 28
Figure 3.4. Specimen and comparator for free drying shrinkage 29
Figure 3.5. Mold, specimen, and data logger for concrete ring tests.....29
Figure 3.6. Layout of creep test 31
Figure 3.7. Surface resistivity test.....32
Figure 3.8. Fundamental transverse frequency measurement for dynamic modulus 33
Figure 4.1. Mix 6 autogenous shrinkages with different SCA dosages.....34
Figure 4.2. Mix 6 free drying shrinkages with different SCA dosages 35
Figure 4.3. Mix 6 restrained ring shrinkages with different SCA dosages.....36
Figure 4.4. Mix 6 stress rates with different SCA dosage 36
Figure 4.5. Autogenous shrinkage of Mix 6 with different SRA dosages.....37
Figure 4.6. Free drying shrinkage of Mix 6 with different SRA dosages.....38
Figure 4.7. Mix 6 restrained ring shrinkages with different SRA dosages.....38
Figure 4.8. Mix 6 stress rates with different SRA dosages.....39

Figure 4.9. Autogenous shrinkage of Mix 8 modified with different percent cementitious material reduction 41
Figure 4.10. Free drying shrinkage of Mix 8 modified with different percent cementitious material reduction 41
Figure 4.11. Restrained ring shrinkage of Mix 8 with different percent cementitious material reduction 42
Figure 4.12. Stress rates of Mix 8 with different percent cementitious material reduction....43
Figure 4.13. Mix 2 autogenous shrinkages with different LWFA replacement percent....44
Figure 4.14. Mix 2 free drying shrinkages with different LWFA replacement percent 44
Figure 4.15. Mix 2 restrained ring shrinkages with different LWFA replacement percent....45
Figure 4.16. Total shrinkage of mixes studied at 56 days 45
Figure 4.17. Slump of original and modified mixes 48
Figure 4.18. Unit weight of original and modified mixes....48
Figure 4.19. Air content of original and modified mixes 49
Figure 4.20. Mechanical properties of Mix 6 and Mix 6-SR1.25....50
Figure 4.21. Mechanical properties of Mix 8 and Mix 8-CM90 51
Figure 4.22. Mechanical properties of Mix 2-0% LWFA and Mix 2-34% LWFA 53
Figure 4.23. Creep of Mix 6 and Mix 6-SR 1.25....54
Figure 4.24. Creep of Mix 8 and Mix 8-CM 90....55
Figure 4.25. Creep of Mix 2 and Mix 2-34%LWFA 56
Figure 4.26. Surface resistivity of selected concrete mixes....58
Figure 4.27. Durability factor of selected concrete mixes 60
Figure 4.28. Samples after F-T cycles 62
Figure 5.1. US 20 over I-35 dual bridge location 64
Figure 5.2. US 20 over I-35 overlay sections 66
Figure 5.3. Crack survey using wet test method (water used to wet concrete surface) 68
Figure 5.4. Crack survey results on the Stage 1 deck surface before new overlay construction 68
Figure 5.5. Crack survey results on the Stage 2 deck surface before new overlay construction 69
Figure 5.6. Cracks on surface of deck after one year of service for the new overlay....70
Figure 5.7. GS3 moisture sensor....70
Figure 5.8. GEOKON strain gages 71
Figure 5.9. Sensor location on the bridge deck....73
Figure 5.10. Installation of GEOKON 4200 and GS3 on deck 76
Figure 5.11. Installation of GEOKON 4000 beneath deck and on girder....76
Figure 5.12. Wires in PVC pipe....77
Figure 5.13. Wires to DAS 77
Figure 5.14. Data acquisition system....78
Figure 5.15. Moisture and strain monitoring system 78
Figure 5.16. Concrete samples used for moisture sensor calibration 79
Figure 5.17. Calibrated VWC equation for Mix 6 80
Figure 5.18. Calibrated VWC equation for modified Mix 6....80
Figure 5.19. Calibrated VWC equation for Mix 8 81
Figure 5.20. Calibrated VWC equation for modified Mix 8....81
Figure 5.21. Concrete overlay construction....84

Figure 5.22. Curing method 85
Figure 5.23. New overlays before opening to traffic 85
Figure 5.24. Formwork of a mini slab and strain gage location 87
Figure 5.25. Mini slabs on the field site 87
Figure 5.26. Compressive strength of laboratory- and field-cast samples (original and modified Mix 6) 88
Figure 5.27. Compressive strength of laboratory- and field-cast samples (original and modified Mix 8) 89
Figure 5.28. 28-day compressive strength for field-cast samples under laboratory and field curing conditions 90
Figure 5.29. Free drying shrinkage of field concrete samples 90
Figure 5.30. Apparatus for CTE 91
Figure 5.31. CTE results of field concrete mixes 91
Figure 5.32. Ambient temperature of the field site 93
Figure 5.33. VWC measurements from Mix 6 series 94
Figure 5.34. VWC measurements from Mix 8 series 95
Figure 5.35. Microstrain for different mixes used in mini slabs 97
Figure 5.36. Strain gage readings at various locations of overlays in the transverse direction 99
Figure 5.37. Comparison of strains in different concrete mixes 100
Figure 6.1. Shrinkage behaviors of different mixes at given ages 104
Figure 6.2. Restrained ring shrinkage behaviors of different mixes at given ages 105
Figure 6.3. Strength and elastic modulus of selected mixes 106
Figure 6.4. Creep behavior of selected mixes 107
Figure 6.5. Durability properties of selected mixes 109
Figure 6.6. Comparison of crack types and locations found before and after overlay construction 113
Figure 6.7. Comparison of moisture sensor readings on different days 114
Figure A.1. First trial on SAP for Mix 2 (presoaked with additional water) 125
Figure A.2. Second trial on SAP for Mix 2 (without presoak) (free drying shrinkage) 126
Figure A.3. Third trial on SAP for Mix 2 (presoaked with mixing water) (free drying shrinkage) 126
Figure A.4. Fourth trial on increased SAP dosage for Mix 2 (presoaked with mixing water) 127
Figure B.1. Strain readings of gages in concrete overlays 129
Figure B.2. Strain readings of gages on the bottom surfaces of concrete decks 129
Figure B.3. Strain readings of gages on the web of concrete girder (strain gage for Mix 8 modified broken during the sensor monitoring) 130

LIST OF TABLES

Table 1.1. Iowa HPC mixes studied for IHRB Phase I project....2
Table 2.1. Hardened concrete properties....11
Table 2.2. Chemical components of SRA....12
Table 2.3. Proportions, constituents, and properties of concrete mixtures....13
Table 2.4. Transportation agencies that have used IC....20
Table 3.1. Concrete materials and their sources....23
Table 3.2. Physical and chemical properties of cementitious materials....23
Table 3.3. Aggregate information....24
Table 3.4. Gradations of aggregates....24
Table 3.5. Dosage of chemical admixtures....26
Table 3.6. Mix proportions of original mixes....26
Table 3.7. Tests performed in lab....27
Table 4.1. Proportions of Mix 8 modified with different amount of cementitious material reduction....40
Table 4.2. Mix proportions of concrete mixes used in an extended study....47
Table 4.3. Fresh concrete properties....48
Table 4.4. Instantaneous elastic modulus and creep rate for all mixes....56
Table 4.5. Penetrability classification....59
Table 4.6. Durability factors of selected mixes....61
Table 5.1. US 20 over I-35 project construction timeline....67
Table 5.2. Sensor locations....75
Table 5.3. Field concrete mix proportions and their shrinkage....83
Table 5.4. Fresh concrete properties in the field....86
Table 5.5. Field samples and their uses....86
Table 6.1. Comparisons of properties of field and laboratory samples....111
Table 6.2. Maximum compressive strain in mini slabs....114

ACKNOWLEDGMENTS

The authors would like to acknowledge the Iowa Department of Transportation (DOT) and Iowa Highway Research Board (IHRB) for their sponsorship of this research. Special thanks are given to technical advisory committee (TAC) members Kevin Jones, Todd Hanson, James Nelson, Ahmad Abu-Hawash, and Wayne Sunday for their technical support throughout the project as well as their valuable comments on this report and to Chengsheng Ouyang for his help on collecting all of the concrete materials used in the project.

The authors would also like to express their appreciation to Cramer and Associates, Inc. for their coordination during the field investigation and to the Bridge Engineering Center and others at Iowa State University (Brent Phares, Doug Wood, Travis Hosteng, Evan Beczek, and Clinton Gross) for their assistance during sensor installation on the overlays on the US 20 over I-35 dual bridge. Song Han from Beijing Jiaotong University and Peng Zhang from Zhengzhou University also participated in field testing during their visit to Iowa State University. Bob Steffes of Iowa State University's Portland Cement Concrete Research Laboratory provided the research team with constant help during this project. All of their contributions are greatly valued.

EXECUTIVE SUMMARY

High-performance concrete (HPC) is increasingly being used in bridge decks and deck overlays because of its high strength, low permeability, and excellent durability. However, due to its high cementitious content, low water-to-binder (w/b) ratio, and use of various admixtures, HPC is also reported to be at high risk for shrinkage cracking, an issue of great concern in Iowa.

A research project conducted from 2011 to 2013 on the shrinkage behavior of the HPC used in Iowa bridge decks and overlays (the Phase I study) relied on a laboratory investigation to evaluate 11 typical Iowa HPC mixes. Based on their shrinkage behavior and mechanical properties, these concrete mixes were characterized as having either high, medium, or low cracking potential. Different shrinkage control technologies were then suggested for the concrete mixes with different cracking potentials.

To build on the research results obtained from the Phase I study, a Phase II study focusing on shrinkage control methods and field investigations has been in progress since 2015. This report summarizes all research activities and results from the Phase II study.

Laboratory and Field Investigation

In the Phase II study, three concrete mixes from the Phase I study with different shrinkage cracking potentials were selected for further investigation:

1. Mix 2 (HPC-O-C20): a mix with low shrinkage cracking potential, made with 80% Ash Grove IP cement and 20% Class C fly ash, with a w/b ratio of 0.40
2. Mix 6 (O-4WR): a mix with high shrinkage cracking potential, made with 100% Lafarge I/II cement, with a w/b ratio of 0.33
3. Mix 8 (HPC-O-C20-S20): a mix with medium shrinkage cracking potential, made with quartzite (Phase I) or limestone (Phase II) as coarse aggregate, 80% Lafarge I/II cement, and 20% ground granulated blast furnace slag (GGBFS), with a w/b ratio of 0.40

For Mix 2, it was found during the Phase II study that when different aggregates and water reducing admixtures were used, the mix exhibited much higher shrinkage than in Phase I.

The following measures were taken to reduce the shrinkage cracking potential of the selected concrete mixes:

- Internal curing (IC) agents were used for Mix 2
- Shrinkage reducing admixtures (SRAs) and shrinkage compensating admixtures (SCA) were used for Mix 6
- Cementitious material (CM) reductions were used for Mix 8

These modifications were conducted through a laboratory investigation where the amounts of IC agents, SRA/SCA dosages, and CM in Mixes 2, 6, and 8 were gradually changed until the optimal shrinkage behavior was achieved. The shrinkage behavior was evaluated by autogenous shrinkage, free drying shrinkage, and restrained shrinkage tests.

These mix modification processes generated the following new, optimal concrete mixes:

1. Mix 2M or Mix2-34%LWFA, obtained by using 34% (by volume) lightweight fine aggregate (LWFA) as an IC agent to sand in Mix 2
2. Mix 6M or Mix6-1.25SRA, obtained by using 1.25 gal of SRA per yd^3 of concrete for Mix 6
3. Mix 8M or Mix8-90CM, obtained by using only 90% (or reducing 10%) of CM in the original Mix 8

In addition to shrinkage behavior, mechanical properties (such as compressive and splitting tensile strength and elastic modulus) of both the modified and original concrete mixes (Mixes 2, 6, 8, 2M, 6M, and 8M) were evaluated at different curing ages. Creep, freeze-thaw (F-T) durability, and surface resistivity tests were performed for these concrete mixes as well.

A field investigation was conducted on the US 20 over I-35 dual bridge, where Mix 6 and Mix 6-1.0SR (instead of Mix 6-1.25SR) as well as Mix 8 and Mix8-90CM were placed side by side for the bridge overlays. Quality control properties, construction conditions, and procedures were recorded. Sensors (strain gages and temperature and moisture sensors) were installed in the concrete overlays to monitor the strain, temperature, and moisture of the concretes for approximately one year. Visual examinations were conducted on the surface of the concretes, and the shrinkage cracks (time, size, and pattern) were recorded regularly.

Results, Observations, and Conclusions

The following observations and conclusions were drawn from the laboratory and field investigations.

Effects of Shrinkage Control Methods on Concrete Properties

Effects on Shrinkage

- Addition of 1.0 or 1.25 gal/yd^3 of SRA in Mix 6 reduced 28-day autogenous shrinkage by approximately 30%, 28-day free drying shrinkage by over 50%, and the stress rate of restrained ring shrinkage by 60%.
- The 10% cementitious material reduction in Mix 8 decreased 28-day autogenous shrinkage and free drying shrinkage by approximately 40% and the stress rate of restrained ring shrinkage by 13%.
- Use of 34% LWFA as an IC material to replace fine aggregate in Mix 2 reduced 28-day autogenous shrinkage by 47.5%, 28-day free drying shrinkage by 11%, and the stress rate of restrained ring shrinkage by only 1.3%.

Effects on Mechanical Properties

- Addition of 1.0 or 1.25 gal/yd^3 of SRA in Mix 6 increased 28-day compressive strength by approximately 5%, splitting tensile strength by about 9%, and compressive elastic modulus by around 22%. It decreased the concrete creep rate by almost 22%.
- The 10% cementitious material reduction in Mix 8 decreased 28-day compressive strength by approximately 12% and splitting tensile strength by about 19% but increased compressive elastic modulus by around 15% and creep rate by almost 18%.
- Use of 34% LWFA as an IC material to replace fine aggregate in Mix 2 increased 28-day compressive strength by approximately 15% and splitting tensile strength by about 12% but decreased compressive elastic modulus by around 8% and creep rate by almost 21%.

Effects on Durability

- Addition of 1.0 or 1.25 gal/yd^3 of SRA in Mix 6 increased concrete surface resistivity by approximately 24% but decreased the concrete F-T durability factor by almost 8%.
- The 10% cementitious material reduction in Mix 8 decreased concrete surface resistivity by approximately 11% but had little effect on the concrete F-T durability factor.
- Use of 34% LWFA as an IC material to replace fine aggregate in Mix 2 increased concrete surface resistivity by only about 5% and the F-T durability factor by nearly 4%.

Field Performance of Concrete Overlays with and without Shrinkage Control

- Cracks were observed on the overlays made with the two original HPC mixes (Mix 6 exhibited five cracks and Mix 8 exhibited two cracks) after the repaired bridge had been opened to traffic for about one year.
- No cracks were found on the overlays made with the modified mixes (Mix 6-1.0SR and Mix 8-CM90) after the repaired bridge had been opened to traffic for about one year.
- There are some differences in compressive strength between the laboratory-cast and laboratory-cured samples and the field-cast and laboratory-cured samples for a given mix. The results suggest that the environmental conditions on the casting day and the first few days of curing play an important role in the development of concrete properties.

Field Sensor Monitoring

Moisture Content

- Moisture sensors generally did well in capturing the major changes in the moisture conditions of the overlays studied. The concrete moisture content decreased rapidly at an early age (before 14 days), mainly due to cement hydration, and gradually stabilized.
- The moisture profiles varied noticeably among the different concrete mixes that were placed on different dates.

- For the same mix, the concrete near the abutment/joint had a higher moisture content and took a little longer to become stable than the same concrete farther away from the abutment.

Strain in Mini Slabs

- The strain measurements in mini slabs provided valuable information on concrete strain under an unrestrained loading condition free of mechanical/traffic loading. The measurements showed that the maximum strain in the mini slabs was the highest and second highest for Mix 6 and Mix 8, respectively, which might be responsible for the cracks observed on the corresponding overlays one year after overlay construction.

Strain in Overlays

- The strains monitored in the concrete overlays in the transverse direction did not appear to vary significantly among the concrete mixes.
- In the longitudinal direction, the strains monitored in the concrete overlays made with Mixes 6 and 6-1.0SR were similar, and they were much higher than the strains monitored in the concrete overlays made with Mixes 8 and 8-CM90, which also showed similar strains.
- The strains monitored by the embedded strain gages in the field concrete overlays resulted from the combined effects of cementitious hydration (autogenous deformation), the exposed conditions (drying/wetting and thermal expansion/contraction), mechanical loading (structural and traffic loads), and creep behavior. Comprehensive combinations of these effects might have made the strain readings more complex.

Ambient Temperature

- A thermocouple monitored the year-round ambient temperature to provide vital information for concrete strain analysis in this project.
- The overall shapes of all of the strain curves of the concrete overlays studied were similar, and the shapes were all opposite to the overall shape of the ambient temperature curve. This implies that thermal strain dominated the total strain in the concrete, while autogenous and drying shrinkage strains were superimposed on it.

Recommendations

The following proposed recommendations are based on these observations and discussions.

Recommendations for Research Implementation

- Addition of 1.0/1.25 gal/yd3 SRA in Mix 6 demonstrated many positive effects on concrete shrinkage control and mechanical property improvements, except for the slight reduction in F-T durability. This shrinkage control method could reduce the concrete ring shrinkage stress

rate by 60%, which is highly effective. This modification is recommended for shrinkage reduction and prevention of premature concrete distress in Iowa bridge decks/overlays.

- The 10% reduction of cementitious material in Mix 8 decreased autogenous and free drying shrinkage significantly, but it reduced the stress rate of restrained ring shrinkage by only 13%. This shrinkage control method also resulted in noticeable reductions in concrete strength, elastic modulus, creep rate, and surface resistivity, which might impair the concrete serviceability. Therefore, this modification should be employed very cautiously.
- Use of LWFA as an IC material in Mix 2 effectively reduced the concrete autogenous shrinkage (48%) but only slightly reduced free drying shrinkage (11%) and had little effect on the ring shrinkage stress rate (1%). This shrinkage control method also helped improve concrete strength, surface resistivity, and F-T durability slightly, though it reduced elastic modulus and creep rate. This modification can be considered for concrete mixes with moderate free drying shrinkage potential and/or concrete with a high autogenous shrinkage potential (low w/b ratio concrete).

Recommendations for Further Research

- This study performed a field investigation on the use of SRA and CM for shrinkage control. The use of LWFA in Mix 2 was studied in the laboratory but not in the field investigation. It is proposed that a field investigation be conducted to verify the effectiveness of LWFA as an IC agent in various HPC mixes (e.g., HPC-O, O-S20-C20, and O-C20).
- Concrete shrinkage behavior and crack resistance are closely related to concrete pore structure and degree of hydration. Moisture content in field concrete is also strongly associated with concrete pore structure. Further study is necessary to find out how the addition of SRA influences cement hydration and pore structure. The results would help researchers further understand the moisture sensor readings obtained from this study.
- The strains monitored by gages in the field concrete overlays showed that strains resulted from the combined effects of cementitious hydration (autogenous deformation), the exposed conditions (drying/wetting and thermal expansion/contraction), mechanical loading (structural and traffic loads), and creep behavior. A comprehensive stress analysis to fully examine these effects should be conducted on the bridge structure with applications of various HPC mixes on the overlays.
- In this project, sensor monitoring was conducted for only one year, and extended monitoring time (up to three to five years) may be beneficial. Extended monitoring could capture the potential concrete cracks that appear at later stages. In this project, sensor data were downloaded manually on site. In the future, data transmitted via the internet could be downloaded at home or at an office.

1. INTRODUCTION

1.1 Summary of Phase I Study

In Phase I of this project for the Iowa Highway Research Board (IHRB), shrinkage behavior and cracking potential of 11 typical HPC mixes used in Iowa bridge decks and overlays were studied. The results are summarized in Table 1.1.

Table 1.1. Iowa HPC mixes studied for IHRB Phase I project

Mix		Cement	Binder,	FA,	Slag (MK),	w/b	Amount of shrinkage			Cracking
No.	Type	type	lb/yd^3	%	%	ratio	Autogenous	Drying	Restrained	potential
1	HPC-O	IP	666.3	0	0	0.40	high	med.	high	medium
2	HPC-O	IP	651.5	20	0	0.40	high	med.	med.	low
3	HPC-S	IP	573.8	20	0	0.40	high	low	low	low
4	HPC-O (control)	I/II	709.2	0	0	0.40	med.	low	high	high
5	HPC-S (control)	I/II	624.5	0	0	0.42	med.	med.	med.	high
6	O-4WR	I/II	825.7	0	0	0.40	high	med.	high	high
7	HPC-O	I/II	692.9	0	25	0.40	med.	high	high	medium
8	HPC-O	I/II	668.8	20	25	0.40	high	med.	med.	medium
9	HPC-S	I/II	588.9	20	25	0.42	low	med.	med.	medium
10	HPC-O	I/II	675.0	20	(5.6)	0.40	high	low	high	medium
11	HPC-S	I	588.9	20	25	0.42	low	high	low	low

In these 11 mixes, the differences in HPC-O and HPC-S mixes are mainly ones of aggregate gradation and chemical admixture. The coarse aggregate gradation of HPC-O mixes is finer than that of HPC-S mixes. Mid-range water reducer (MRWR) is used in HPC-O mixes, while normal-range water reducer (NRWR) is used in HPC-S mixes. A retarding admixture and limestone coarse aggregate are used in all mixes, except that Mix 6 does not have the retarding admixture, and Mix No. 8 has quartzite as the coarse aggregate. The mixes consisted of three types of cements (Type I, I/II, and IP) and the various supplementary cementitious materials (CM) are Class C fly ash (FA), ground granulated blast furnace slag (GGBFS), and metakaolin (MK). Chemical shrinkage of pastes, free drying shrinkage, autogenous shrinkage of mortar and concrete, as well as restrained ring shrinkage of the concrete were monitored. Mechanical properties such as elastic modulus and compressive and splitting tensile strength of these concrete mixes were measured at different ages. Creep coefficients of these concrete mixes were estimated using the models in NCHRP Report 496 (Tadros et al. 2003). Cracking potential of the concrete mixes was assessed based on both ASTM C1581 and simple stress-to-strength ratio methods (Wang et al. 2013).

The results in Table 1.1 indicate that Mixes 4, 5, and 6 have high cracking potential; Mixes 1, 7, 8, 9, and 10 have medium cracking potential; and Mixes 2, 3, and 11 have low cracking potential. Different concrete materials (cementitious type and admixtures) and mix proportions (cementitious material content) affect concrete shrinkage in different ways. The stresses in the concrete are associated with the shrinkage as well as the elastic modulus, tensile strength, and creep behavior of the concretes. In the Phase I study, creep of concrete was not measured, but the creep coefficients of the concrete mixes were estimated based on a model reported in the literature (Tadros et al. 2003). The investigators had suggested testing concrete creep behavior and using available shrinkage control technologies, such as use of an internal curing (IC) agent and shrinkage-reducing admixture (SRA), to reduce the concrete shrinkage and minimize the cracking potential (Wang et al. 2013).

1.2 Objectives of Phase II Study

The objectives of the Phase II study were as follows:

1. Investigate different methods and identify the most practical and effective method applicable to control shrinkage cracking for Iowa HPC mixes
2. Investigate field performance of the Iowa HPC mixes and compare the performance of mixes with different shrinkage cracking potential and the field performance of concrete mixes with and without shrinkage control methods
3. Compare the test results and observations obtained from the laboratory and field investigations and provide rational recommendations for the Iowa concrete industry to effectively control shrinkage of HPC

1.3 Scope and Tasks

The scope of the Phase II study was to address the shrinkage behavior and cracking potential of selected mixes through a review of current methodologies and testing of selected shrinkage reduction methods in the laboratory and field. The study covered the following tasks:

Task 1: Conduct a literature survey on effective materials and methods used for controlling concrete shrinkage and shrinkage cracking.

Task 2: Reduce shrinkage cracking potential of Mix 6 (identified in Phase I as a mix with high shrinkage cracking potential) by using SRA, shrinkage compensating admixture (SCA), etc.

Task 3: Reduce shrinkage cracking potential of Mix 8 (identified in Phase I as a mix with medium shrinkage cracking potential) by reducing cementitious material.

Task 4: Reduce shrinkage cracking potential of Mix 2 (identified in Phase I as a mix with low shrinkage cracking potential) by using IC materials. (Note: This task was added to the project to examine the effectiveness of IC materials.)

Task 5: Evaluate general engineering properties (including workability, strength development, and creep behavior) of the modified concrete mixes and compare them to those of the original concrete mixes.

Task 6: Conduct a field investigation and comparing the field performance of selected concrete mixtures (Mixes 6, 8, 6M, and 8M) with and without shrinkage reduction modification measures.

Task 7: Monitor concrete behavior in the field, using various sensors such as temperature and moisture sensors and strain gages.

Task 8: Analyze all tested and monitored data and provide recommendations for future shrinkage cracking control of HPC used for Iowa bridge decks and overlays.

2. LITERATURE REVIEW

In this Phase II study, a literature review was conducted with a focus on the effects of cementitious materials, shrinkage controlling admixtures, and internal curing agents on shrinkage behavior of concrete.

2.1 Effects of Cementitious Materials

It has been widely accepted that paste is the primary contributor to the shrinkage of normal weight concrete. Aggregates in concrete have two major effects on reducing paste shrinkage: dilution and restraint (Fulton 1986). Dilution achieves shrinkage reduction by adding non-shrinkable aggregates in the matrix, and restraint decreases concrete shrinkage by increasing the stiffness of the aggregate. Since aggregate is much cheaper than cementitious materials, the most cost effective way to control concrete shrinkage is to reduce cementitious material content. However, this method of reduction has its limits. The amount of cementitious materials in concrete has to be sufficient to fill the voids between aggregate particles to achieve proper density/strength and provide the excessive paste layer required for concrete workability (Yurdakul et al. 2013).

For a given concrete mix proportion, concrete shrinkage behavior is largely affected by the types or properties of cementitious materials used. Tazawa and Miyazawa (1997) did experiments on autogenous shrinkage using 10 different cements. The cement types consisted of normal (N), moderate heat (M), high early-strength (H), sulfate resisting (S), geothermal (G), oil well (O), alumina (A), white (W), blast furnace slag (B), and low heat (L) cements. They found that the samples made with high early strength cement and alumina cement displayed higher early age autogenous shrinkage than Portland cement, while the samples made with moderate heat cement, low heat cement, and sulfate-resisting cement clearly exhibited lower early-age autogenous shrinkage. Blast furnace slag (BFS) cement showed high shrinkage at a later age. Based on this study, they concluded that high alumina content in cement could help increase autogenous shrinkage, while high C_2S content in cement (like that in a low heat cement) could lead to much lower autogenous shrinkage (Figure 2.1).

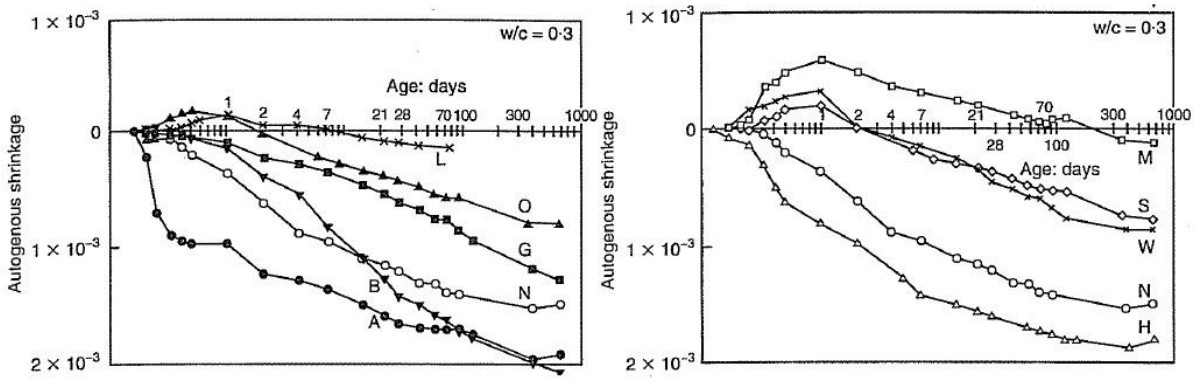

Tazawa and Miyazawa 1997, Copyright © ICE Publishing 1997, reused with permission through the Copyright Clearance Center, Inc.

Figure 2.1. Influence of cement type on autogenous shrinkage

Satio et al. (1991) investigated the effect of expansive cements and aggregate type on shrinkage of mortar. A significant reduction in concrete shrinkage was achieved by use of expansive cement. As illustrated in Figure 2.2, the shrinkage behavior for samples made with both cements was similar at early ages, but clear differences were seen in the shrinkage at later ages.

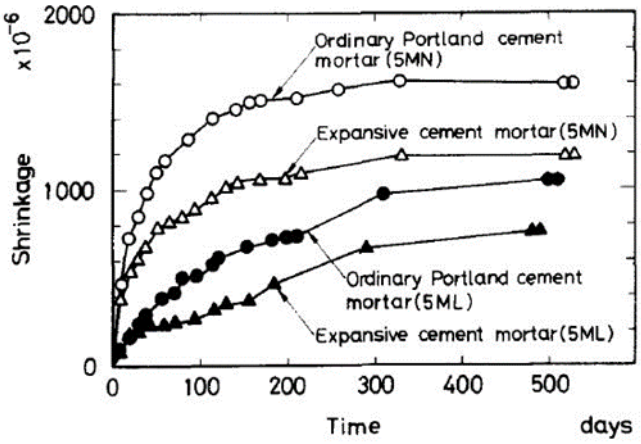

MN and ML refer to natural and lightweight aggregate, respectively.
Satio et al. 1991, Copyright © 1991 Elsevier Science Publishers Ltd, England. Reprinted with permission from Elsevier

Figure 2.2. Shrinkage of OPC and expansive cements concrete

Jianyong and Yan (2001) investigated shrinkage and creep of HPC made with different types of cementitious materials: Concrete A, consisting of pure ordinary Portland cement (OPC); Concrete B, consisting of 70% OPC and 30% ultrafine GGBFS (fineness > 600m^2/kg); and Concrete C, consisting of 60% OPC, 30% ultrafine GGBFS, and 10% silica fume (SF). As shown in Figure 2.3, the results suggested that ultrafine supplementary cementitious material reduced both shrinkage and creep of the HPC in a comparison with OPC.

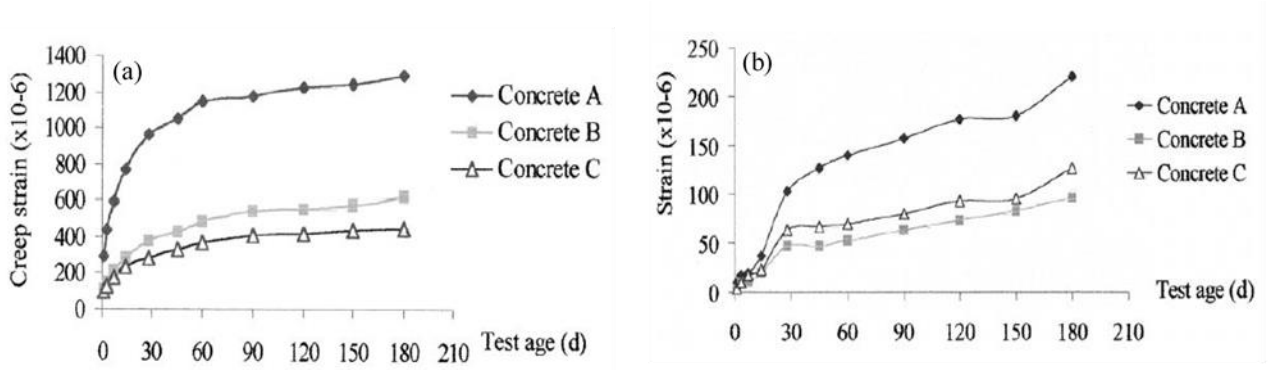

Figure 2.3. Creep (a) and drying shrinkage (b) strains of HPC

Nakarai and Ishida (2008) conducted experiments on autogenous and drying shrinkage of concrete containing different amounts of fly ash (FA) as a replacement for OPC. The results showed that both autogenous shrinkage and drying shrinkage of the concrete were reduced with increased FA replacement (Figure 2.4).

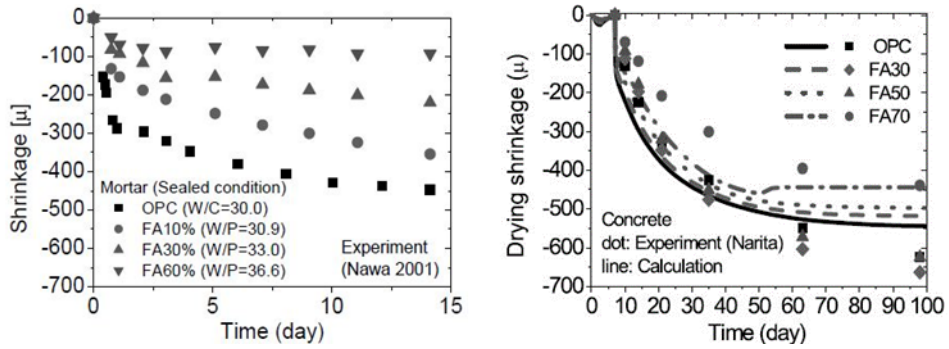

Figure 2.4. Autogenous shrinkage (a) and drying shrinkage (b) of concrete with fly ash

Miyazawa et al. (2008) studied restrained shrinkage of concrete made with OPC (N), moderate heat cement (M), and two types of slag cements (BB and LBB). The two slag cements differ in fineness (4080 cm^2/g for BB and 3380 cm^2/g LBB), slag content (40% for BB and 58% for LBB), and SO_3 content (2.39% for BB and 3.90% for LBB). Their experimental results showed that the samples made with the moderate heat cement (M) and LBB slag cement had much less restrained stress than the samples made with OPC and BB slag cement (Figure 2.5).

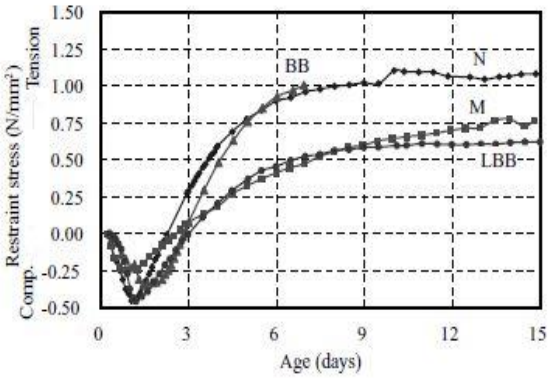

Miyazawa et al. 2008, © 2009 Taylor & Francis Group, LLC. Reprinted with permission

Figure 2.5. Development of restraint stress

Whiting et al. (2000) studied the effect of SF on drying shrinkage and strength of concrete. They conducted experiments for both base and overlay mixes, where base mixes were moist cured for seven days while the overlay mixes were moist cured for three days. Their results revealed that the effects of SF on concrete shrinkage depended on both the dosage and the duration of curing (Figure 2.6).

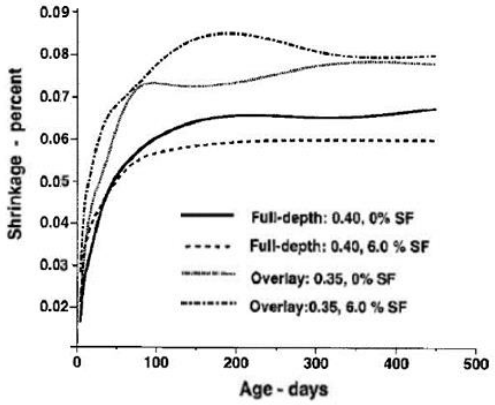

Whiting et al. 2000, © 2000 American Concrete Institute, used with permission

Figure 2.6. Effect of curing and w/c ratio on drying shrinkage of silica fume concrete

Brooks and Johari (2001) investigated the effect of MK on shrinkage of concrete. As shown in Figure 2.7, when only 5% MK was used as a replacement for OPC, autogenous shrinkage declined at a very early age (< 24hrs), but increased after 24 hours. When 10% or 15% MK was used, the autogenous shrinkage of the concrete decreased at both early and later ages.

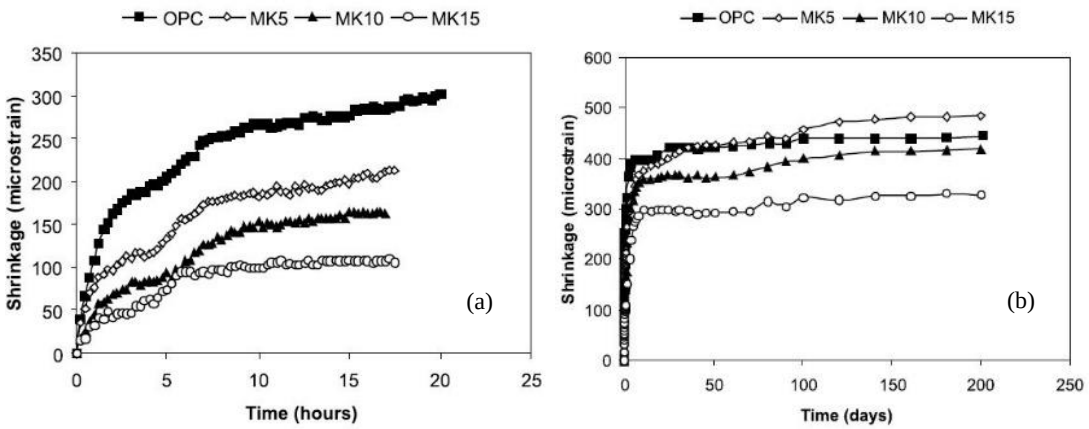

Figure 2.7. Effect of metakaolin on (a) early age shrinkage (less than 24 hrs) and (b) after 24 hrs

An interesting observation was made regarding the pure drying shrinkage and total shrinkage of concrete with an MK replacement for OPC. The amount of total shrinkage was reduced as MK amounts increased. The total shrinkage of concrete with MK was attributed predominantly to autogenous shrinkage since the pure drying shrinkage of MK concrete was very low when compared with that of OPC concrete. It implies that the MK replacement for cement had refined the pore structure of the concrete, which might have promoted self-desiccation, rather than permitting diffusion of water to the environment (Figure 2.8).

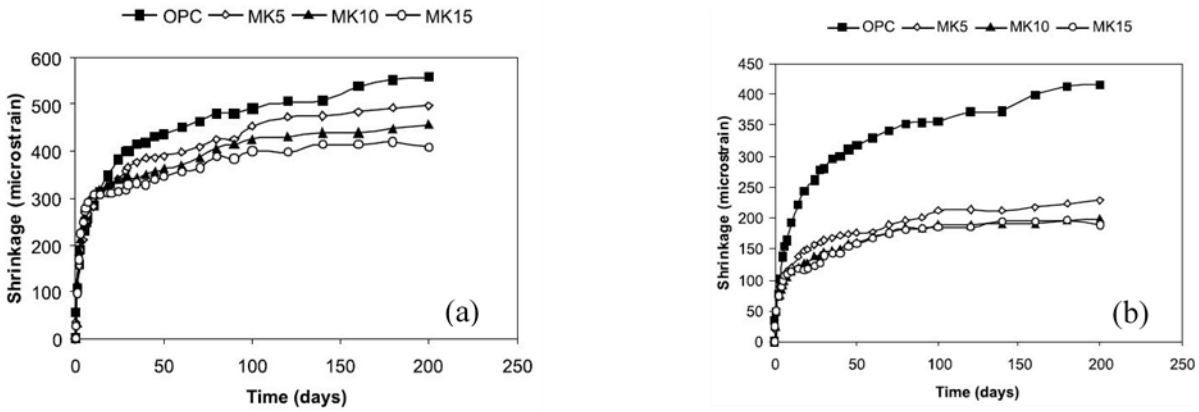

Figure 2.8. Effect of metakaolin on (a) total shrinkage and (b) pure drying shrinkage of concrete

Camiletti et al. (2013) investigated the effects of adding nano- and micro-limestone to ultra-high-performance concrete (UHPC). The results showed that the inclusion of micro- and nano-limestone reduced the drying shrinkage of the concrete (Figure 2.9).

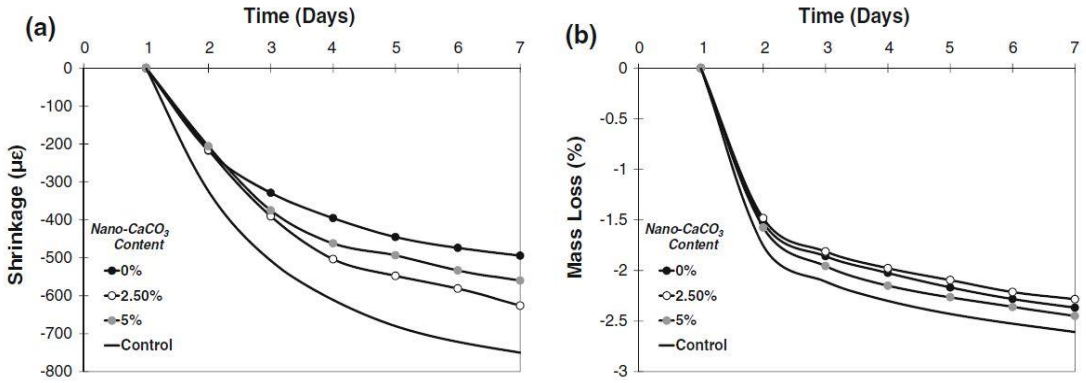

Camiletti et al. 2013, Copyright © 2012 RILEM, reprinted with permission from Springer Nature

Figure 2.9. Effect of nano- and micro-limestone on (a) drying shrinkage and (b) mass loss

2.2 Effects of Shrinkage-Reducing Admixtures

SRA is a chemical admixture that usually reduces the surface tension of pore solution in concrete pores (Folliard and Berke 1997), thus easing the capillary stress, a driving force of concrete shrinkage. Researchers have found that SRA addition can delay the age of cracking and reduce the corresponding crack width (Weiss et al. 1999). However, it may also result in decreases in concrete strength and a change in concrete pore structure (Ribeiro et al. 2006).

Bentz et al. (2001) and Bentz (2006) studied the effect of SRA on the internal relative humidity (RH) of cement pastes with and without a 2% mass addition of SRA and with a given w/c ratio of 0.3 and cement fineness of 654 m^2/kg (ultrafine). In their study, all samples were cured and measurements were taken at a temperature of 25°C under sealed conditions. As shown in Figure 2.10, they found that the internal RH in the samples with 2% SRA was much higher than that in the sample without SRA (Figure 2.10a). They concluded that SRAs may beneficially reduce evaporative water loss from fresh concrete and reduce autogenous shrinkage (Figure 2.10b).

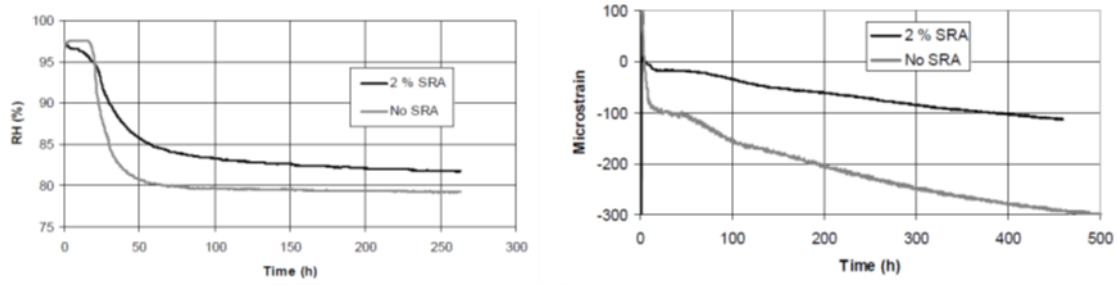

(a) Internal relative humidity (b) Autogenous shrinkage

Bentz 2006, adapted from Bentz et al. 2001, Copyright © 2006 Japan Concrete Institute

Figure 2.10. Internal RH and autogenous shrinkage of cement pastes with and without SRA

Folliad and Berke (1997) studied shrinkage behavior of two sets of HPC mixes: an OPC mix with and without 1.5% SRA (by mass of binder) and an SF mix (containing 92.5% OPC-7.5%) with and without 1.5% SRA. After 24 hours, the concrete prisms were demolded and stored at 20°C and 50% RH. They found that SRA significantly reduced drying and restrained shrinkage of the concretes (Figure 2.11).

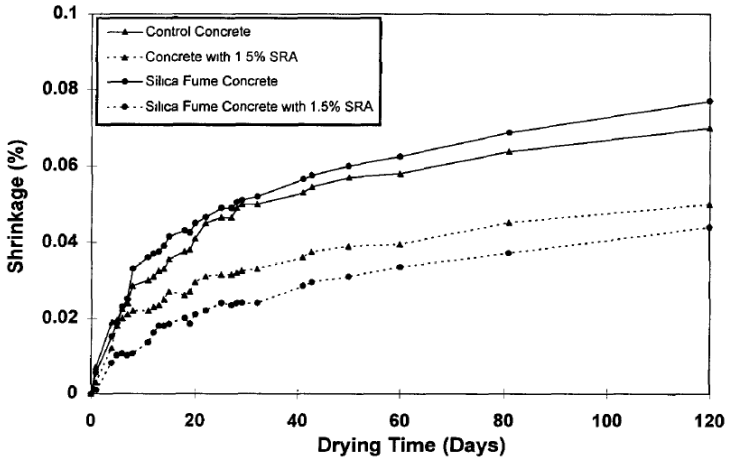

Folliard and Berke 1997, Copyright © 1997 Elsevier Science Ltd. Reprinted with permission from Elsevier

Figure 2.11. Drying shrinkage of HPC with and without SRA

The concrete containing SRA also exhibited slightly lower early age strengths than the corresponding concrete without SRA (Table 2.1).

Table 2.1. Hardened concrete properties

	Compressive Strength (MPa)			
Mixture Description	**1 day**	**7 days**	**28 days**	**90 days**
Control Concrete	31.2	51.9	63.9	74.1
Concrete with 1.5% SRA	25.0	48.2	58.7	67.6
Silica Fume Concrete	30.6	56.0	76.4	83.6
Silica Fume Concrete with 1.5% SRA	25.5	50.7	71.7	76.9

Source: Folliard and Berke 1997

Weiss et al. (1998) studied the shrinkage of both normal strength concrete (NSC) and high strength concrete (HSC) according to ASTM C341. They found that SRA significantly reduced the free drying shrinkage of both NSC and HSC (Figure 2.12).

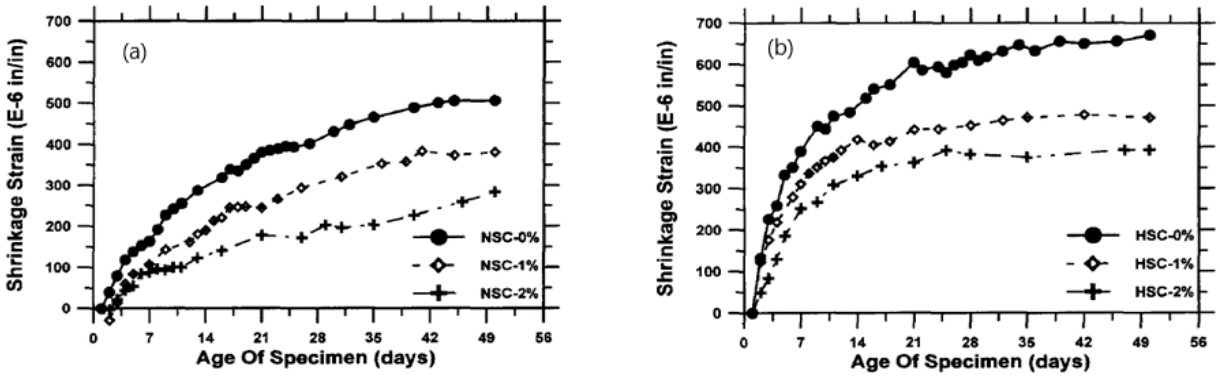

Weiss et al. 1998, Copyright © 1998 ASCE, used with permission from ASCE

Figure 2.12. Shrinkage strain of (a) NSC and (b) HSC with 0-2% SRA

Ribeiro et al. (2006) studied the effect of SRA on pore structure of mortars. They conducted experiments using a reference mixture (no SRA), a SRA-1 mix (6.7 ml of SRA 1), and a SRA-2 mix (9 ml of SRA 2). The information on the two SRAs used appears in Table 2.2.

Table 2.2. Chemical components of SRA

Admixture	Main component
SRA-1	High molecular weight polyglycol
SRA-2	Alkyl-ether

Source: Ribeiro et al. 2006

Free drying shrinkage was measured on 40 mm×40 mm×160 mm mortar bars, which were kept in molds for 24 hours in a moist chamber at 20 ± 1°C (RH>90%) and then maintained at 20 ± 2°C and 60 ± 5% RH. The results showed that the addition of SRA reduced free drying shrinkage of the mortar (Figure 2.13), and it decreased the capillary suction and oxygen permeability as well. They hypothesized that the reduction in shrinkage resulted from the decrease in surface free energy and a variation in disjoining pressure on the pore structure of the mortars.

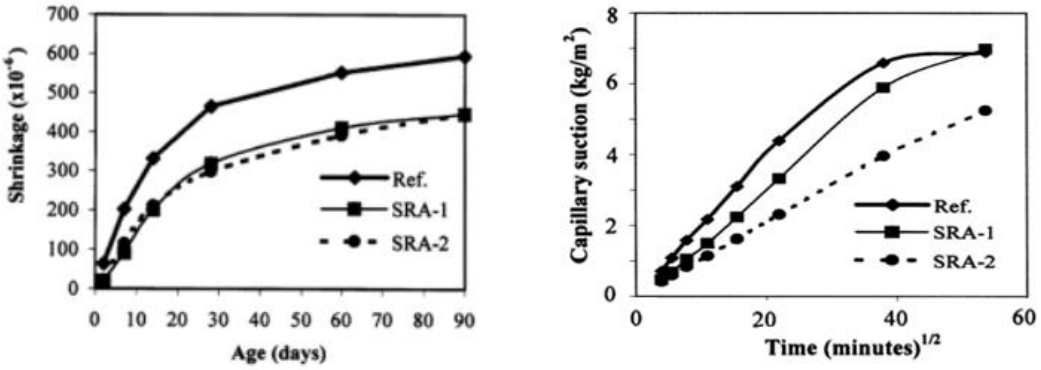

(a) Free drying shrinkage (b) Capillary suction

Ribeiro et al. 2006, Copyright © 2006 RILEM, reprinted with permission from Springer Nature

Figure 2.13. Shrinkage and capillary suction of samples with 0–2% SRA

Maltese et al. (2005) investigated the combined effect of expansive and shrinkage-reducing admixtures on shrinkage of mortars. They conducted experiments using samples: without admixtures, with 3% (by mass of cement) of a calcium oxide based expansive agent, with 3% of a propylene glycol ether based SRA, and with 3% of the SRA and the expansive agent. Restrained expansion was measured according to ASTM C845. They found that the use of the combined expanding agent and SRA made the mortars less sensitive to drying. A synergistic effect was observed between these two admixtures (Figure 2.14).

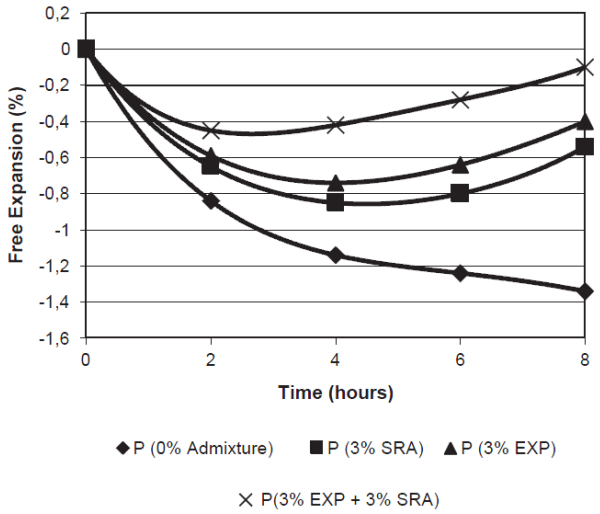

Figure 2.14. Free expansion test

Saliba et al. (2011) investigated the influence of shrinkage-reducing admixtures on plastic and long-term shrinkage of four different concrete mixes with and without SRA. The information on their concrete mixtures is listed in Table 2.3.

Table 2.3. Proportions, constituents, and properties of concrete mixtures

Concrete mixture properties	C43	C43SRA	C65	C65SRA
Gravel (rolled gravel 4/12) (kg/m^3)	836	833	836	833
Sand (river sand 0/4) (kg/m^3)	824	821	824	821
Cement (CEM | 52.5) (kg/m^3)	383	383	283	283
Filler (limestone) (kg/m^3)	163	163	192	192
Water (kg/m^3)	165	165	185	185
Superplasticizers (kg/m^3)	13.7	13.7	3.5	3.5
SRA (kg/m^3)	0	5.5	0	4.8
w/c	0.43	0.43	0.65	0.65
w/(c + A)	0.3	0.3	0.39	0.39
Sp/*(c + A)* (%)	1.77	1.78	0.79	0.74
SRA/*(c + A)* (%)	0	1	0	1
Slump flow (mm)	-	-	650	680

Source: Saliba et al. 2011

After casting, specimens were covered and maintained at 20°C and 100% RH for 24 hours, then they were demolded and exposed to environmental conditions of 20 ± 1°C and RH of 50 ± 5%. The researchers found that SRA was more effective when the internal humidity was relatively high or when a higher porosity existed in the concrete materials (Figure 2.15).

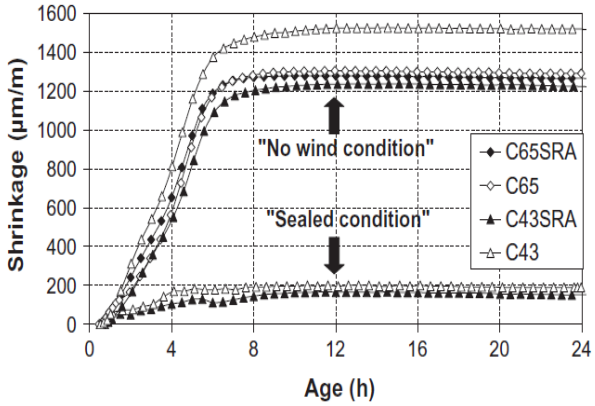

Figure 2.15. Plastic shrinkage of concretes with and without SRA

In addition to shrinkage and strength, researchers have found that many SRAs, such as polypropylene glycol based SRA, have a plasticizing effect and often lead to an increase in the workability of the concrete (Gettu et al. 2002). Yoo et al. (2015) studied the effectiveness of SRA in reducing autogenous shrinkage stress of ultra-high-performance fiber-reinforced concrete (UHPFRC). They found that the 28-day tensile strength of non-steam-cured UHPFRC slightly increased with a rise in the SRA content, and autogenous shrinkage stress decreased at lower reinforcement ratios and higher SRA contents.

2.3 Shrinkage Compensating Admixture (SCA)

SCA is a chemical admixture that typically causes concrete to expand through specific chemical reactions during early-age cement hydration, thus offsetting shrinkage that occurs with concrete drying. These chemical reactions often involve formation of ettringite from a sulfoaluminate based agent or calcium hydroxide from a CaO (lime)-based expansive agent. A sulfoaluminate based SCA commonly has a slower rate of expansion than a CaO-based SCA, the latter of which is more suitable for early age strength concrete with a short curing time (Collepardi et al. 2005). SCAs are also used to produce expansive cement varieties such as Types K, M, and S cement (ASTM C845).

Mo et al. (2014) investigated the history, performance, industrial manufacturing, and application of MgO expansive cement and concrete. They found that the expansion properties of MgO depend on its hydration reactivity and microstructure, which are influenced by the calcination conditions. For the manufacturer, precise control of the calcination temperature, residence time, and homogeneous heating of the magnesite are the important elements to manufacture MgO-based SCA. As shown in Figure 2.16, when calcined at higher temperatures or for longer

durations, the MgO could undergo crystal growth. A large size of MgO grains with small specific surface area generally displayed lower hydration reactivity, thus reducing the rate of expansion.

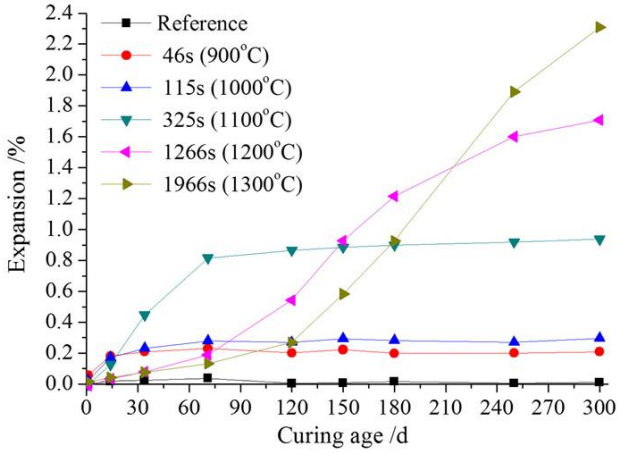

Figure 2.16. Expansion of cement pastes containing 8% MEA with various hydration reactivities calcined under different temperatures for 1 hr (cured in 40°C water)

Chen and Brouwers. (2012) investigated ettringite-based, mineral shrinkage-compensating admixtures (MSAs) made with differing proportions of GGBFS, fly ash, and anhydrite. They used the MSAs to replace 0% to 20% Portland cement and measured the mortar samples for length change and compression. They found that a 10% MSA replacement could provide a significant reduction in autogenous shrinkage with very limited loss of mortar strength (Figure 2.17).

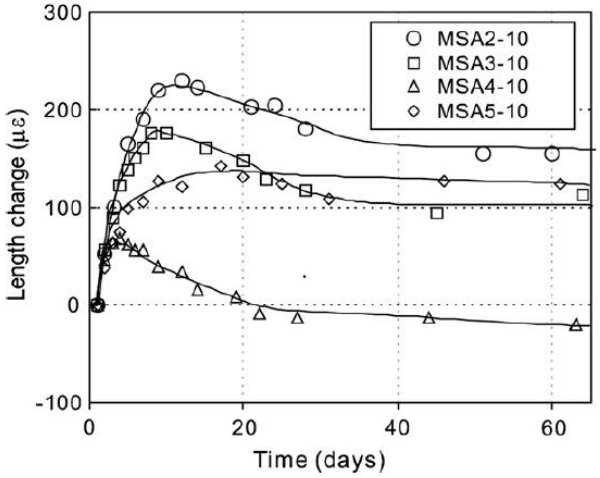

Figure 2.17. Effect of MSA composition on the autogenous length change of mortar

Collepardi et al. (2005) reported that neither an expansive agent nor SRA, when used separately, can definitively and safely deter the risk of cracking caused by drying shrinkage in real concrete structures under the practical conditions of curing on many jobsites. They showed the advantages of the combined use of an SRA and CaO-based expansive agent to produce SCA even in the absence of an adequate wet curing.

As seen in Figure 2.18, concrete C (with SRA + CaO) performs much better than that with CaO only (concrete B) or with SRA only (concrete D).

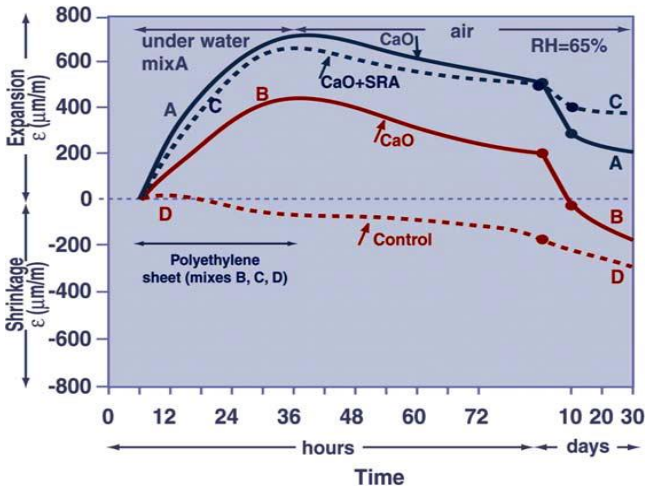

Figure 2.18. Effects of CaO-based SCA and SRA on concrete length change

In a recent study, Treesuwan and Maleesee (2017) considered shrinkage behavior of mortar made with various combinations of SRA (polyoxyalkylene alkyl ether type), CaO-based expansive additive (EX), and 20% and 40% FA. As shown in Figure 2.19, they found that under a normal curing condition, expansion was observed in the mortar with a combination of SRA, EX, and FA.

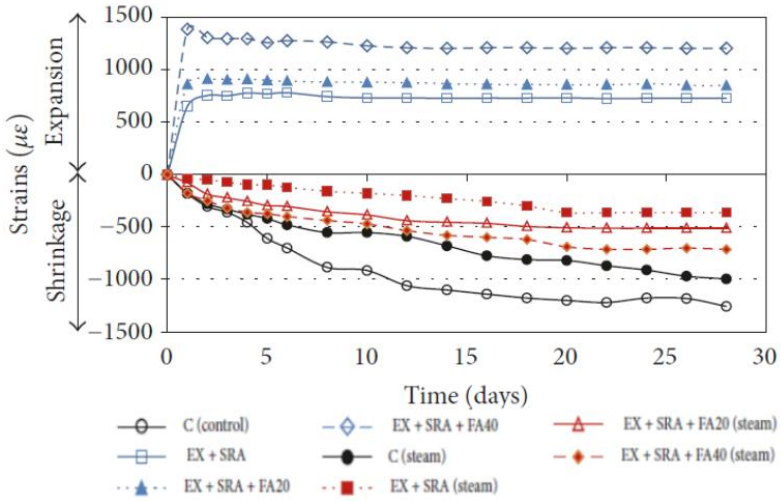

Figure 2.19. Combined effects of EX, SRA, and FA on mortar length change

While under a steam curing condition, shrinkage, rather than expansion, was observed for up to 28 days of curing. They believed that such shrinkage of the steam cured concrete resulted from the accelerated pozzolanic reaction of the FA at the elevated temperature.

Wang et al. (2011) studied the effects of delayed ettringite formation from U-type expansive agents (UEA). (In China, UEA is the most commonly used of all the calcium sulphoaluminate expansive agents.) They found that early stage curing was very important for large volumes of concrete containing the expansive agent, and delayed ettringite formation (DEF) could be a great concern. Keeping water from entering the concrete and controlling internal concrete temperature were critical for avoiding the problems caused by DEF.

2.4 Effects of Internal Curing

IC is a method to increase internal water supply through addition of a “water-entraining” agent, such as saturated superabsorbent polymer particles (SAPs) or lightweight fine aggregate (LWFA), in a concrete mixture. The water supplied from these saturated particles can counterbalance the moisture lost in concrete from drying or self-desiccation, thus reducing shrinkage. Internal curing can also improve concrete compressive strength at later stages due to the increased degree of hydration (Geiker et al. 2004). There are several literature reviews on IC of concrete, and a recent one by Liu et al. (2017), covered the effects of various commonly used IC materials (such as SAP, LWFA, and porous superfine powders) on shrinkage behavior of concrete, especially HPC, as well as their shrinkage reduction mechanisms. To date, internally cured concrete has been used most often in bridge decks, while some extended investigation has also been conducted on its use in pavements. In addition to reducing shrinkage reduction, IC could also help decrease slab curling/warping (Weiss 2016a).

2.4.1 Use of Superabsorbent Polymer

SAPs are often made of covalently cross-linked acrylamide/acrylic acid copolymers, and they can be produced by solution or suspension polymerization to obtain particles of different sizes and shapes. Use of SAP as an IC agent for concrete has been investigated by many researchers since 2000 (Jensen and Hansen 2002, Friedemann et al. 2006, Kovler and Jensen 2007, Mechtcherine and Reinhardt 2012, Schröfl et al. 2012, Sensale and Goncalvas 2014). Researchers have found that the water absorbed/desorbed by SAP in concrete largely depends upon its molecular structure. Some SAPs, with high anionic functional group density, can take up and release water within 1 to 3 hours, while others take days after being mixed with concrete (Schröfl et al. 2012). SAP can be used as a dry concrete ingredient since it takes up water during the mixing process. The addition of SAP can change the setting and rheology of concrete, and more importantly, agglomeration and grinding of SAP particles during concrete mixing is sometimes a concern (Sensale and Goncalvas 2014).

Sensale and Goncalves (2014) employed a SAP in mortar. The SAP was based on a cross-linked polyacrylic sodium salt with a particle size of 45 to 150 μm and specific gravity of 680 kg/m^3. As shown in Figure 2.20, they found that additions of 0.3 and 0.6% SAP led to a small successive reduction of autogenous shrinkage. However, complete elimination of autogenous deformation was not achieved with a higher SAP content. The reduction of autogenous shrinkage by use of the SAP reported in this paper was much less than that brought about by use of lightweight fine aggregate as an IC agent.

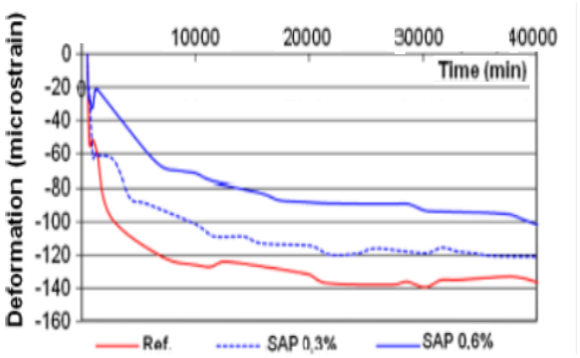

Sensale and Goncalves 2014, used with open access/Creative Commons permission

Figure 2.20. Effect of SAP on autogenous deformation of mortars

Shen et al. (2016) studied the effect of IC on the early age autogenous shrinkage of internally cured concrete with different amounts of IC water provided by SAP. They found that the concrete with SAP experienced a period of early age expansion. The amount and time of the maximum expansion of the concrete increased with the amount of IC water provided by SAP. Both the autogenous shrinkage and compressive strength of concrete at 28 days decreased with the increase of IC water provided by SAP.

Kong et al. (2015) studied the effect of pre-soaked SAP on shrinkage of HSC with a water-to-binder (w/b) ratio of 0.34 (HSC-1) and 0.39 (HSC-2). They found that the addition of pre-soaked

SAP clearly alleviated the early age shrinkage related to moisture loss. The autogenous shrinkage-reducing effect provided by the pre-soaked SAP is much stronger than that of the additional mixing water.

Pourjavadi et al. (2013) studied the interactions between SAP and cement-based composites. They used distilled water, artificial pore solution, 0.9% NaCl solution, and cement paste filtrate as swelling media. As shown in Figure 2.21, they found that the swelling behavior of SAP due to absorption in cement paste filtrate was very different from that in distilled water.

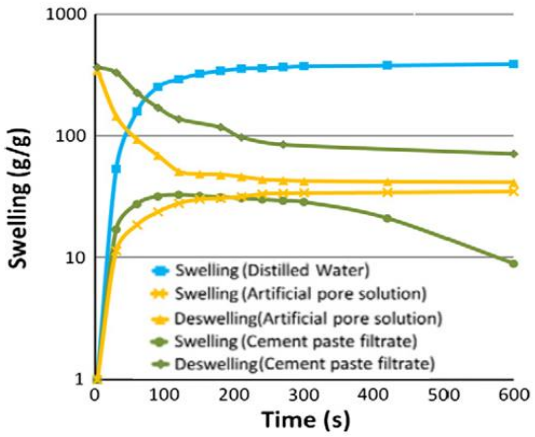

Figure 2.21. Kinetics of swelling of dry SAP and de-swelling of water-swollen SAP upon immersion in artificial pore solution and cement paste filtrate

Chen et al. (2011) investigated the presence of shrinkage for a concrete slab with SAP. They found that use of SAP clearly improved the concrete shrinkage cracking performance. Compared to the concrete without SAP, the slab with SAP had a 50% reduction in total cracking area and a 65% decrease in free shrinkage (Figure 3 at https://www.scientific.net/MSF.675-677.697.pdf), and the reduction was greater than that seen in the slab with lightweight ceramisite.

Pang at el. (2011) studied effects of SAP dosages (0.05, 0.15, and 0.25% by weight of binder) on free drying shrinkage of mortar (w/b ratio = 0.5). In order to allow SAP to reduce autogenous shrinkage, more water was added to some mortar mixtures based on the amount of SAP used. They found that SAP addition increased the internal RH of the mortar samples that were tested. If no additional water was added, the mortar shrinkage generally decreased as the dosage of SAP increased. However, if the amount of additional water was high for a high dosage of SAP, the shrinkage of the mortar with SAP was higher than that of corresponding mortar without SAP.

It has been noted in the literature that there are some conflicting results on use of SAP as an IC agent for reducing concrete shrinkage. Generally, use of SAP reduces autogenous shrinkage, but does not always effectively reduce free drying shrinkage. These conflicts had not been explained until recently when Kang et al. (2018) studied the importance of monovalent ions on water retention capacity of SAP. The researchers revealed that SAP releases monovalent cations such

as Na^+ into pore solutions of a cement paste upon absorption of Ca^{2+}. The retention capacity of the SAP declines with the amount of Ca^{2+} absorbed by the SAP. Although the SAP in concrete has suitable absorption capacity, if its water retention capacity is low, the internal curing water will be released prematurely (i.e., before setting or starting autogenous shrinkage). As a result, the added water that originally acted to reduce autogenous shrinkage can just increase the w/c of the cement paste, thus resulting in higher free drying shrinkage.

2.4.2 Use of Lightweight Fine Aggregate (LWFA)

A literature review on the impacts of IC on concrete properties was conducted in Iowa under IHRB Project TR-676 (Babcock and Taylor 2015). The basic IC concept, IC concrete mix design method, and the effects of IC on concrete shrinkage, strength, elastic modulus, permeability, and freeze-thaw (F-T) durability etc. were briefly summarized. Related studies have also been conducted by other transportation agencies (Jones et al. 2014, Guthrie et al. 2014). Table 2.4 lists the transportation agencies that have used IC for bridge decks and pavements (Castrodale 2015).

Table 2.4. Transportation agencies that have used IC

State	IC applications
Illinois (Tollway)	Bridge decks
Indiana	Bridge decks, HESC (high early strength concrete) pavement repair
Iowa	Bridge decks
Kansas	Bridge decks, pavement
New York	Bridge decks
Texas	Bridge decks, pavement
Utah	Bridge decks
Virginia	Bridge decks and overlays
Ontario, Canada	Bridge decks

Source: Castrodale 2015

Based on laboratory studies and field experiences over the past decade, the *Guide Specification for Internally Curing Concrete* was developed (Weiss and Montanari 2017). The research and practices have consistently indicated that use of LWFA as an IC agent can reduce both autogenous and drying shrinkage, improve compressive strength, reduce ion diffusion, and maintain workability, and intact freezing-thawing durability of the concrete. To avoid repetition, detailed literature review results on use of LWFA as an IC agent do not appear in this report.

The literature review presented here indicates that there are various concrete shrinkage reduction methods, including use of FA (especially Class F fly ash) and minimal binder content, shrinkage control admixtures (SRA/SCA), and IC agents (SAP and LWFA). Except for SAP materials, which primarily reduce only autogenous shrinkage, most of the shrinkage reduction methods can reduce both autogenous and drying shrinkage and decrease concrete shrinkage cracking potential. The effectiveness of the shrinkage reduction generated by shrinkage control admixtures or IC agents depends not only upon the admixtures/agents used, but also on the concrete materials and conditions under which they have applied. For instance, SRA often

displays a plasticizing effect in concrete, and it might be more beneficial for use in concrete with a low w/b ratio. Or, due to large pore structure, LWFA may cause a decline in concrete strength, thus raising a concern for its use in high strength and high-performance concrete.

Based on the literature review results as well as the input from the project technical advisory committee, three different shrinkage reduction methods were selected for investigation in this project:

- Use of shrinkage control admixture (SRA/SCA) for Mix 6, with a w/b ratio of 0.33 and binder content of 825.7 lb/yd^3
- Cementitious material (or binder) content reduction for Mix 8, with a w/b ratio of 0.40 and binder content of 668.8 lb/yd^3
- Use of IC (SAP and LWFA) for Mix 2, with a w/b ratio of 0.40 and binder content of 651.5 lb/yd^3

Besides measuring the autogenous, free drying, and restraint drying shrinkage, the effects of the shrinkage reduction methods on other properties of the concrete mixes, such as workability, compressive strength, elastic modulus, creep behavior, etc., were also investigated.

3. LABORATORY INVESTIGATION

A laboratory investigation was conducted to achieve these major objectives:

1. Determine the type and/or optimal quantity of the material to be used in each individual shrinkage reduction method. (For instance, SRA or SCA would be selected for modification of original Mix 6 and the dosage of the selected admixture should be determined based on the laboratory test results.)

2. Understand how the individual shrinkage reduction methods could affect the key properties of three HPC mixes (Mix 6, Mix 8, and Mix 2), including their fresh properties (slump, unit weight, and air content), mechanical properties (compressive and splitting strength, elastic modulus, and creep), shrinkage behaviors (drying shrinkage, autogenous shrinkage, and restrained shrinkage), F-T durability, and surface resistivity.

3. Provide necessary inputs for use of the selected shrinkage reduction methods (SRA for Mix 6 and binder content reduction for Mix 8) for field investigations of this project.

The materials, tests, methods, and results of the laboratory investigation are presented as follows.

3.1 Materials

The concrete materials used in the laboratory investigation include cementitious materials, aggregates, and admixtures. The types and sources of these materials are listed in Table 3.1.

Table 3.1. Concrete materials and their sources

Materials	Type	Source
Cementitious Materials		
Portland cement (PC)	Type I	Continental Cement
Fly ash (FA)	Class C	Headwaters Resources
Ground granulated blast furnace slag (GGBFS)	Grade 100	Holcim
Aggregates		
Coarse aggregate (CA)	Limestone	Martin Marietta, Ames
Fine aggregate (S)	River sand	Hallet Materials, Ames
Chemical Admixtures		
Air-entraining agent (AEA)	Daravair 1000	W. R. Grace
Normal-range water reducer (NRWR)	WRDA-82	W. R. Grace
Mid-range water reducer (MRWR)	MIRA 62	W. R. Grace
Retarder (R)	Recover	W. R. Grace
Shrinkage Control Admixtures/Materials		
Shrinkage-reducing admixture (SR)	Eclipse 4500	W. R. Grace
Shrinkage-compensating admixture (SC)	PREVent-C	Premier CPG
Superabsorbent polymer (SAP)	HydroMax	ProCure
Lightweight fine aggregate (LWFA)	HydroCure expanded shale	Kentucky Solite

3.1.1 Cementitious Materials

Cementitious materials used in the laboratory investigation of the Phase II study included Type I cement, Class C fly ash, and GGBFS. Their physical and chemical properties are presented in Table 3.2. Type IP cement was used for Mix 2 in the Phase I study. However, Type I cement was used for all mixes studied in Phase II.

Table 3.2. Physical and chemical properties of cementitious materials

Composition, %	PC	FA	GGBFS
Na_2O	0.09	1.64	0.29
MgO	2.40	4.87	9.63
Al_2O_3	4.60	17.68	8.54
SiO_2	20.20	31.92	36.50
SO_3	3.40	1.68	0.60
K_2O	0.67	0.43	0.44
CaO	63.10	30.90	41.10
Fe_2O_3	3.20	6.54	0.83
Others	1.20	4.34	2.07
Specific Gravity	3.14	2.69	2.50
Fineness (m^2/kg)	429	419.6	455.0

3.1.2 Aggregates

The coarse aggregate used was 1/2 in. crushed limestone and the fine aggregate was #4 river sand. Both coarse and fine aggregates were used in oven-dried condition. The absorption of coarse aggregate is 0.7% and sand is 1.4%. The specific gravity for coarse aggregate is 2.7 and 2.63 for fine aggregate. Table 3.3 shows the properties of the aggregates used.

Table 3.3. Aggregate information

Aggregate type	Source	Type	Specific gravity	Absorption, %		Desorption at 100% RH
				24 hours	Ultimate	
Coarse aggregate	Martin Marietta, Ames, IA	Limestone	2.68	-	0.8	-
Fine aggregate	Hallet, Ames, IA	River sand	2.66	-	0.9	-
LWFA (HydroCure)	Kentucky Solite, Brooks, KY	Expanded shale	1.75	17.6	24.0	0.95

The gradations of the limestone coarse aggregate and river sand used are shown in Table 3.4, Figure 3.1, and Figure 3.2. The coarse aggregate gradation complies with Iowa Standard No. 6 (Repair and Overlay), and fine aggregate gradation is within the ASTM C33 specification limits.

Table 3.4. Gradations of aggregates

Sieve size	Percent passing, %	
	Limestone	Sand
1 in.	100.0	-
3/4 in.	100.0	-
1/2 in.	97.8	-
3/8 in.	67.8	100.0
No.4	11.5	99.7
No.8	2.1	90.8
No.16	0.9	70.8
No.30	-	37.1
No.50	-	6.9
No.100	-	0.4

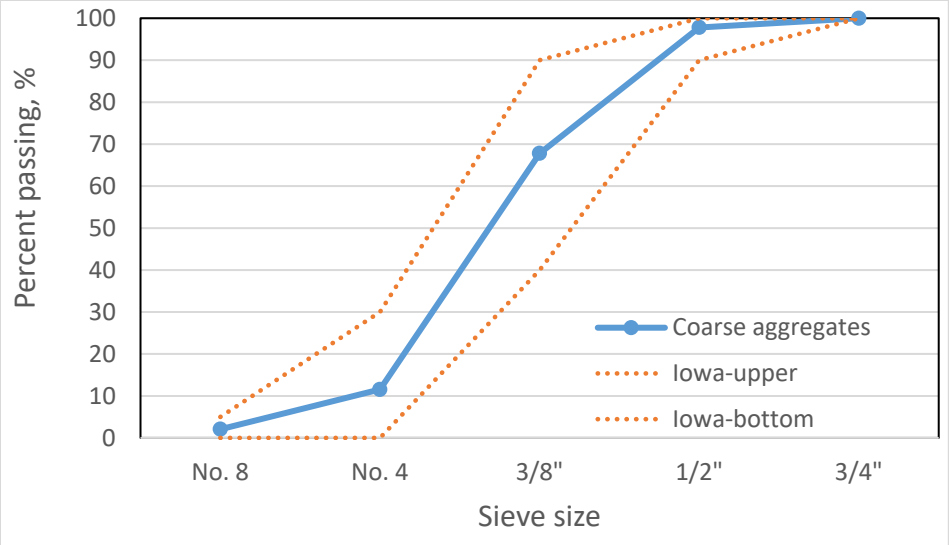

Figure 3.1. Coarse aggregate gradation

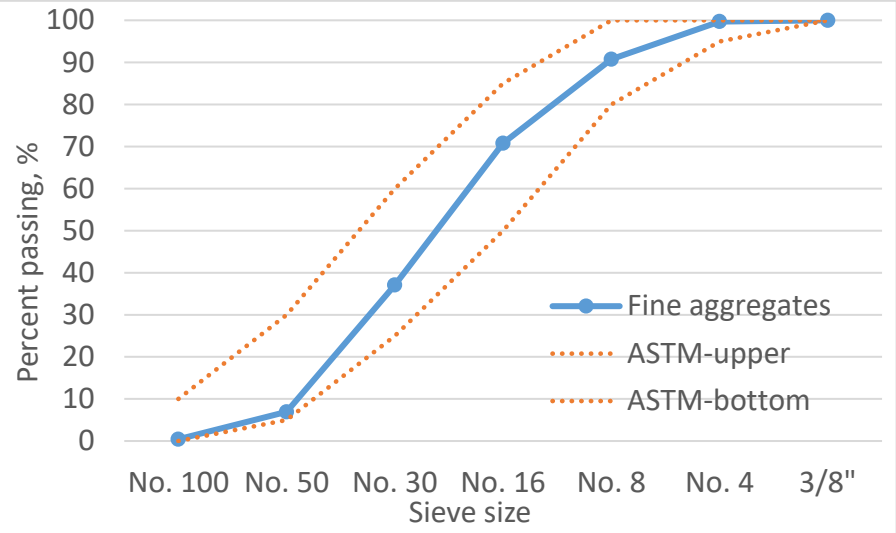

Figure 3.2. Fine aggregate gradation

3.1.3 Admixtures

The chemical admixtures used included MRWR, NRWR, R, and an AEA. The dosage of AEA was determined based on the trial mix and the target air content is 7%. The dosages of water reducer, retarder, and shrinkage reducer were determined based on suggestions from the Iowa Department of Transportation (DOT) and recommendations provided by the manufacturers. Table 3.5 shows the dosages of the chemical admixtures used in this project.

Table 3.5. Dosage of chemical admixtures

	Dosage, oz/cwt		
Admixture	**Mix 6**	**Mix 8**	**Mix 2**
AEA	2.5	0.5	1.0
MRWR	-	6	1.0
NRWR	3.5	-	-
Retarder	-	2	1.0

3.2 Mixture Proportions

Mixes 2, 6, and 8, as denoted in the Phase I study, were selected for Phase II study. The mix proportions of these original mixes appear in Table 3.6. These mixes were selected based on the Phase I study results as well as their historical field performance.

Table 3.6. Mix proportions of original mixes

Mix	**Iowa DOT Designation**	**Cement lb/yd^3**	**FA lb/yd^3**	**GGBFS lb/yd^3**	**Limestone lb/yd^3**	**Sand lb/yd^3**	**Water lb/yd^3**	**w/b ratio**	**WRA**
6	HPC-O	825.4	-	-	1386.3	1365.6	269.9	0.33	NRWA
8	HPC-O-C20-S25	367.9	133.8	167.2	1430.8	1404.9	267.6	0.40	MRWA
2	HPC-O-C20	527.9	132.0	-	1458.0	1431.8	263.9	0.40	NRWA

Mix 6 was identified as a mix with high cracking potential in the Phase I study. It was made with 825.4 lb/yd^3 of Type I cement and a low w/b ratio of 0.33. In order to reduce shrinkage of this mix with impaired workability, SRA and SCA were added to the mixture at different dosages and the effects of the shrinkage control admixtures on shrinkage and concrete properties were evaluated.

Mix 8 was identified as a mix with medium cracking potential in the Phase I study. It was made with 55% Type I cement, 20% FA, and 25% GGBFS at a binder content of 668.9 lb/yd^3 and a w/b ratio of 0.40. In order to reduce shrinkage of this mix, cementitious material or binder content was reduced from 100% to 85% by increments of 5%. It should be noted that cementitious material reduction can cause reduction in mechanical properties and durability; therefore, it needs to be pursued cautiously.

Mix 2 was identified as a mix with low cracking potential in the Phase I study. It was made with 80% Type IP cement and 20% Class C fly ash at a binder content of 659.9 lb/yd^3 and a w/b ratio of 0.40. In an application of Mix 2, early age cracking was a concern for a bridge overlay in Iowa. Therefore, the IC method was proposed for this mix and SAP and LWFA were both employed as IC agents. Since the shrinkage test results obtained from the application of SAP were not conclusive, this study focused more on the use of LWFA for modification of Mix 2. Based on the design method provided by Weiss (2016b), 34% (by volume) of fine aggregate in

the original Mix 2 was replaced by LWFA to provide 7 lbs of water for every 100 lbs of cementitious materials used.

The details of the modification procedures and test results of these mixes are given in the following sections.

3.3 Tests and Methods

The four types of tests performed for both original and modified concrete mixes were (1) fresh concrete properties, (2) shrinkage tests, (3) mechanical property tests, and (4) durability tests. The fresh concrete property tests were slump, unit weight, and air content. Shrinkage tests included free drying shrinkage, autogenous shrinkage, and restrained ring shrinkage. The hardened concrete property tests were strength (splitting tensile and compressive), elastic modulus, and creep. Durability tests were surface resistivity tests and freezing-thawing tests. Table 3.7 summarizes the sample sizes and test methods.

Table 3.7. Tests performed in lab

Concrete properties	Tests	Sample dimension	Method
Fresh concrete properties	Slump	Slump cone	ASTM C143
	Unit weight	0.25 ft^3	ASTM C138
	Air content	0.25 ft^3	ASTM C231
Shrinkage tests	Free drying shrinkage	3×3×11.25 in.	ASTM C157
	Autogenous shrinkage	3×3×11.25 in.	ASTM C157
	Restrained ring shrinkage	16(ϕ_o)×13(ϕ_i)×6(t) in.	ASTM C1581
Hardened concrete properties	Compressive strength	4×8 in. cylinder	ASTM C39
	Splitting tensile strength	4×8 in. cylinder	ASTM C496
	Elastic modulus	4×8 in. cylinder	ASTM C469
	Creep	4×8 in. cylinder	ASTM C512
Durability	Surface resistivity	4×8 in. cylinder	AASHTO TP 95
	Freezing-thawing tests	3×4×16 in.	ASTM C666

3.3.1 Fresh Concrete Properties

Concrete was mixed and cast according to ASTM C192 (standard practice for making and curing concrete test specimens in the laboratory). Oven-dried aggregates were used. Slump tests were performed based on ASTM C143. Unit weight and air content tests were conducted according to ASTM C138 and C231, respectively. Iowa DOT specifies Class O mix (Mix 6) to have a slump of 3/4 to 1 in. and HPC (Mix 8 and Mix 2) to have a specified slump of 1 to 4 in., with a maximum of 5 in. The air content requirement is 6.5%, with a maximum variation of plus 2.0% and minus 1.0% (Section 2413. Bridge Deck Surfacing, Repair, and Overlay). The dosages of water reducing agents and air-entraining agents for the concrete mixtures were adjusted to reach the slump and air content requirements.

3.3.2 Shrinkage Tests

Autogenous Shrinkage

To measure autogenous shrinkage, all concrete mixtures were cast according to ASTM C192. Three 3×3×11.25 in. prisms were cast for each concrete mix. To prepare the samples, molds were oiled and had a stud installed in each of the two interior ends. Fresh concrete was placed in one layer, and consolidated with a vibrating table at a frequency of 3,600 vpm for 5 seconds. After surfacing, the specimens were covered with a plastic sheet and wet towels to avoid moisture loss. After 24 hours, the specimens were demolded, immediately coated in wax, and wrapped tightly with multiple layers of a self-sealing polythene film to prevent moisture loss. Next, the initial length and weight of the specimens were measured, and the specimens were stored in an environmental chamber at a constant 73°F.

As shown in Figure 3.3, length changes of these specimens were measured using a comparator according to ASTM C157 (the standard test method for length change of hardened hydraulic-cement mortar and concrete). The measurements and weights of the specimens were taken at 4, 7, 14, 21, 28, and 56 days.

(a) Mold of sample (b) Setup for length measurement

Figure 3.3. Specimen mold and comparator for concrete autogenous shrinkage measurement

Free Drying Shrinkage

The specimen preparation for free drying shrinkage tests was the same as that for the autogenous shrinkage tests, and the concrete mixtures came from the same batch. After being demolded at 24 hours, the specimens were cured in a standard moist curing room (73.5 ± 3.5°F and 100% RH) for 7 days. The specimens were then stored (without sealing) in a drying environment (73°F and 50% RH) right after initial lengths of the specimens were taken. Subsequently, the lengths and weights of the specimens were measured at 3, 7, 14, 21, 28, and 56 days, following the same procedure as for the autogenous shrinkage test (Figure 3.4).

Figure 3.4. Specimen and comparator for free drying shrinkage

Restrained Ring Shrinkage Test

The restrained ring test was performed for each mix according to ASTM C1581 (the standard test method for determining age at cracking and induced tensile stress characteristics of mortar and concrete under restrained shrinkage). As seen in Figure 3.5, the test apparatus included two steel rings, two strain gages, and a data acquisition system.

(a) Ring mold

(b) Concrete ring sample

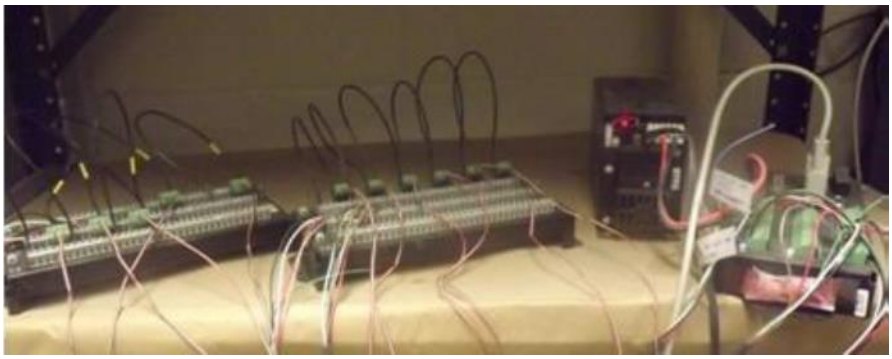

(c) Data logger

Figure 3.5. Mold, specimen, and data logger for concrete ring tests

The two strain gages were used to measure the strain along the circumferential direction of the ring specimens, and they were horizontally attached on the interior surface of the inner steel ring at mid-height locations diametrically opposite to each other. The manufacturer's specifications were used for mounting and waterproofing the gages on the steel ring and connecting the lead wires to the strain gage modules. The ring molds were held in place using four 3 in. C-clamps (Figure 3.5a) and oiled just before concrete casting.

The fresh concrete was placed in the space between the outer and inner steel rings in two layers, and each layer was rodded 75 times. The specimens were covered with a polythene sheet and a wet towel to prevent the moisture loss, and were maintained in a laboratory room with a temperature of 73.5 ± 3.5°F. The next day, the clamps were removed, and the lead-wires of the strain gages were connected to modules immediately after the clamps were released. The outer steel ring was removed (Figure 3.5b), and the top surfaces of the specimens were sealed with paraffin wax. The specimens were then stored in a drying environment set at 73.5 ± 3.5°F and 50% RH to achieve drying on the lateral surface along the circumferences of the rings.

The data logger recorded response data from the strain gages automatically once per minute, which were then converted to the shrinkage strains with time. The testing time and ambient temperature were also recorded. Any sudden decrease in the compressive strain measured by one or both strain gages indicated cracking of the concrete ring specimen being tested. The specimens were examined every 3 days for cracks. The test ended at 28 days of drying regardless of whether cracking was detected in the tested specimens.

3.3.3 Mechanical Properties

Strength and Elastic Modulus

For each concrete mix, 18 4×8 in. cylinder specimens were cast in two equal layers, and each layer was rodded 25 times. After being demolded at 24 hours, the specimens were cured in a 75°F and 100% RH curing room. Compressive strength, splitting tensile strength, and elastic modulus tests were performed at the ages of 3, 7, 14, 28, and 56 days, according to ASTM C39 (the standard test method for compressive strength of cylindrical concrete specimens), C496 (the standard test method for splitting tensile strength of cylindrical concrete specimens), and C469 (the standard test method for static modulus of elasticity and Poisson's ratio of concrete in compression), respectively.

Creep Test

Creep behavior of the mixes was investigated according to ASTM C512 (standard test method for creep of concrete in compression). For each concrete mix, 10 4×8 in. cylinder specimens were cast from the same batch and stored under the same environmental conditions. Four specimens were subjected to a constant load for the creep test, three specimens were not loaded and served as reference specimens for drying shrinkage strain measurements under the given

testing environment, and the remaining three specimens were tested for determining the creep load, which was 40% of the 28-day compressive strength of the tested concrete.

The specimens were cast at 73.5 ± 3.5°F and demolded at 1 day. They were then stored in a standard curing room (73.5 ± 3.5°F and 100% RH) for 7 days. After curing, 2 strain gages were attached on the lateral surface of the specimens in the vertical direction which evenly divided the specimen in height. Then, the ends of each specimen were capped with a sulfate compound to provide a completely contactable surface. The capped specimens were stored in a drying environment at a temperature of 73.5 ± 1.5°F and relative humidity of 50 ± 4% for 28 days.

After 28 days of drying, three specimens from each concrete mix were tested for compressive strength of the concrete and four specimens were loaded. The loading frame consisted of 4 square jack plates, 26 3 in. plugs, 3 springs, 3 threaded rods, 2 ball joints, and nuts in corresponding numbers as seen in Figure 3.6(a).

(a) Loading frames

(b) Creep test specimens

(c) Portable comparator

Figure 3.6. Layout of creep test

The four cylinder specimens were vertically stacked in the line between two plugs so they were subjected to a uniform load. Four plates and three springs were assembled with 3 threaded rods inserted. Springs were used to maintain the load for the system. The threaded rod was used to gauge the reaction of the loaded system. With the ball joint bearing the load between plate and plug, uniform loading of the cylinders was expected to be ensured.

The specimens were then loaded up to 40% of the 28-day compressive strength. As shown in Figure 3.6(c), an external portable comparator was used to measure the strain of the specimens at the time right before and after loading. Subsequently, the strain measurements were taken at four hours, then once a day (for one week), once a week (for one month), and once a month until the end of one year. Similarly, the shrinkage strain of the three control specimens was also measured on the same schedule as the loaded specimens for the offset of the strain from creep.

3.3.4 Durability Tests

Surface Resistivity

The surface resistivity test was conducted for all mixes according to AASHTO TP 95 (standard test method for surface resistivity of concrete's ability to resist chloride ion penetration) (Figure 3.7). Research has indicated that this test constitutes a promising alternative to the standard rapid chloride permeability test (RCPT, ASTM C1202) (Ardani and Tanesi 2012).

Figure 3.7. Surface resistivity test

For each concrete mix, three cylinder specimens at various curing ages were used for the test, and eight readings were taken from evenly spaced locations on the lateral surface of each specimen.

Freeze-Thaw Resistance

FT resistance was tested in accordance with ASTM C666 (standard test method for resistance of concrete to freezing and thawing) Method A for all mixes. Three 3×4×16 in. prisms were cast for each concrete mix. The prisms were demolded after 24 hours and subsequently stored in a standard moist curing room (73.5 ± 3.5°F and 100% RH) until the age of 28 days. After the 28 days of curing, the initial fundamental transverse frequency (Figure 3.8) and mass of the prism specimens were measured, and the prisms were placed into a FT chamber, as described in ASTM C666-B, and subjected to FT cycles under a cyclic temperature from 40°F to 0°F and then to 40°F again. The fundamental transverse frequency and mass change of the specimens were measured weekly until the end of 300 cycles.

Figure 3.8. Fundamental transverse frequency measurement for dynamic modulus

4. LABORATORY TESTS RESULTS AND DISCUSSION

4.1 Shrinkage Behavior of Mixes with and without Modifications

The results of the shrinkage tests of all project mixes (original and modified) are presented here. Discussions focus on how the shrinkage control methods affected the test results.

4.1.1 Mix 6: Modified with Different Dosages of SCA

In this study, Mix 6 was modified first since it was identified as having high shrinkage cracking potential. SCA was used first, followed by SRA. The results of the autogenous, free drying, and restrained ring shrinkage tests conducted on Mix 6 with various SCA dosages are shown in Figures 4.1 through 4.4. The modified mixes were designated as 6-SC2.5, where 6 denotes Mix 6; SC, shrinkage compensating admixture; and 2.5, a dosage of SCA that is 2.5% (by weight) of the cementitious materials in Mix 6.

Figure 4.1 shows that autogenous shrinkage of Mix 6 was reduced with increasing dosages of SCA. The autogenous shrinkage reached 0.041% (or 410×10^{-6}) for the mix with no SCA (6-SC0.0), while it was only 0.01% (or 100×10^{-6}) for the mix with 7.5% SCA (6-SC7.5) at 56 days.

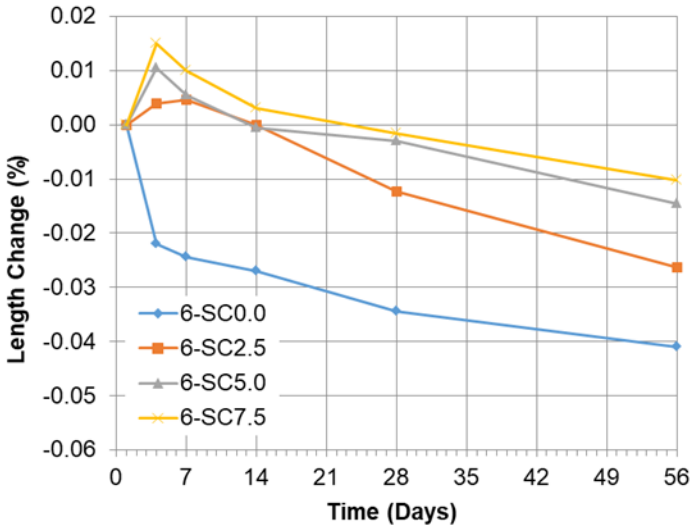

Figure 4.1. Mix 6 autogenous shrinkages with different SCA dosages

This shrinkage reduction was more effective at a later age (> 28 days) when the SCA dosage increased from 0 to 5.0%, and it was less effective when the SCA dosage increased from 5.0 to 7.5%. It was noted that even when the specimens were all sealed, the concrete containing SCA showed expansion before 14 to 22 days, depending on its SCA dosage. After the expansion was compensated, the mix displayed shrinkage.

For free drying shrinkage tests, as seen in Figure 4.2, the mixes with SCA had more significant expansion during -7 days to 0 days of moist curing.

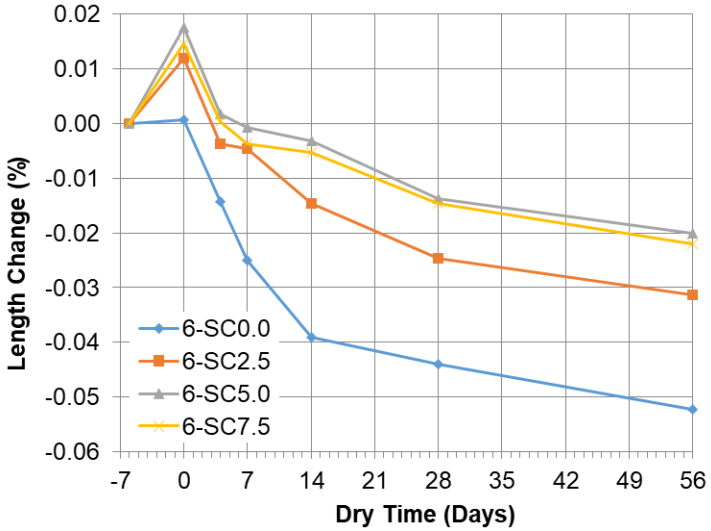

Figure 4.2. Mix 6 free drying shrinkages with different SCA dosages

After being subjected to drying, the specimens with SCA had substantially less free drying shrinkage. The free drying shrinkage reached 0.052% (or 520×10^{-6}) for concrete without SRA, and it was only 0.02% (or 200×10^{-6}) for concrete with 7.5% SCA at 56 days. When the SCA dosage increased from 2.5% to 5.0%, the free drying shrinkage reduction showed a corresponding increase. However, when the SCA dosage increased from 5.0% to 7.5%, the free drying shrinkage reduction decreased, implying diminishing effectiveness for using a SCA dosage higher than 5.0%. This observation supports the manufacturer's recommendation of a 5.0% maximum dosage.

Figures 4.3 and 4.4 show that SCA addition significantly reduced the strain of the steel ring used in the restrained drying shrinkage tests.

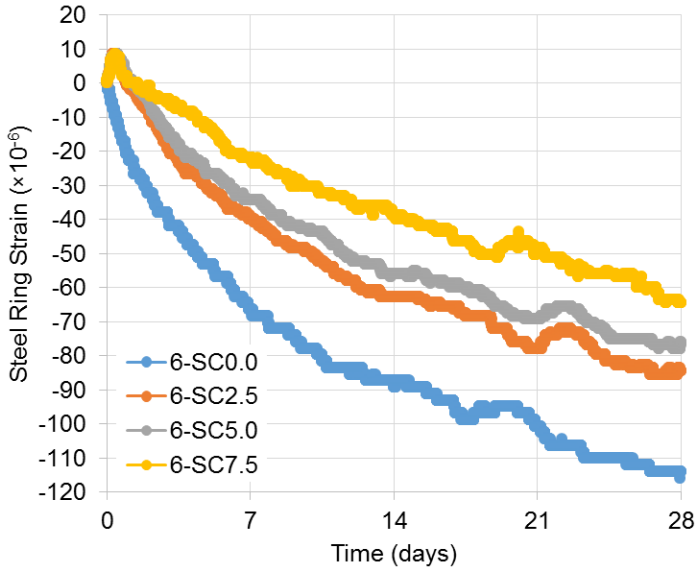

Figure 4.3. Mix 6 restrained ring shrinkages with different SCA dosages

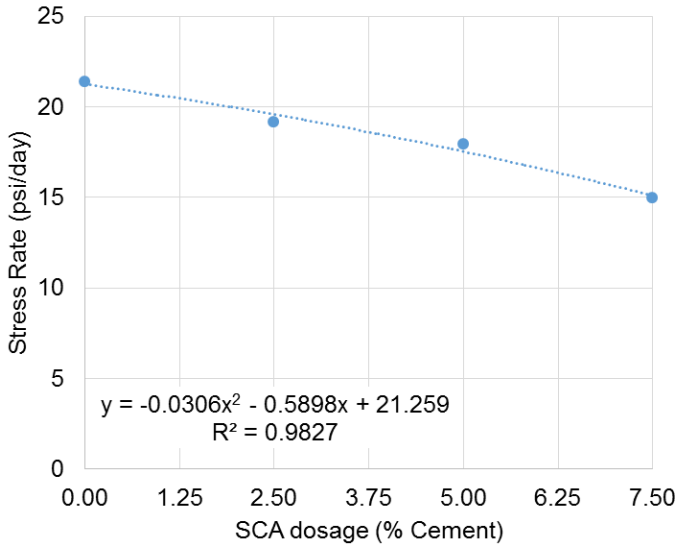

Figure 4.4. Mix 6 stress rates with different SCA dosage

At the age of 28 days, the shrinkage strain was 115×10^{-6} for the mix without SCA, but it was only 65×10^{-6} for the mix with 7.5% SCA. The reduction increased with increasing SCA dosage (up to 7.5%). The limiting dosage (5.0%) that was seen in free drying shrinkage tests (Figure 4.2) was not observed in the restrained shrinkage tests.

Generally, if the shrinkage strain exceeds the concrete cracking resistance, the measured strain will become zero due to cracking. Figure 4.3 shows that at 28 days, no mix had a measured strain of zero, indicating that no cracking occurred in these tested specimens.

According to ASTM C1581, the rate of stress resulting from the drying shrinkage in a tested concrete ring specimen can be calculated using Equation 1:

$$q = \frac{G\left|\alpha_{avg}\right|}{2\sqrt{t_r}} \quad (1)$$

Where, G is the concrete elastic modulus, given as 10.47×10^6 psi in this study; α_{avg} is the average strain rate factor; and t_r is the elapsed testing time. A concrete mix is considered to have low shrinkage cracking potential when the calculated stress rate is less than 15 psi/day.

The stress rates of Mix 6 with various SCA dosages at t_r = 28 days were plotted in Figure 4.4. As seen in Figure 4.4, only Mix 6-SC7.5 had shrinkage stress rates equal to or lower than 15 psi/day. This indicates that a dosage of 7.5% SCA would be more appropriate for shrinkage cracking prevention of Mix 6 for the present study.

4.1.2 Mix 6: Modified with Different Dosages of SRA

Mix 6 was also modified by adding different dosages of SRA (Eclipse 4500, WR Grace) to the mix. The dosages of the SRA studied were 0.0, 0.5, 1.0, 1.5, and 2.0 gal/yd^3. The modified mixes were designated as 6-SR1.5, where 6 denotes Mix 6; SR, shrinkage-reducing admixture; and 1.5, a dosage of 1.5gal/yd^3. Figures 4.5 through 4.8 show the measurements from the autogenous shrinkage, free drying shrinkage, and the restrained ring shrinkage strain and strain rate of these mixes.

As seen in Figures 4.5 and 4.6, both autogenous shrinkage and drying shrinkage of Mix 6 decreased with the dosage of SRA used.

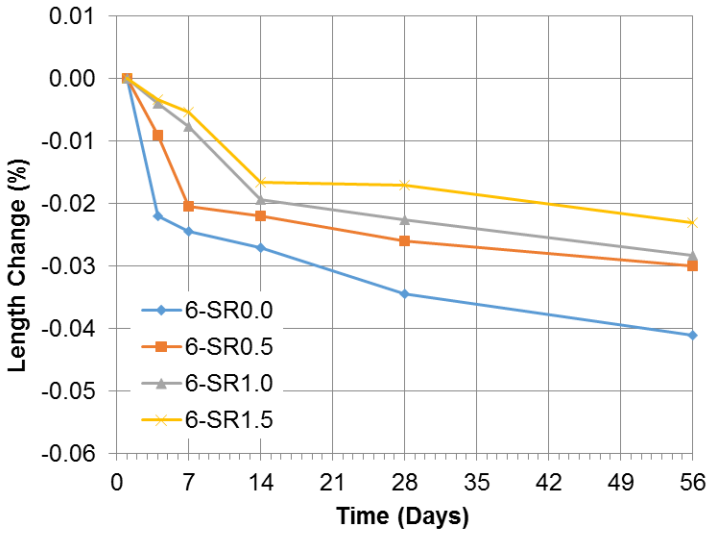

Figure 4.5. Autogenous shrinkage of Mix 6 with different SRA dosages

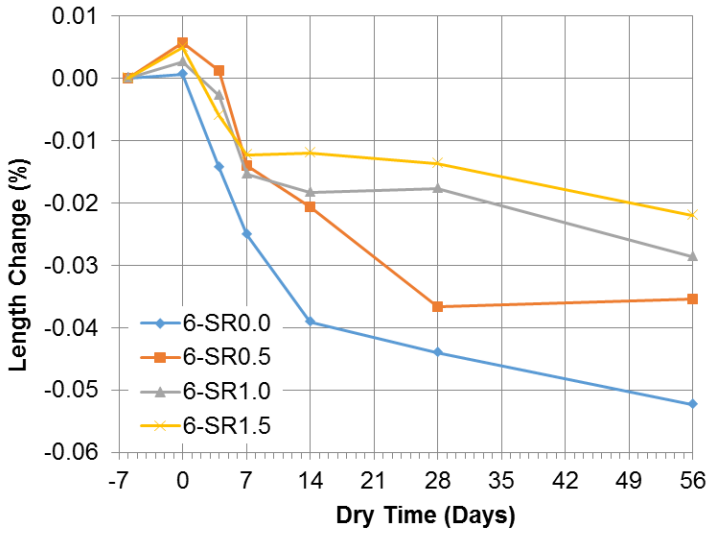

Figure 4.6. Free drying shrinkage of Mix 6 with different SRA dosages

Unlike the addition of SCA, specimens with SRA showed no expansion during the autogenous shrinkage tests when they were sealed. In the free drying shrinkage tests during the moisture curing period (-7 to 0 days), concrete mixes with SRA expanded noticeably more than the mix without SRA (6-SR0.0) when exposed to approximately 100% RH. However, the expansion values were much lower (< 0.05%) than those of specimens with SCA (> 0.10%).

Figures 4.7 and 4.8 show that SRA addition significantly reduced the strain of the steel ring used in the restrained drying shrinkage tests.

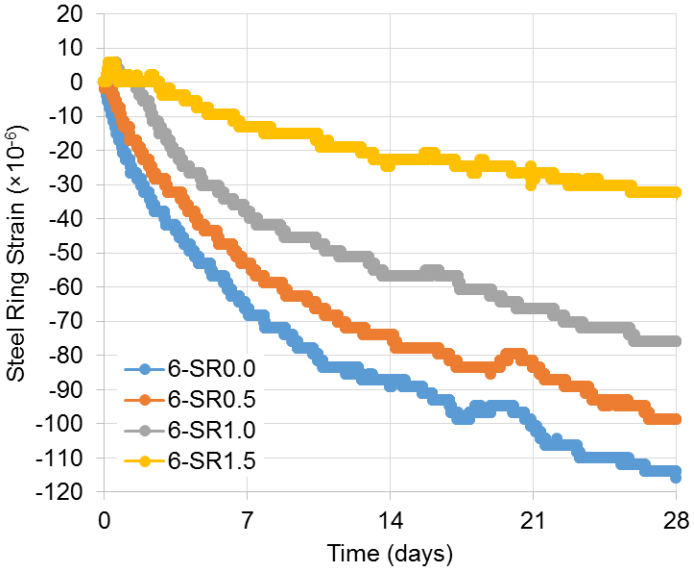

Figure 4.7. Mix 6 restrained ring shrinkages with different SRA dosages

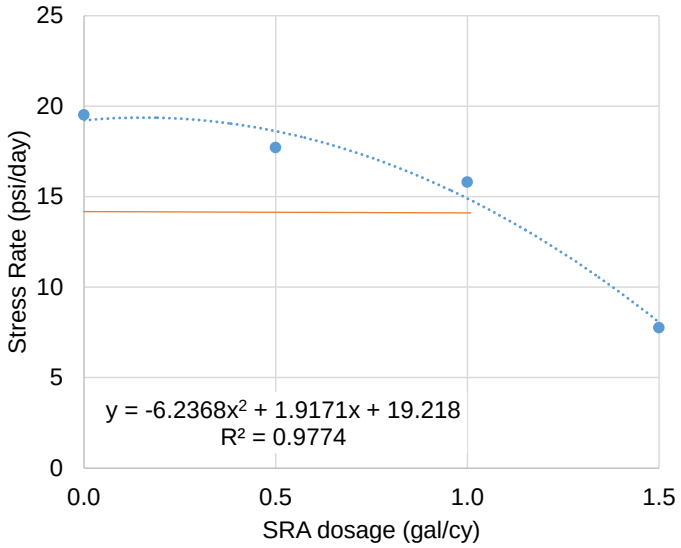

Figure 4.8. Mix 6 stress rates with different SRA dosages

At 28 days, the shrinkage strain was 115×10^{-6} for the mix without SRA, 75×10^{-6} for the mix with 1.0 gal/yd^3 SRA, and only 32×10^{-6} for the mix with 1.5 gal/yd^3 SRA. At 28 days, no mix had a measured strain of zero, indicating that no cracking occurred in the specimens.

The stress rates of Mix 6 with various SRA dosages at t_r = 28 days were plotted in Figure 4.8. As seen in the figure, Mixes 6-SR1.0 and 6-SR1.5 had a stress rate lower than 15 psi/day and therefore they can be considered as low shrinkage crack potential mixes. Compared with the use of SCA, use of SRA appeared to provide more effective shrinkage reduction and cracking prevention since considerable change could be made merely by adding a small amount of SRA.

Considering that SRA might have some negative effects on other concrete properties, such as strength, the dosage of 1.0 gal/yd^3 (or Mix 6-SR1.0) was selected for further research in the laboratory and field.

4.1.3 Mix 8: Modified with Reduction of Cementitious Materials

In order to investigate the effect of cementitious material or binder content on concrete shrinkage, the cementitious material or binder content of the original Mix 8 was reduced from 100% to 85% in increments of 5% (by weight). Table 4.1 provides the proportions of the new, modified mixes, where 8 denotes Mix 8; CM, cementitious materials; and 100 to 85% binder (by weight of the original Mix 8). The w/b and limestone-to-sand ratios remained the same for all the mixes listed. It can be noted from Table 4.1 that in order to maintain good workability and sufficient strength, the percentage content of cement and FA in the mixes increased approximately 10 and 3 lb/yd^3, respectively, for each 5% binder reduction. As a result, significant binder reduction came from the GGBFS content.

Table 4.1. Proportions of Mix 8 modified with different amount of cementitious material reduction

Mix ID	Cement	FA	GGBFS lb/yd^3	Limestone	Sand	Water	Wt. % of binder			Binder Reduction
							Cement	FA	GGBFS	Wt. %
8-CM100 (original)	367.8	133.8	167.2	1430.4	1404.6	267.5	55.0	20.0	25.0	0.0
8-CM95	376.0	136.7	128.2	1462.0	1435.6	256.3	58.7	21.3	20.0	4.2
8-CM90	386.8	140.7	75.7	1504.0	1476.8	241.2	64.1	23.3	12.5	9.8
8-CM85	396.5	144.2	28.5	1541.7	1513.9	227.6	69.7	25.3	5.0	14.9

Figures 4.9 to 4.11 show the shrinkage tests results for Mix 8 with different amounts of cementitious material reduction (100%, 95%, 90%, and 85% of the cementitious materials of the original Mix 8).

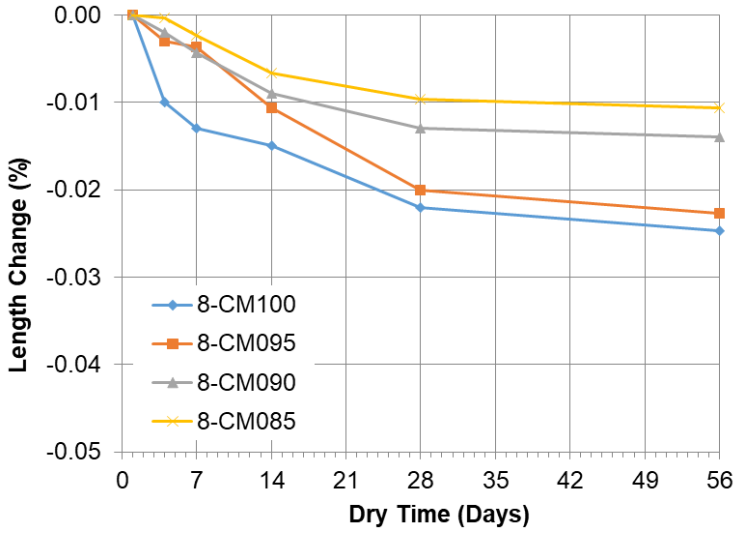

Figure 4.9. Autogenous shrinkage of Mix 8 modified with different percent cementitious material reduction

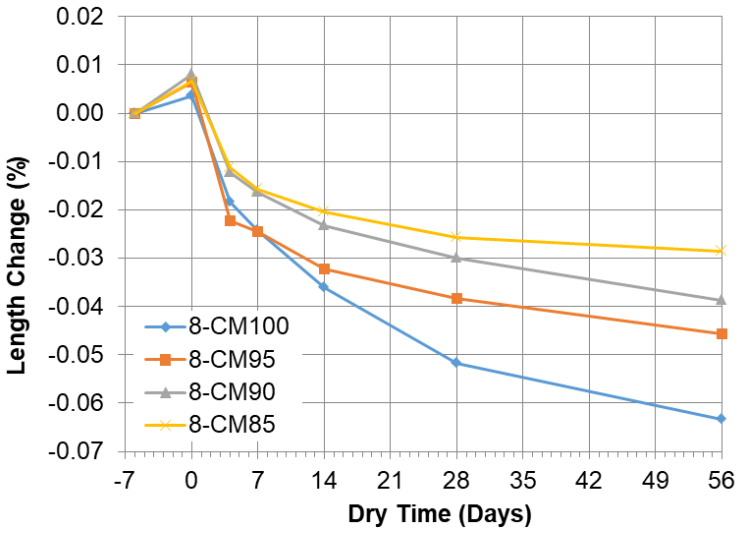

Figure 4.10. Free drying shrinkage of Mix 8 modified with different percent cementitious material reduction

It can be seen from Figures 4.9 and 4.10 that both autogenous shrinkage and free drying shrinkage of Mix 8 declined with increased cementitious material reductions. The autogenous shrinkage reached 0.025% (or 250×10^{-6}) for the original Mix 8 (8-CM100, no reduction), while it was only 0.011% (or 110×10^{-6}) for the mix with a 15% cementitious material reduction (8-CM85) at 56 days. The free drying shrinkage was 0.063% (or 630×10^{-6}) for the original Mix 8

(8-CM100, no reduction), while it was only 0.029% (or 290×10^{-6}) for the mix with 15% cementitious material reduction (8-CM85) at 56 days.

Figure 4.11 shows that the effect of binder content reduction on the strain of the steel ring of Mix 8 in the restrained drying shrinkage tests.

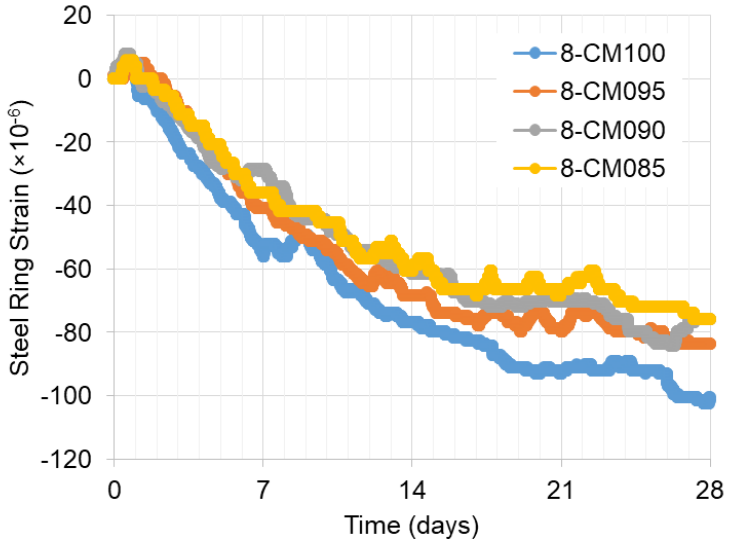

Figure 4.11. Restrained ring shrinkage of Mix 8 with different percent cementitious material reduction

At 28 days, the shrinkage strain was 100×10^{-6} for the original Mix 8 (8-CM100, no binder reduction) and 75×10^{-6} for the mix with 15% binder content reduction (8-CM85). Compared with the effect caused by SRA on Mix 6, the drop in shrinkage strain due to binder content reduction of Mix 8 appeared very limited. However, at 28 days, Figure 4.11 shows that no mix had a sudden strain drop, indicating that no cracking occurred in any of the specimens.

Figure 4.12 presents the effect of binder content reduction on the stress rate of Mix 8.

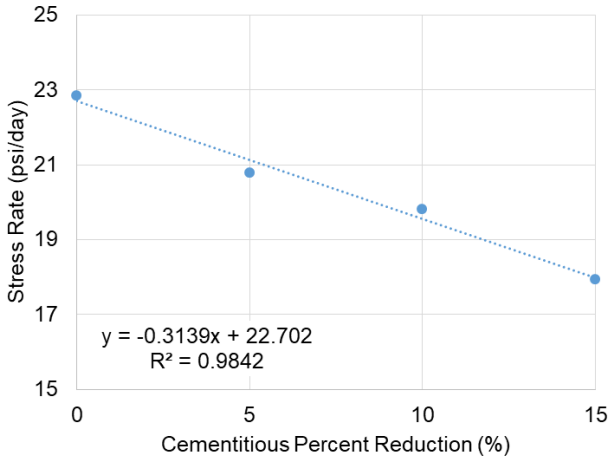

Figure 4.12. Stress rates of Mix 8 with different percent cementitious material reduction

The figure shows that the stress rate decreased linearly with an increasing amount of binder content. Based on this linear regression equation, the concrete stress rate would reduce to 15 psi/day (a criterion for a low shrinkage cracking potential) only when it reached the point of 25% binder reduction.

To avoid a significant decrease in concrete strength due to excessive reduction in cementitious materials, a 10% reduction in cementitious material for Mix 8 was proposed for the field investigation of this project. The cracking potential classification of Mix 8 with a 10% reduction of cementitious materials (8-CM90) is "moderate-low" according to ASTM C1581.

4.1.4 Mix 2 with Internal Curing Agent (LWFA)

Mix 2 was modified by using LWFA to replace 34% of the fine aggregate in the original mix. The free drying, autogenous, and restrained ring shrinkage test results for both original and modified Mix 2 are shown in Figures 4.13 through 4.15. The designation of 2-34% LWFA indicates Mix 2 with 34% LWFA replacement of fine aggregate.

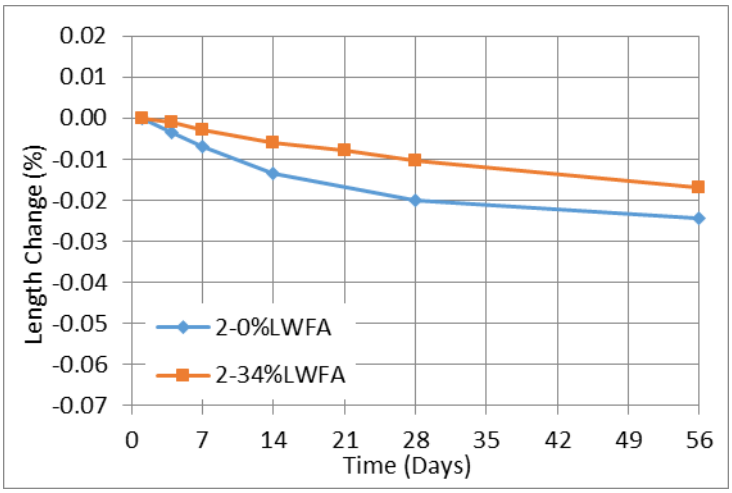

Figure 4.13. Mix 2 autogenous shrinkages with different LWFA replacement percent

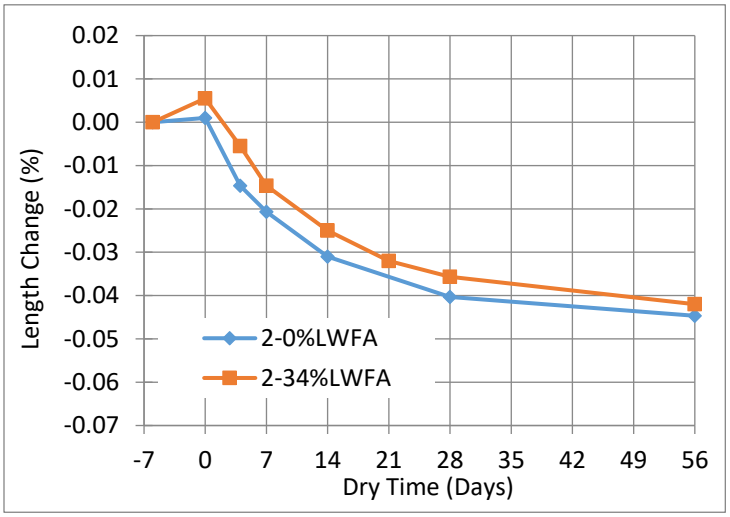

Figure 4.14. Mix 2 free drying shrinkages with different LWFA replacement percent

The figures show that using LWFA as an internal curing admixture reduced all measured shrinkage values because the water in the LWFA was released gradually as a supplier to the drying concrete. However, the reductions in the free drying and restrained ring shrinkage were not significant.

Although no cracking was observed, Figure 4.15 shows that the stress rates obtained from ring tests of both Mix 2-0%LWFA and Mix 2-34%LWFA were about the same (approximately 31.00 psi/day). Both of them were considered to have a moderate-low cracking potential according to ASTM C 1581. As mentioned previously, Type IP cement was used for Mix 2 in Phase I, while Type I cement was used in Phase II, which may be responsible for the increased cracking potential of the mix.

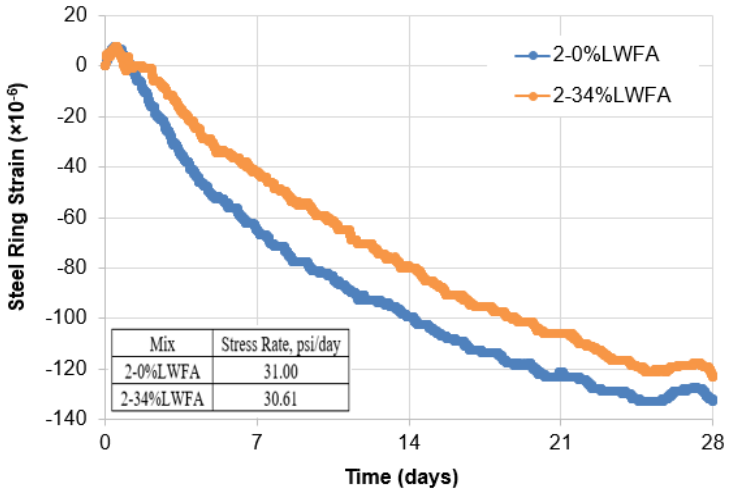

Figure 4.15. Mix 2 restrained ring shrinkages with different LWFA replacement percent

4.1.5 Comparison of Shrinkage Behavior of the Mixes Studied

Figure 4.16 shows the comparison of autogenous and free dry shrinkage of all mixes studied at 56 days.

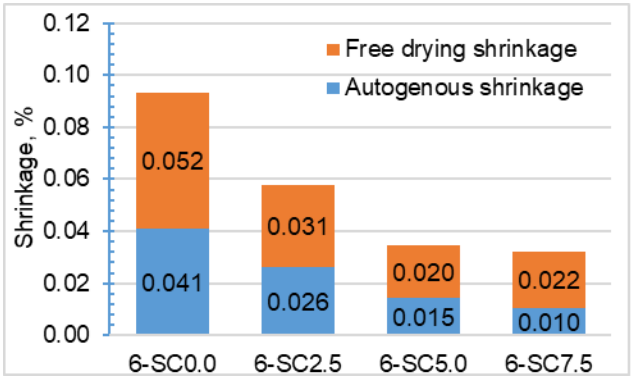

(a) Mix 6 with different amounts of SCA

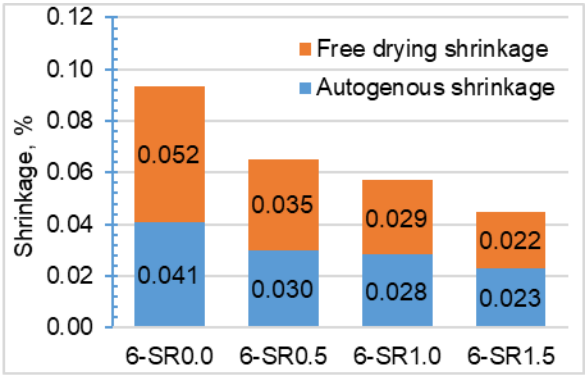

(b) Mix 6 with different amounts of SRA

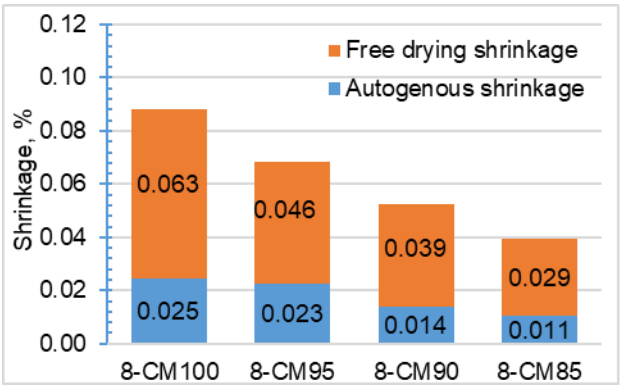

(c) Mix 8 with binder content reduction

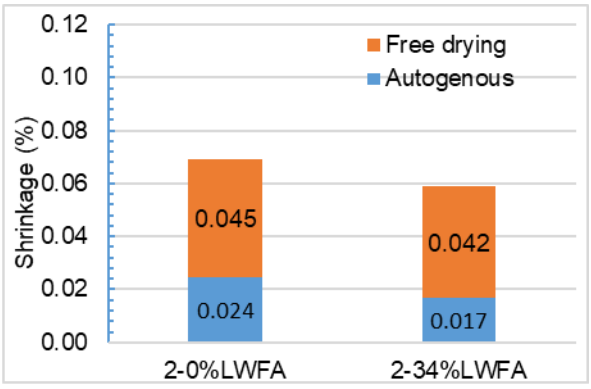

(d) Mix 2 with and without IC (LWFA)

Figure 4.16. Total shrinkage of mixes studied at 56 days

It can be seen from the figure that the original Mix 6 (Class O mix), which had a binder (pure cement) content of 825.4 lb/yd^3 and w/b ratio of 0.33, had an autogenous shrinkage value of 0.041% (410 microstrain) and a free drying shrinkage value over 0.051% (510 microstrain), given a total shrinkage value over 0.092% (920 microstrain). As mentioned previously, additions of SCA and SRA reduced both autogenous and free drying shrinkage. With the dosages used, shrinkage reduction provided by SCA was more effective than that provided by SRA. It is interesting to note that SRA seemed to reduce free drying shrinkage more effectively than autogenous shrinkage.

The original Mix 8 (HPC-O-C20-S25), with a binder content of 668.9 lb/yd^3 and w/b ratio of 0.40, had an autogenous shrinkage value of 0.025% (250 microstrain) and a free drying shrinkage value over 0.063% (630 microstrain), given a total shrinkage value over 0.088% (880 microstrain), similar to that of Mix 6 (900 microstrain). The high free drying shrinkage might be attributed to the high w/b ratio. The binder content reduction noticeably reduced both autogenous and free drying shrinkage.

The original Mix 2 (HPC-O-C20) had a binder content of 659.9 lb/yd^3 and w/b ratio of 0.40, and compared with the original Mix 8, there was a lower volume of binder. The test results showed that the original Mix 2 had an autogenous shrinkage value similar to the original Mix 8 (0.025%, or 250 microstrain), but much lower free drying shrinkage value (0.045% or 450 microstrain) than that of the original Mix 8 (0.063%, or 630 microstrain). Thus, the total shrinkage value of the original Mix 2 was 0.070% (700 microstrain), much lower than that of Mix 6 (900 microstrain), and Mix 8 (880 microstrain). The high free drying shrinkage might be attributed to the high w/b ratio. Use of 34% LWFA as an IC agent significantly decreased autogenous shrinkage, but only slightly reduced free drying shrinkage. Further study may be necessary to investigate the effectiveness of LWFA in shrinkage reduction of Iowa HPC mixes.

4.1.6 Proposed Mixes for Further Study

As discussed above, the six mixes listed in Table 4.2 were selected for an extended study to evaluate their fresh concrete properties, mechanical properties, and durability. The tests and results are presented in the sections that follow.

Table 4.2. Mix proportions of concrete mixes used in an extended study

Mix	ID	Cement lb/yd^3	FA lb/yd^3	GGBFS lb/yd^3	Limestone lb/yd^3	Sand lb/yd^3	LWFA lb/yd^3	Water lb/yd^3	SR gal/yd^3	w/b ratio
6	6-SR0.0	825.4	-	-	1386.3	1365.6	-	269.9	-	0.33
6M	6-SR1.0	825.4	-	-	1386.3	1365.6	-	269.9	1.0	
8	8-CM100	367.9	133.8	167.2	1430.8	1404.9	-	267.6	-	0.40
8M	8-CM90	342.1	124.4	155.5	1478.1	1451.4	-	248.8	-	0.40
2	2-0%LWFA	527.9	132.0	-	1458.0	1431.8	-	263.9	-	0.40
2M	2-34%LWFA	527.9	132.0	-	1458.0	944.0	325.0	263.9	-	0.40

M = modified mix, SR = shrinkage reducer, CM = % of the original binder content, LWFA = lightweight fine aggregate

4.2 Fresh Concrete Properties

The fresh concrete properties, such as slump, unit weight, and air content, of all the mixes were evaluated. The test results are presented in Table 4.3 and Figures 4.17 through 4.19.

Table 4.3. Fresh concrete properties

Property	Mix 6	Mix 6-SR 1.25	Mix 8	Mix 8-CM 90	Mix 2	Mix 2-LWFA
Slump, in.	1.75	0.75	8.50	7.00	3.20	1.75
Unit weight, pcf	138.8	146.4	138.6	140.2	143.0	135.6
Air content, %	9.5	5.5	9.0	8.0	6.5	7.5

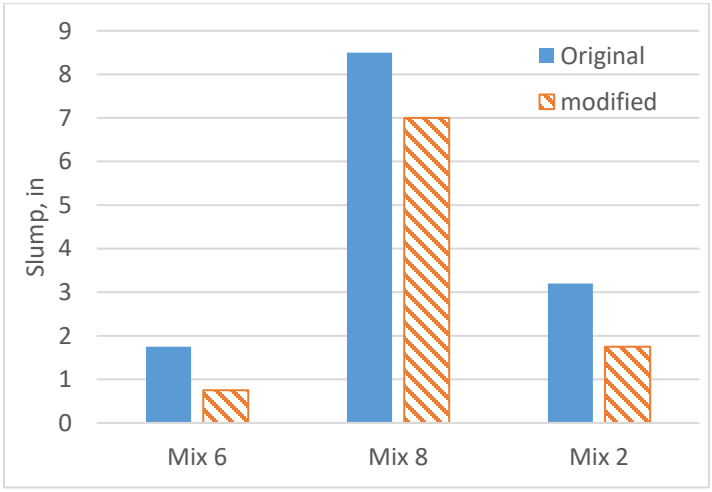

Figure 4.17. Slump of original and modified mixes

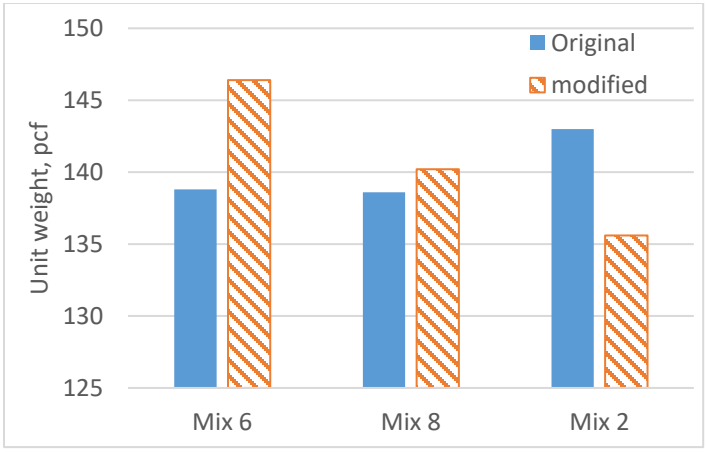

Figure 4.18. Unit weight of original and modified mixes

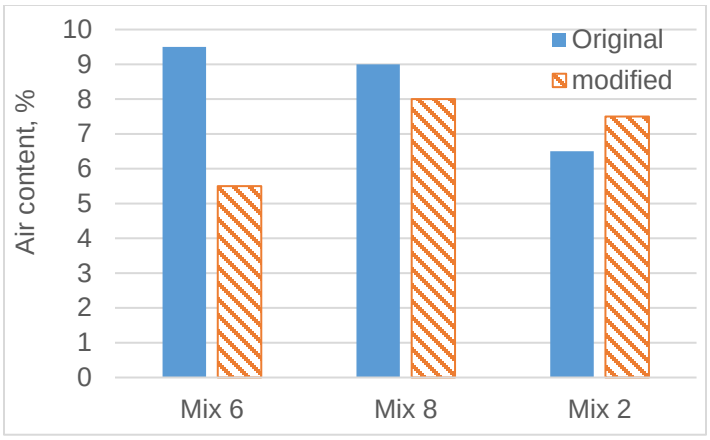

Figure 4.19. Air content of original and modified mixes

As seen from the table and figures, the addition of SRA decreased slump and air content and increased unit weight of Mix 6. It is possible that the decreased air content was related to the decreased slump of the concrete. The deduction of 10% cementitious materials in Mix 8 resulted in a lower slump and a slightly lower air content, but it had little or no effect on unit weight. Use of 34% (by volume) LWFA as an IC agent to replace sand reduced both the slump and unit weight of Mix 2, and the measured air content of Mix 2-34% LWFA was higher, probably due to the test method (pressure method).

4.3 Mechanical Properties

The mechanical properties, such as compressive strength, elastic modulus, splitting tensile strength and creep, were measured for all six mixes. All measurements were performed on 4×8 in. cylinders.

4.3.1 Compressive Strength, Elastic Modulus, and Splitting Tensile Strength

Figures 4.20 to 4.22 show the compressive strength, elastic modulus, and splitting tensile strength of all six mixes studied. As seen in Figure 4.20, addition of 1.25 gal/yd^3 SRA slightly increased strength and elastic modulus of Mix 6. Generally, it is believed that SRA does not modify the mineralogical composition of cement pastes, and it does not change the degree of cement hydration (Bentz 2006).

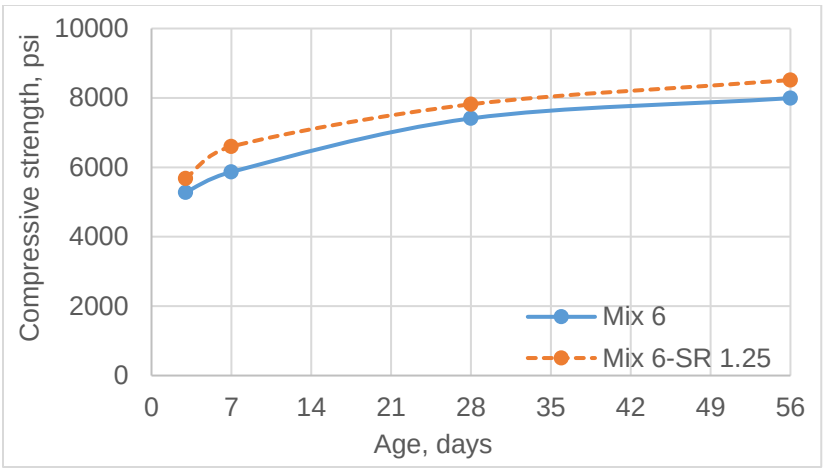

(a) Compressive strength

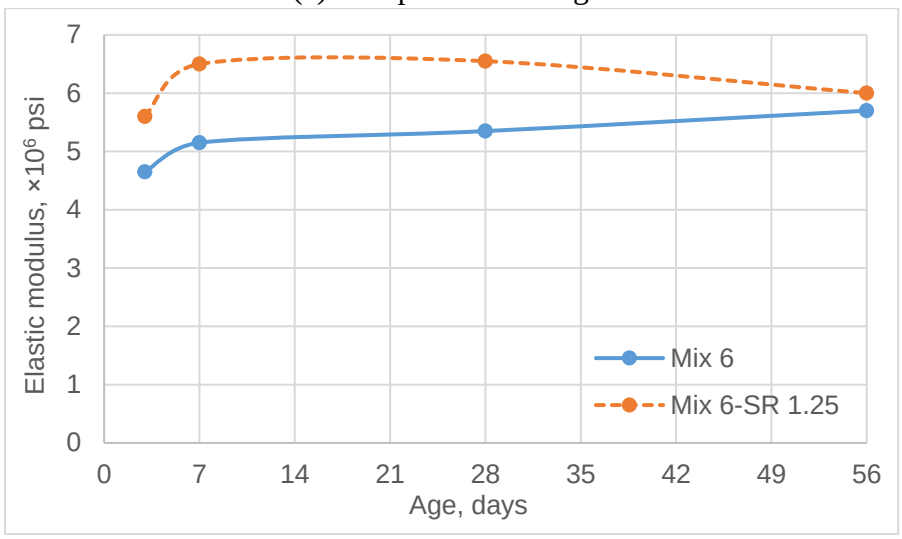

(b) Static elastic modulus

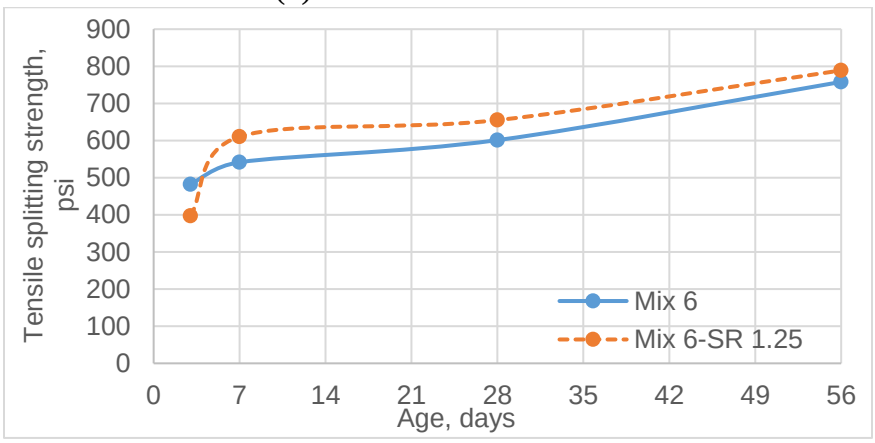

(c) Tensile splitting strength

Figure 4.20. Mechanical properties of Mix 6 and Mix 6-SR1.25

Figure 4.21 shows that a 10% reduction (Mix 8-CM90) in cementitious content of the original Mix 8 (Mix 8-CM100) resulted in a 9% reduction in the concrete compressive strength. It did not

reduce the concrete elastic modulus before the age of 14 days, but did decrease the concrete elastic modulus after 14 days. The tensile splitting strength of Mix 8-CM90 declined more significantly (600 psi vs. 713 psi at the age of 56 days, about 18% reduction).

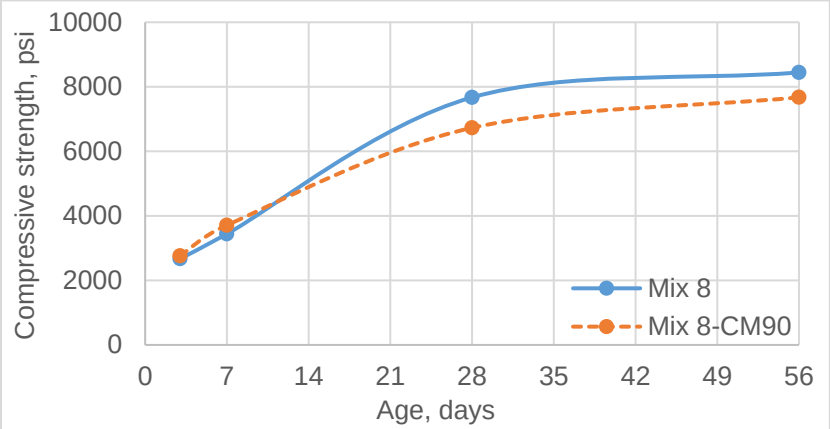

(a) Compressive strength

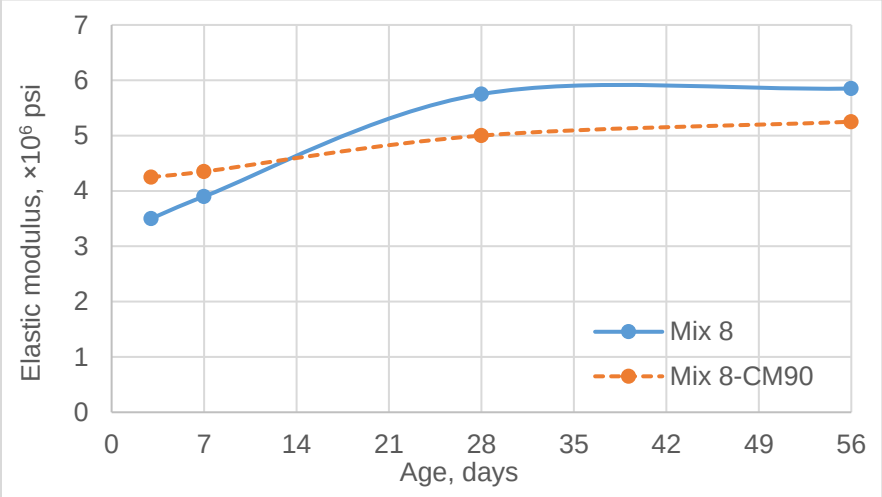

(b) Static elastic modulus

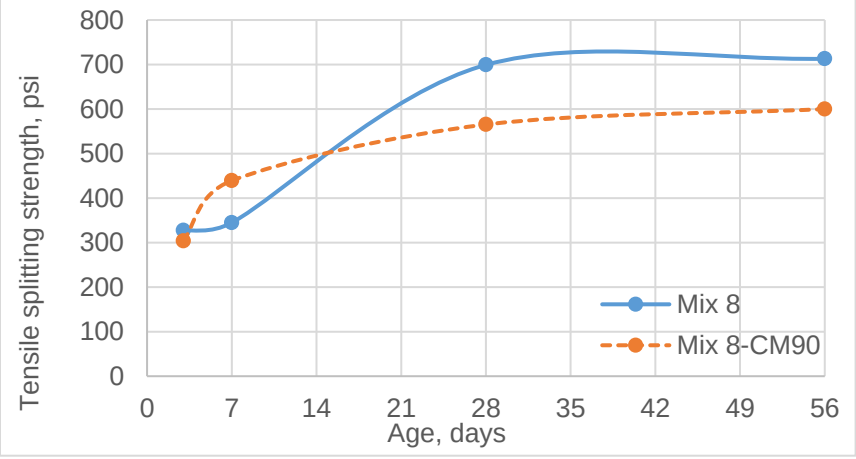

(c) Tensile splitting strength

Figure 4.21. Mechanical properties of Mix 8 and Mix 8-CM90

These reductions in concrete mechanical properties might be related to the paste content of Mix 8-CM90.

Figure 4.22 reveals that use of 34% LWFA as an IC agent to replace fine aggregate in Mix 2 increased both the concrete compressive strength and splitting tensile strength by 10% and 9%, respectively. Such strength improvement is mainly attributed to the additional water supplied by LWFA throughout the bulk concrete specimens, which enhanced cement hydration. However, due to low elastic modulus of LWFA, Mix 2-34% LWFA had approximately 10% lower elastic modulus than Mix 2-0% LWFA.

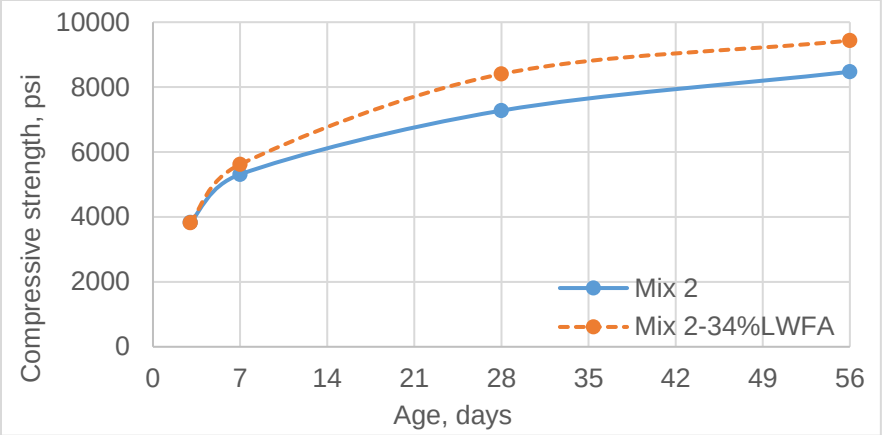

(a) Compressive strength

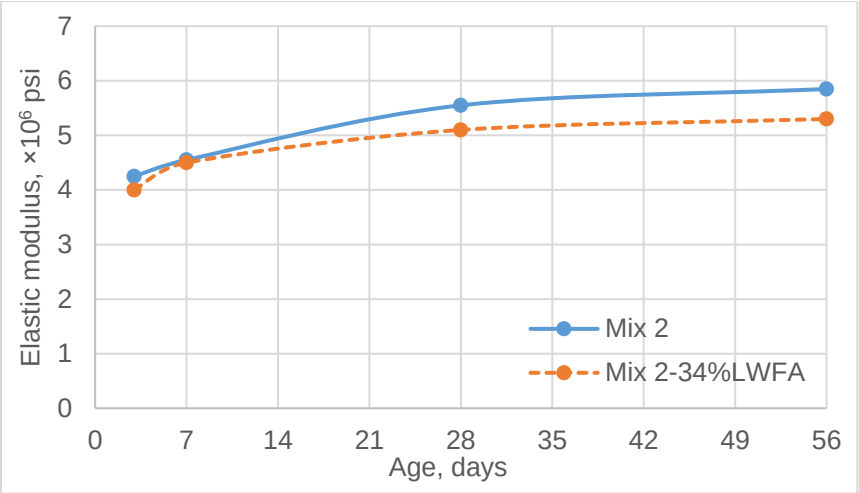

(b) Static elastic modulus

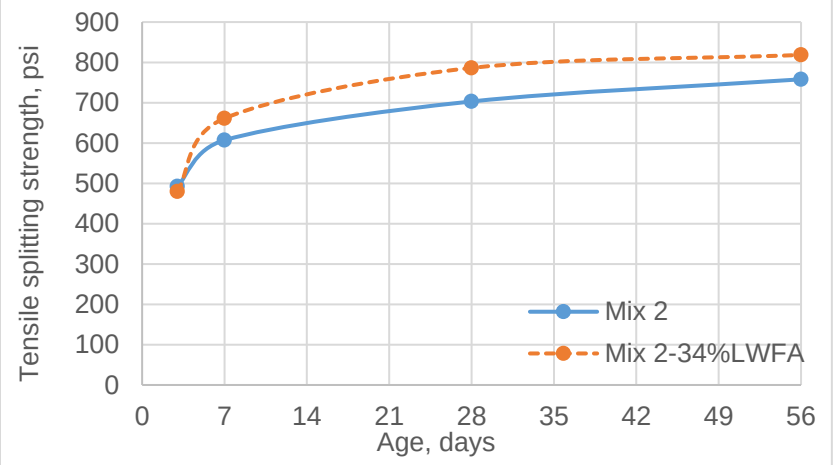

(c) Tensile splitting strength

Figure 4.22. Mechanical properties of Mix 2-0% LWFA and Mix 2-34% LWFA

4.3.2 Creep

According to ASTM C512, the total strain of a concrete specimen under a creep test could be expressed by Equation 2:

$$\varepsilon = \left(\frac{1}{E}\right) + F(K)\ln(t+1) \quad (2)$$

Where, Ɛ is total strain per unit stress in psi-1; E is instantaneous elastic modulus in psi; F (K) is creep rate, which can be determined by the slope of a straight line representing the creep curve on the semi-log plot (Ɛ vs. ln(t+1)); and t is time after loading in days.

Figures 4.23 through 4.25 show the total strain per unit stress from the creep tests of all six mixes studied and Table 4.4 lists the instantaneous elastic modulus and creep rate for all mixes.

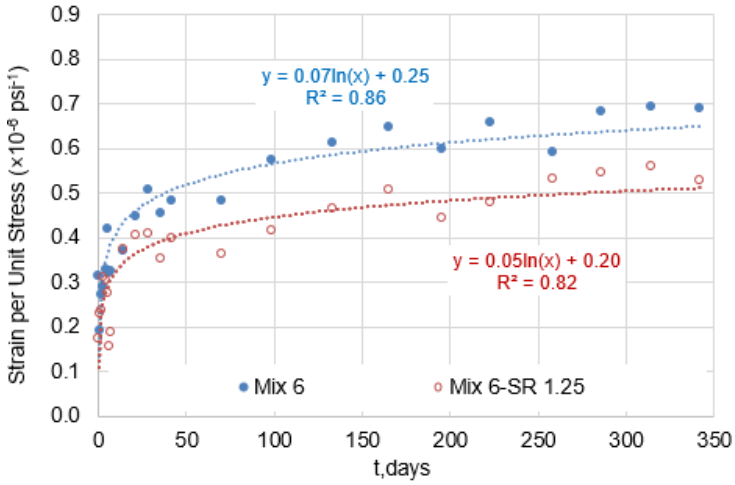

(a) Total strain vs t

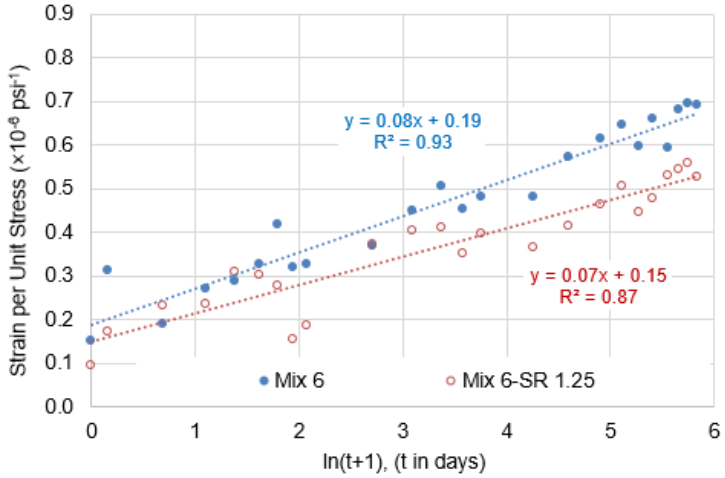

(b) Total strain vs ln(t+1)

Figure 4.23. Creep of Mix 6 and Mix 6-SR 1.25

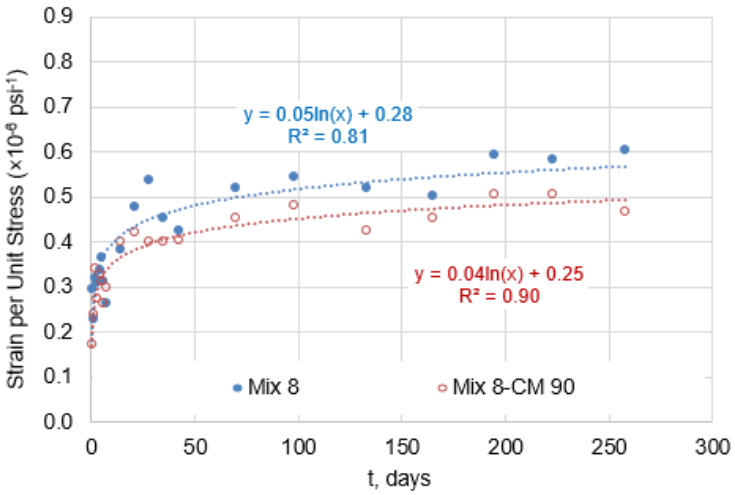

(a) Total strain vs t

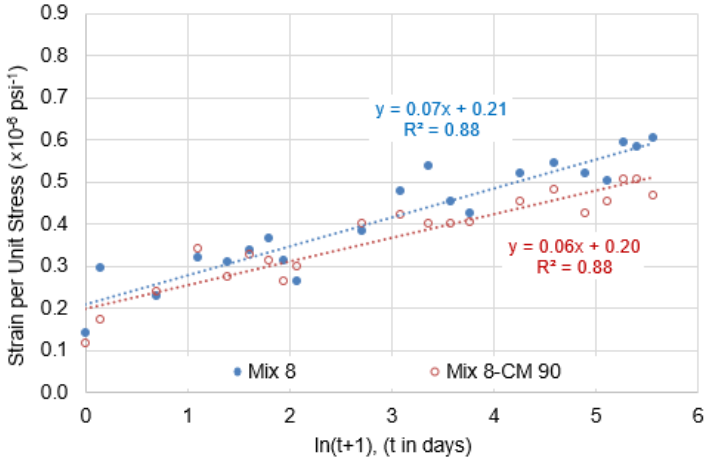

(b) Total strain vs ln (t+1)

Figure 4.24. Creep of Mix 8 and Mix 8-CM 90

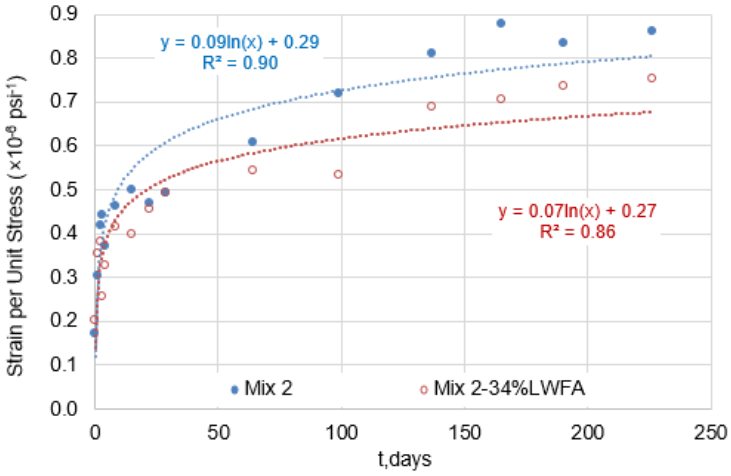

(a) Total strain vs t

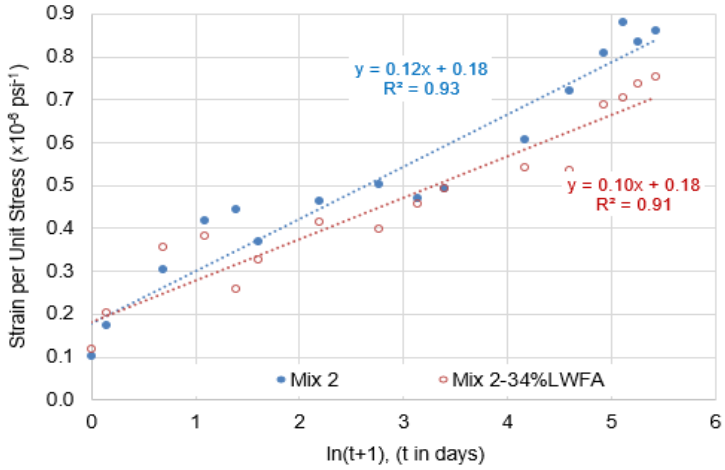

(b) Total strain vs ln (t+1)

Figure 4.25. Creep of Mix 2 and Mix 2-34%LWFA

Table 4.4. Instantaneous elastic modulus and creep rate for all mixes

Mix	Instantaneous Elastic Modulus E (psi)	Creep rate, F(K)
Mix 6	5335063	8.296E-08
Mix 6-SR 1.25	6731294	6.501E-08
Mix 8	4746254	6.875E-08
Mix 8-CM 90	5038317	5.618E-08
Mix 2	5561982	1.213 E-07
Mix 2-34%LWFA	5452105	0.9646E-07

The trends of all the above strain curves show high statistical confidence. It is interesting to see that the total strains per unit stress and creep rates of all modified mixes (Mix 6-SR1.25, Mix 8-CM90, and Mix 2-34%LWFA) were lower than those of original mixes (Mix 6, Mix 8-CM100, and Mix 2-0%LWFA). The addition of SR in Mix 6 increased instantaneous elastic modulus by 26% but decreased creep rate by 22%. The 10% cementitious material reduction in Mix 8

increased instantaneous elastic modulus by 6% but decreased creep rate by 18%. The 34% fine aggregate replacement by LWFA in Mix 2 reduced instantaneous elastic modulus very slightly and decreased creep rate by 20%.

4.4 Surface Resistivity and F-T Durability

4.4.1 Surface Resistivity

Figure 4.26 shows the surface resistivity test results for all six mixes studied.

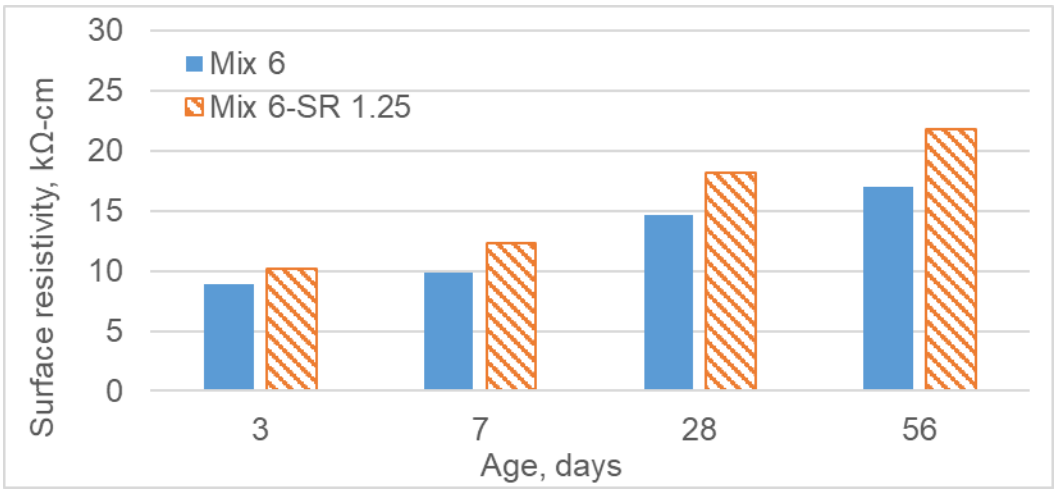

(a) Mix 6 and Mix 6-SR1.25

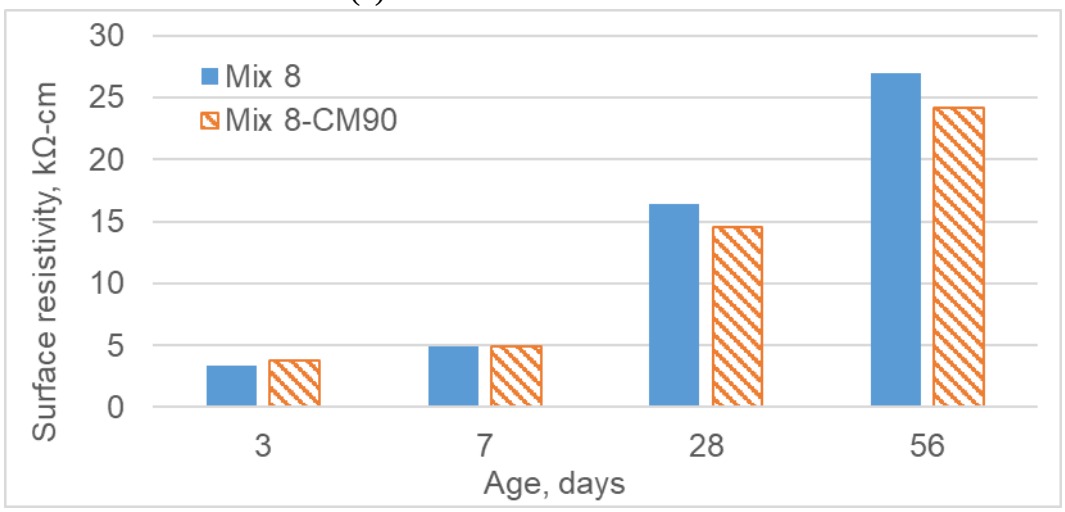

(b) Mix 8 and Mix 8-CM90

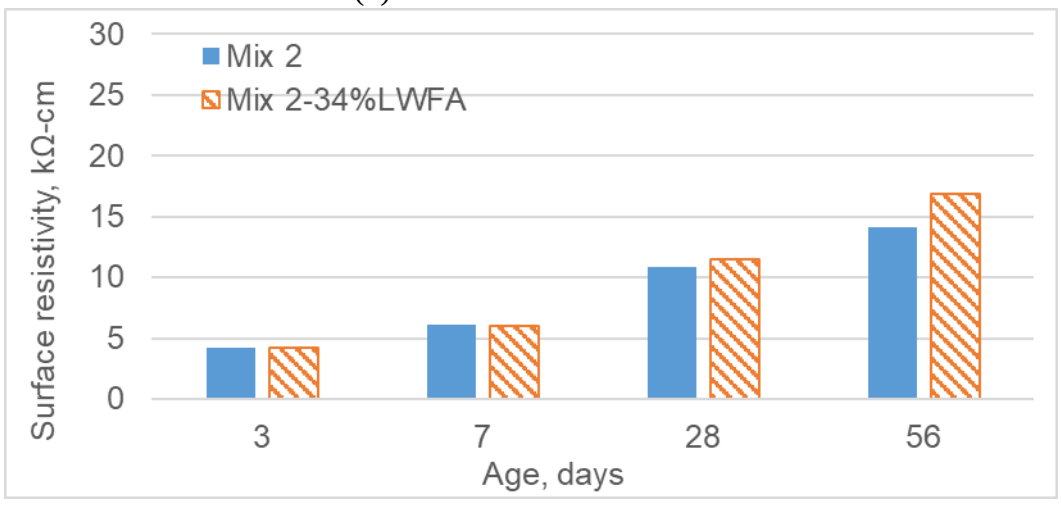

(c) Mix 2 and Mix 2-34%LWFA

Figure 4.26. Surface resistivity of selected concrete mixes

The AASHTO 95 penetrability classification used in Table 4.5 suggests that with curing time the concrete surface resistivity of all the mixes increased or the permeability of all the mixes decreased.

Table 4.5. Penetrability classification

Penetrability	AASHTO 95 (kΩ-cm)
High	<12
Moderate	12-21
Low	21-37
Very low	37-254
Negligible	>254

The addition of 1.25 gal/yd^3 SRA increased surface resistivity of Mix 6. Mix 8 and Mix 8-CM90 had much higher surface resistivity than the other mixes. The 10% reduction of cementitious materials in Mix 8 did not affect surface resistivity of the concrete at 3 and 7 days but decreased surface resistivity or increased permeability of Mix 8 at 28 and 56 days. This is probably related to the slag (GGBSF) used in the mixes, which is effective in refining concrete pore structure. The 34% LWFA replacement for fine sand in Mix 2 did not affect the surface resistivity of the concrete very much before 28 days but increased the surface resistivity or reduced permeability of Mix 2 noticeably at 56 days. This could be due to the slow FA hydration.

4.4.2 F-T Durability

According to ASTM C666, the relative dynamic modulus of elasticity of a sample subjected to an F-T durability test can be calculated as follows:

$$P_c = \left(\frac{{n_1}^2}{n^2}\right) \times 100 \quad (3)$$

Pc (%) is the relative dynamic modulus of elasticity (RDME) after c cycles of freezing and thawing, n is the fundamental transverse frequency at 0 cycles of freezing and thawing, and n_1 is the fundamental transverse frequency after c cycles of freezing and thawing.

The durability factor (DF) could be obtained by the following:

$$DF = PN/M \quad (4)$$

Where, DF is the durability factor of the test specimen; P is relative dynamic modulus of elasticity at N cycles in percent; N is number of cycles at which P reaches the specified minimum value for discontinuing the test or the specified number of cycles at which the exposure is to be terminated, whichever is less; and M is the specified number of cycles at which the exposure is to be terminated. If the minimum RDME is greater than 50%, DF and RDME are the same.

The F-T test results of all six mixes studied are shown in Figure 4.27, and the DF values of the mixes at 300 F-T cycles are listed in Table 4.6.

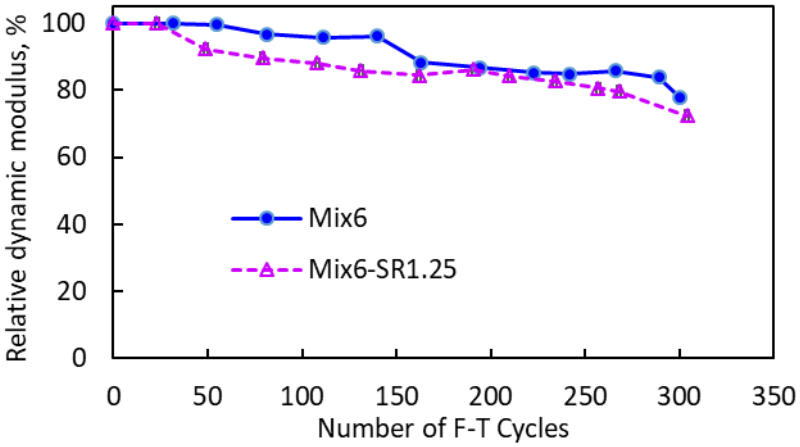

(a) Mix 6 and Mix 6-SR1.25

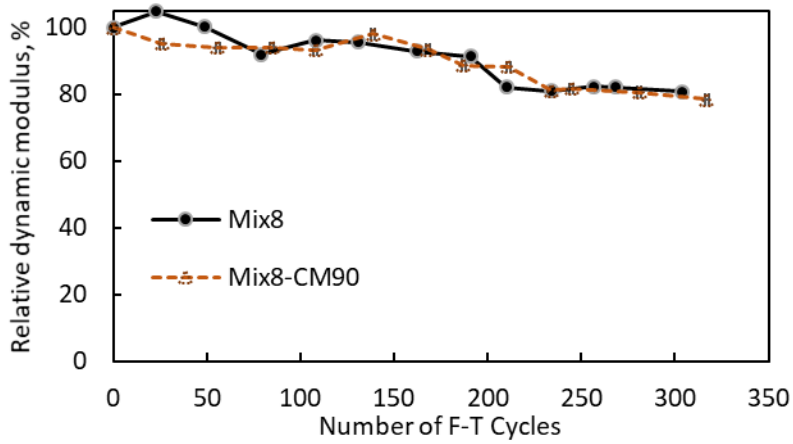

(b) Mix 8 and Mix 8-CM90

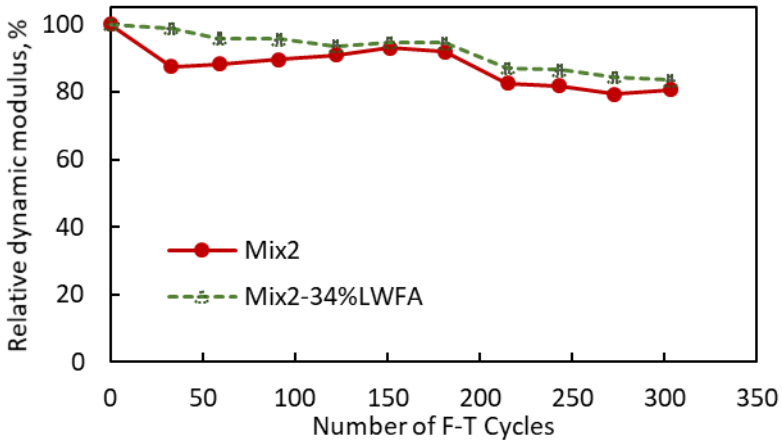

(c) Mix 2 and Mix 2-34%LWFA

Figure 4.27. Durability factor of selected concrete mixes

Table 4.6. Durability factors of selected mixes

Mix	Durability factor (%) @ 300 F-T cycles
Mix 6	79.0
Mix 6-SR1.25	73.0
Mix 8	81.0
Mix 8-CM90	80.0
Mix 2	81.0
Mix 2-34%LWFA	84.0

It can be seen from Figure 4.27 that when compared with the corresponding original mixes, Mix 6-1.0SR reduced F-T durability slightly. Mix 8-CM90 had F-T durability comparable to Mix 8 (or Mix 8-CM100). Mix 2-34% LWFA slightly improved the concrete F-T durability, probably due to enhanced cement hydration. The DF values in Table 4.6 show the same trend as described by Figure 4.27, although the differences in the DF values between the original and modified mixes were not significant.

Figure 4.28 shows the concrete beam samples after 300 F-T cycles.

(a) Mix 6

(b) Mix 6-SR1.25

(c) Mix 8

(d) Mix 8-CM90

(e) Mix 2

(f) Mix 2-34%LWFA

Figure 4.28. Samples after F-T cycles

Samples of the modified Mix 6 (Mix 6-SR1.25) and modified Mix 8 (Mix 8-CM90) displayed more deterioration than their original mixes. However, modified Mix 2 (Mix 2-34%LWFA) showed less damage. The literature has shown conflicting results on the effect of SRA on concrete F-T resistance. In a Virginia DOT report (Nair et al. 2016), it was stated that both the SRA and control mixtures showed excellent freeze-thaw durability, while Bae et al. (2002)

pointed out that some SRA might reduce concrete F-T resistance because it impairs the development of a proper air system in the concrete.

5. FIELD INVESTIGATION

The project's field investigation was conducted on the US 20 over I-35 dual bridge, where Mix 6 and Mix 6-1.25SRA as well as Mix 8 and Mix 8-90CM were placed side by side for the bridge overlays. Quality control properties, construction conditions, and procedures were recorded. Sensors (strain gages, temperature and moisture sensors) were installed in the concrete overlays to monitor the strain, temperature, and moisture of the concretes for approximately one year. Mechanical properties of field concrete samples were tested and the results compared with those of laboratory-cast concrete samples. Visual examinations were conducted on the surface of the concretes, and data on the shrinkage cracks (time, size, and pattern) were recorded regularly. The detailed information on the field investigation is presented as follows.

5.1 Field Preparation

5.1.1 Site and Description

A dual bridge, the US 20 over I-35 bridge, was selected for this shrinkage project. The investigators were allowed to place Mix 6 and Mix 6-1.25SRA as well as Mix 8 and Mix 8-90CM side by side as the new overlays on the bridge. A more accurate comparison of the mix performance could be made since these new overlays were on a structure with similar geometries, restraints, environmental exposure, and perhaps similar traffic loads. The project site was located south of Williams, Iowa. As shown in Figure 5.1, the bridge runs from east to west.

Map data © 2017 Google

Figure 5.1. US 20 over I-35 dual bridge location

As shown in Figure 5.2, each of the dual bridges was 262 ft, 4 in. long and 50 ft wide. There were two construction stages on the bridge: Stage 1 for driving lanes (slower traffic) and Stage 2 for passing lanes (faster traffic).

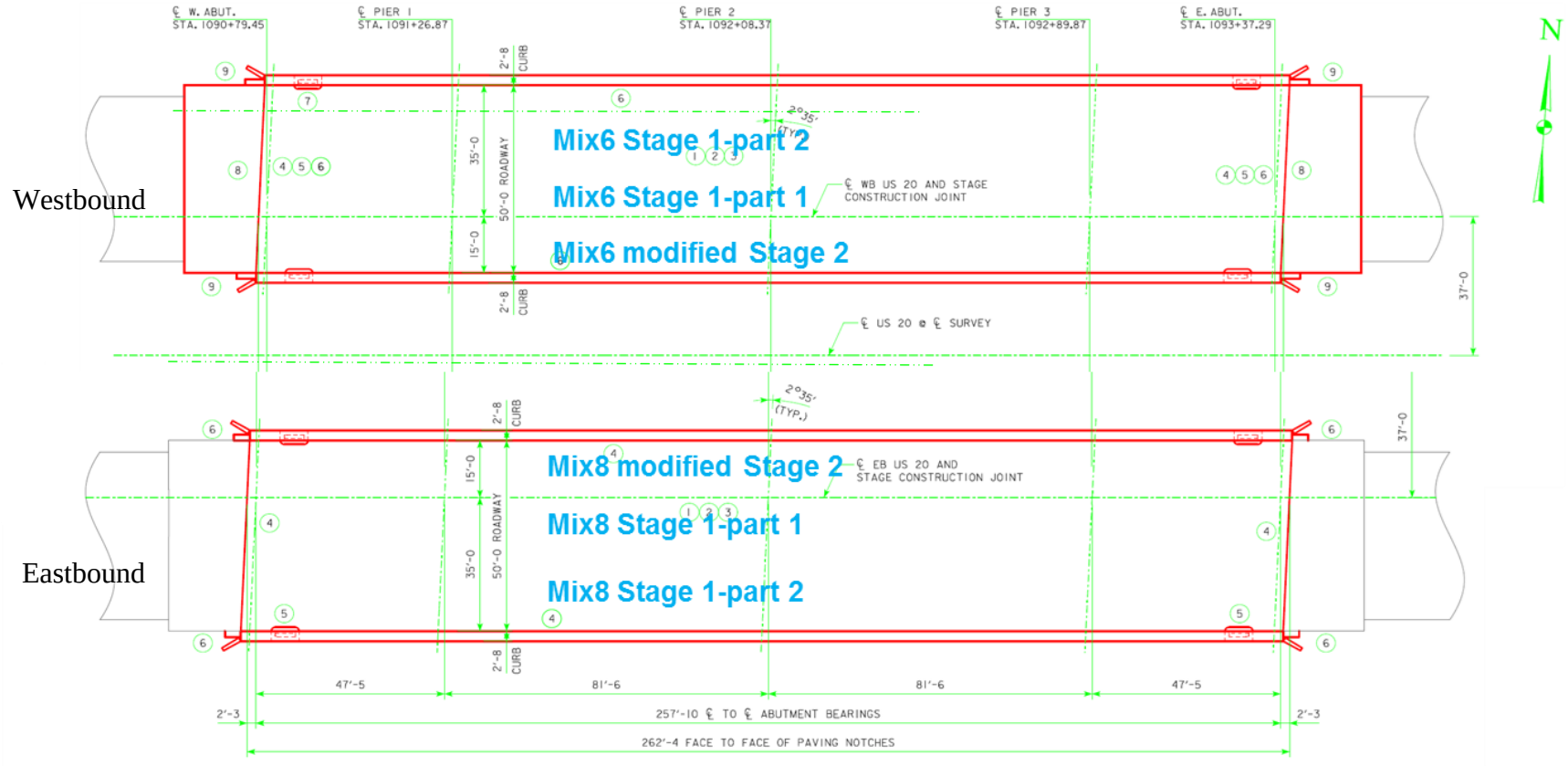

Figure 5.2. US 20 over I-35 overlay sections

Mix 6 (original and modified) was placed on the westbound bridge, and Mix 8 (original and modified) was placed on the eastbound bridge. For both east- and westbound bridges, the original concrete mixes (Mix 6 and Mix 8 or 8-CM100) were placed in the Stage 1 location, while the modified concrete mixes (Mix 6-SR1.25 and Mix 8-CM90) were placed in the Stage 2 location. The new concrete overlays were all 2 in. thick. Table 5.1 shows the construction timeline related to this field study.

Table 5.1. US 20 over I-35 project construction timeline

Date	Activity
7/6/2016	Conducted crack survey (visual inspection) on bridge surfaces (Stage 1) before overlay construction
7/21/2016	Installed sensors on Westbound, Stage 1, part 2 (Mix 6 overlay)
7/22/2016 (Day 0)	Placed Mix 6 concrete overlay on Westbound, Stage 1, part 2
7/27/2016	Installed sensors on Eastbound, Stage 1, part 2 (Mix 8 overlay)
7/28/2016 (Day 6)	Placed Mix 8 concrete overlay on Eastbound, Stage 1, part 2
8/15/2016	Conducted crack survey (wet test) on new overlay of Stage 1 (Mixes 6 and 8)
8/23/2016	Conducted crack survey on bridge surfaces (Stage 2) before overlay construction
8/26/2016	Installed sensors on Westbound, Stage 2 (for Mix 6M or 6-SR1.26 overlay)
8/29/2016 (Day 38)	Placed Mix 6-SR1.26 concrete overlay on Westbound, Stage 2
8/31/2016 (Day 40)	Installed sensors on Eastbound, Stage 2, and also placed Mix 8M or 8-CM90 concrete overlay on Eastbound, Stage 2
9/7/2016	Conducted crack survey (wet test) on new overlay of Westbound, Stage 2 (Mix 6-SR)
9/14/2016	Conducted crack survey (wet test) on new overlay of Eastbound, Stage 2 (Mix 8-CM90)

Day 0 indicates the starting day of sensor monitoring.

5.2 Crack Survey

In this project, crack surveys were conducted three times on the US 20 over I-35 dual bridge deck surfaces, as follows:

1. Visual inspections were performed to locate cracks on the old concrete bridge decks before new concrete overlays were placed.
2. Shortly after the new overlay construction, another crack survey was carried out (using the wet test method, see Figure 5.3) shortly before the bridge was opened to traffic.
3. Finally, a crack survey was conducted, again using the wet method, to identify cracks after the new overlays had one year of service.

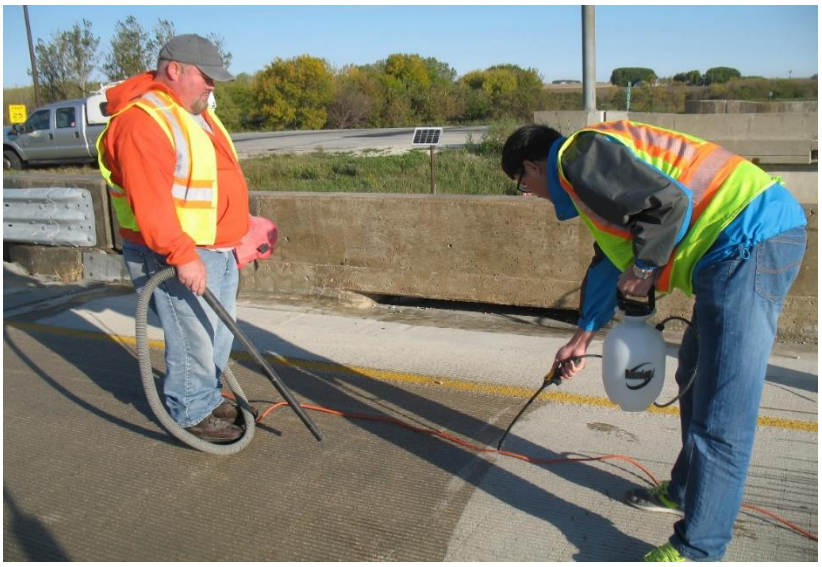

Figure 5.3. Crack survey using wet test method (water used to wet concrete surface)

5.2.1 Crack Survey before New Overlay Construction

On July 6 and August 23, 2016, the cracks on bridge deck surfaces (Stage 1 and Stage 2, respectively) were examined shortly before the new overlay construction. As shown in Figure 5.4 and Figure 5.5, map cracks, longitudinal cracks, and potholes were found on the deck surface in Stage 1, and longitudinal cracks, transverse cracks, spalling, and joint deterioration were observed on the deck surface in Stage 2.

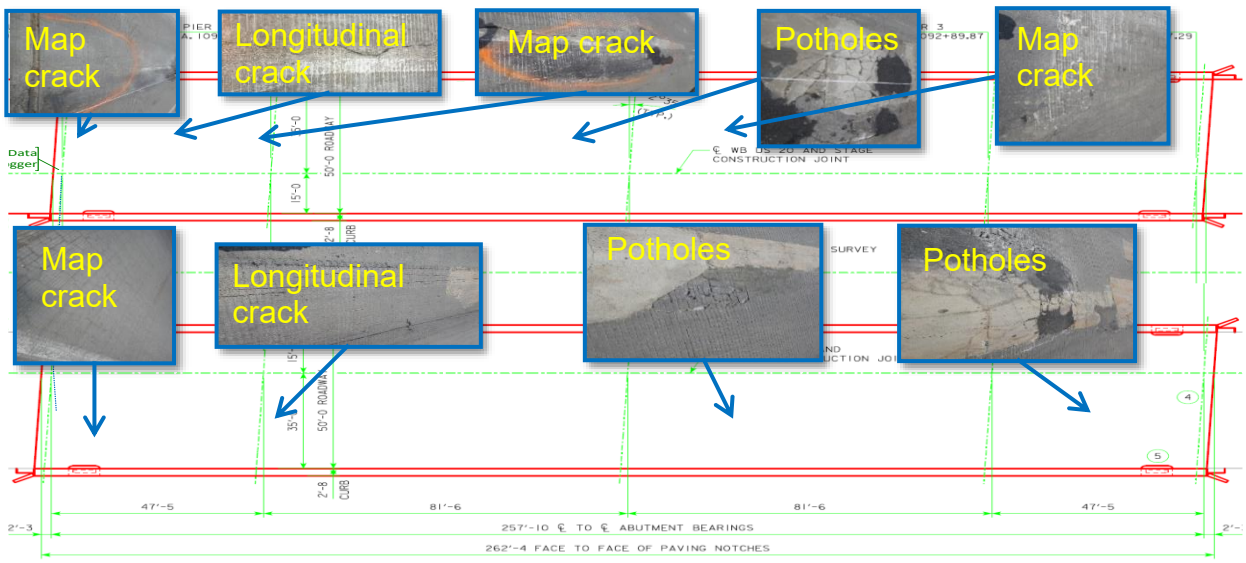

Figure 5.4. Crack survey results on the Stage 1 deck surface before new overlay construction

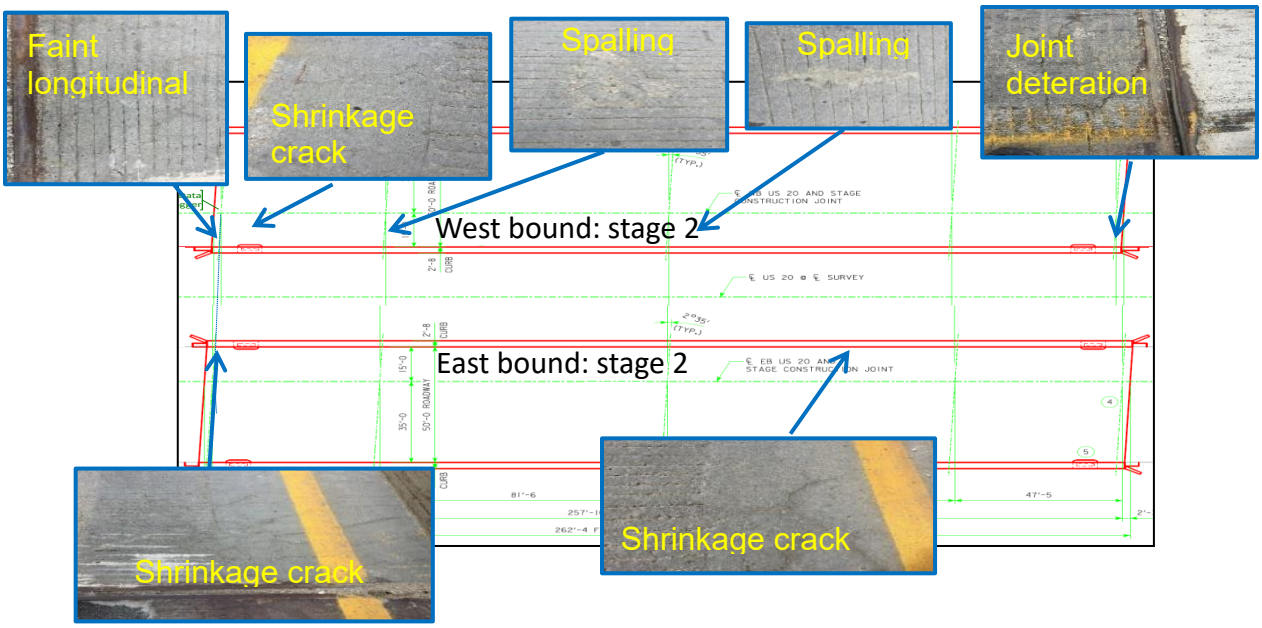

Figure 5.5. Crack survey results on the Stage 2 deck surface before new overlay construction

5.2.2 Crack Survey before Repaired Bridge Opened to Traffic

A second crack survey was conducted shortly before the repaired bridge (with new overlays) was opened to traffic. No cracks were found on any of the new overlays.

5.2.3 Crack Survey after the Repaired Bridge in Service for One Year

On October 9, 2017, cracks were surveyed on the surface of overlays that had one year of traffic service. Figure 5.6 shows the locations and patterns of the cracks.

As shown in the figure, five cracks were found on the overlay made with the original Mix 6 and two cracks appeared on the overlay made with the original Mix 8. The width range of the cracks is from 0.3 mm to 1 mm. They were mostly transverse cracks located near the piers, and probably were related to negative bending moments at the supports. It is not clear if any of these cracks on the new overlays (Figure 5.6) were related to the cracks in the old bridge decks (Figure 5.4) since many cracks on the old bridge decks might not have been identified.

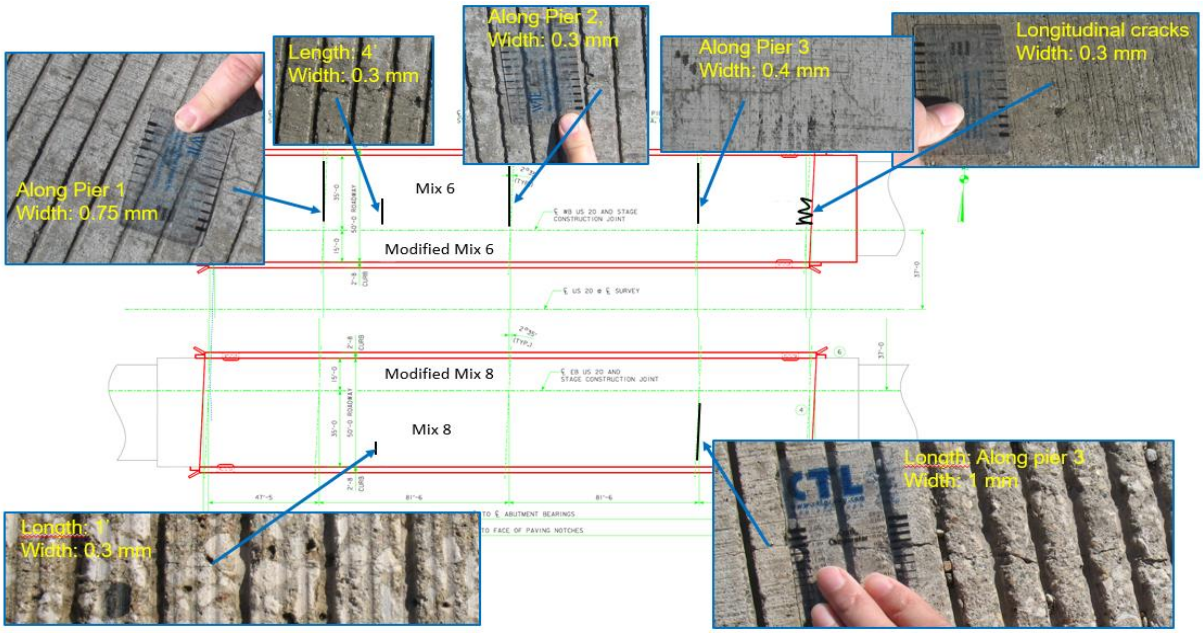

Figure 5.6. Cracks on surface of deck after one year of service for the new overlay

There were no visible cracks found on either of the modified mix (Mix 6-SR and Mix 8-CM90) segments.

5.3 Sensor Installation

5.3.1 Sensor Description and Location

Thirty-six sensors (moisture sensors, Type T thermocouple, and strain gages) were installed in the newly constructed concrete bridge overlays and field concrete samples used in this study. The moisture sensors used were Decagon model GS3, and the strain gages used were Geokon model 4200 and model 4000. A detailed description of each type of sensor follows.

Moisture Sensor

The GS3 from Decagon Devices, Inc., shown in Figure 5.7, was selected for moisture monitoring due to its high stability and accuracy in concrete.

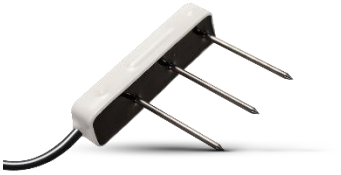

Figure 5.7. GS3 moisture sensor

This type of sensor uses an electromagnetic field to measure the dielectric permittivity of the surrounding medium. The sensor supplies a 70 MHz oscillating wave to the sensor prongs that charges according to the dielectric of the material. The stored charge is proportional to the substrate dielectric and substrate volumetric water content. The GS3 microprocessor measures the charge and outputs a value of dielectric permittivity from the sensor. The dielectric value is then converted to substrate water content by a calibration equation specific to the concrete.

Strain Gages

The strain gages (shown in Figure 5.8) used in this project were the Model 4200 and 4000 vibrating wire strain gages manufactured by GEOKON.

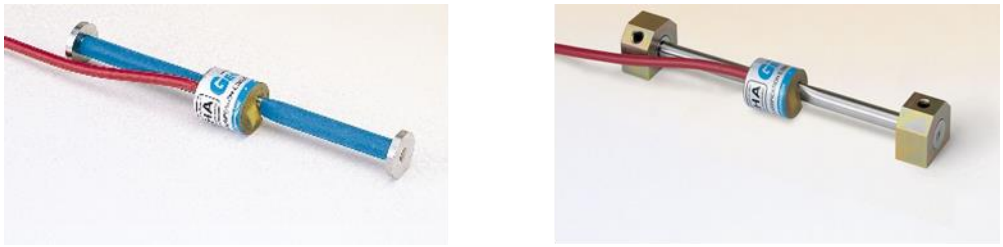

(a) Model 4200 (b) Model 4000

Figure 5.8. GEOKON strain gages

Model 4200 is a 6 in. static strain sensor designed for direct embedment in concrete; its measurements are based on a vibrating wire principle. When the gage is embedded in concrete, strain changes cause the two metal blocks to move relative to one another, and the resulting tension generated in the steel wire can be determined by plucking the wire and measuring its resonant frequency of vibration. The manufacturer cites these advantages of the Model 4200 vibrating wire strain gage: excellent long-term stability, maximum resistance to the effects of water, and a frequency output suitable for transmission over very long cables. Use of stainless steel ensures that it is waterproof and corrosion-free, but strain measurement is affected by temperature, so the Model 4200 strain gage incorporates an internal thermistor for simultaneous measurement of temperature. Model 4000 was used to monitor strain changes on the concrete surface. Strains are measured using the vibrating wire principle. A length of steel wire is stretched between two mounting blocks that are welded to the steel surface being studied. Deformations of the surface will cause the two mounting blocks to move in relation to each other, altering the tension in the steel wire. This change in tension is measured as a change in the resonant frequency of vibration of the wire.

Location of Sensors

Twenty-four GEOKON model 4200 strain gages were used, 20 of which were embedded in the new overlays while 4 were placed in field concrete samples (mini slabs). In addition, 4 GEOKON model 4000 strain gages were installed on the concrete surface beneath bridge deck. Eight GS3 moisture sensors were also embedded in the new overlays.

The sensor locations were varied from the edges of the abutment to the middle point between pier 1 and pier 2. Figure 5.9 shows the details of sensor installation on the bridge decks. For each of the dual bridges, 4 strain gages (GEOKON 4200) were installed transversely at 3 ft, 23 ft 8 in., 61 ft, and 74 ft 7 in. from the abutment, respectively; 2 moisture sensors (GS3) were installed at the location 23 ft 8 in. and 74 ft 7 in. from the abutment, respectively; and 1 GEOKON model 4200 was installed at the location 74 ft 7 in. from the abutment. All sensors were at the depth of 1 in. from the new overlay surface. The directions of the sensors are as shown in Figure 5.9.

In addition, for each of the dual bridges, one GEOKON Model 4000 strain gage was installed on the concrete surface beneath the deck in the transverse direction. Another strain gage was installed on the surface of girder in the longitudinal direction (the same direction as the girder), located 74 ft 7 in. from the abutment. The longitudinal installation runs along with the traffic direction, and the transverse installation is perpendicular to the traffic direction.

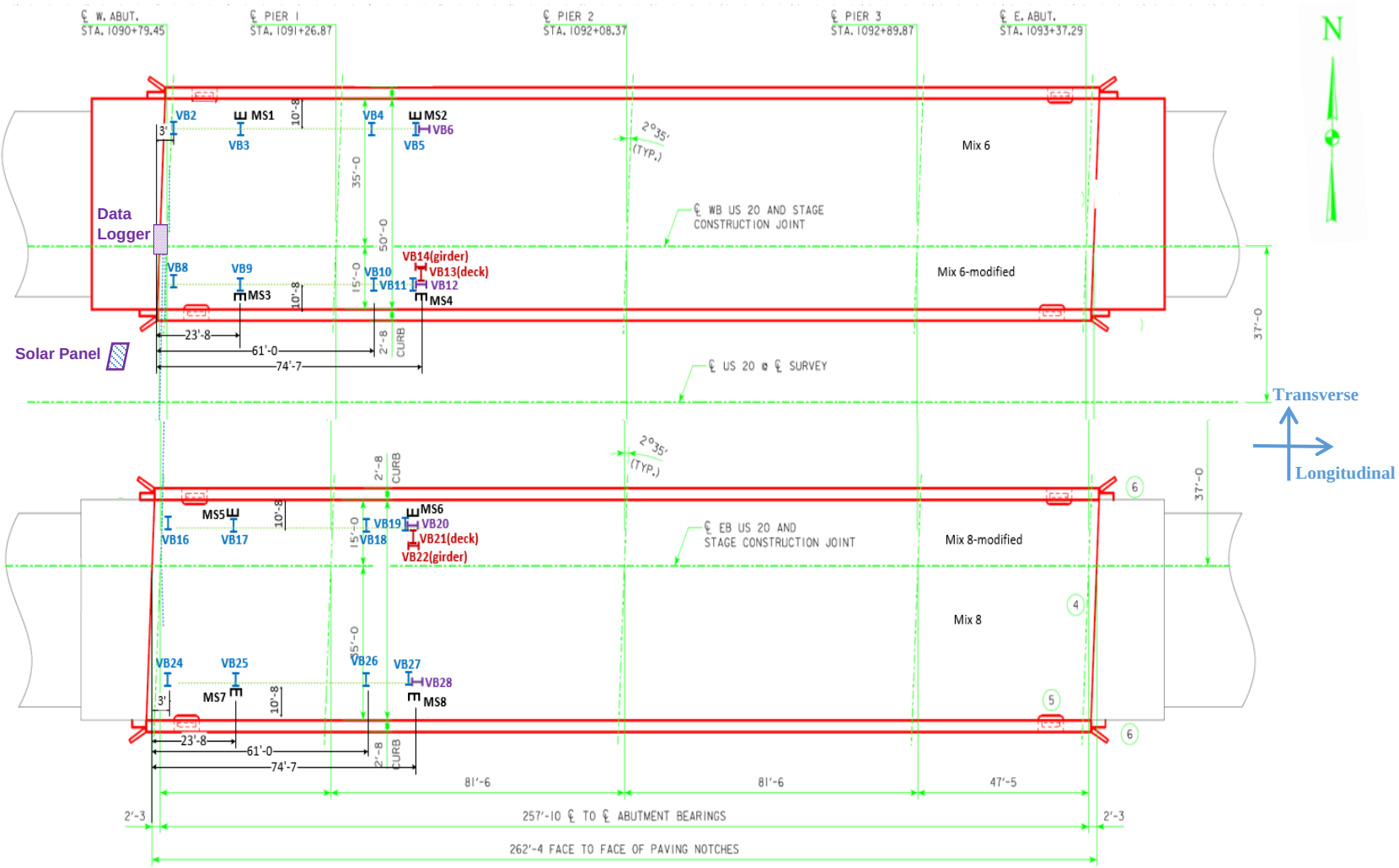

Figure 5.9. Sensor location on the bridge deck

Four mini slabs, one for each field concrete mix, were cast in the field. A GEOKON Model 4200 strain gage was embedded in each mini slab to measure the slab strain under free shrinkage. Information on the mini slabs is detailed in a later subsection titled Field Sample Preparation, and the sensor identifications are listed in Table 5.2.

Table 5.2. Sensor locations

Location	Distance from abutment	Direction	Sensor type	Part of bridge	Westbound		Eastbound	
					Stage1	Stage 2	Stage 1	Stage 2
1	3 ft	Transverse	GEOKON 4200	Overlay	VB 2	VB8	VB 24	VB16
2	23 ft 8 in.	Transverse	GEOKON 4200	Overlay	VB3	VB9	VB25	VB17
		Longitudinal	GS3	Overlay	MS1	MS3	MS7	MS5
3	61 ft	Transverse	GEOKON 4200	Overlay	VB4	VB10	VB26	VB18
4	74 ft 7 in.	Transverse	GEOKON 4200	Overlay	VB5	VB11	VB27	VB19
			GEOKON 4000	Deck	-	VB13	-	VB21
		Longitudinal	GEOKON 4200	Overlay	VB6	VB12	VB28	VB20
			GEOKON 4000	Girder	-	VB14	-	VB22
			GS3	Overlay	MS2	MS4	MS8	MS6

VB = vibrational strain gage sensor, MS = moisture sensor

Installation Procedures

All sensors were installed before the concrete overlays were placed. Each strain gage was affixed on 2 plastic seats that were screwed on the substrate as shown in Figure 5.10. This ensured that the height of the sensors in the new overlays was 1 in. Each moisture sensor was glued and screwed onto the substrate, and some aggregate particles were used to support the sensor and ensure that it was in the middle of the new overlays (Figure 5.10). Strain gages were installed in a similar way underneath the decks and girders of the dual bridge (Figure 5.11).

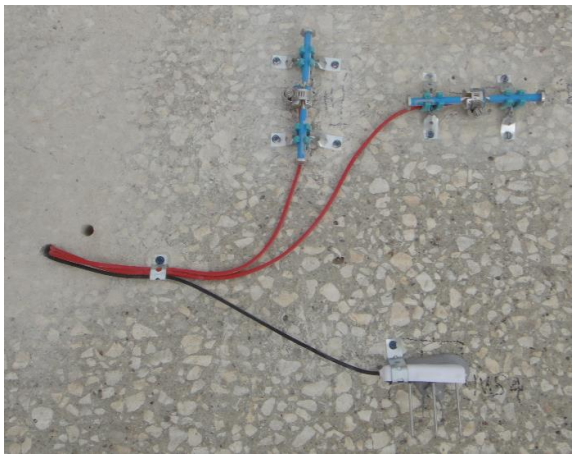

Figure 5.10. Installation of GEOKON 4200 and GS3 on deck

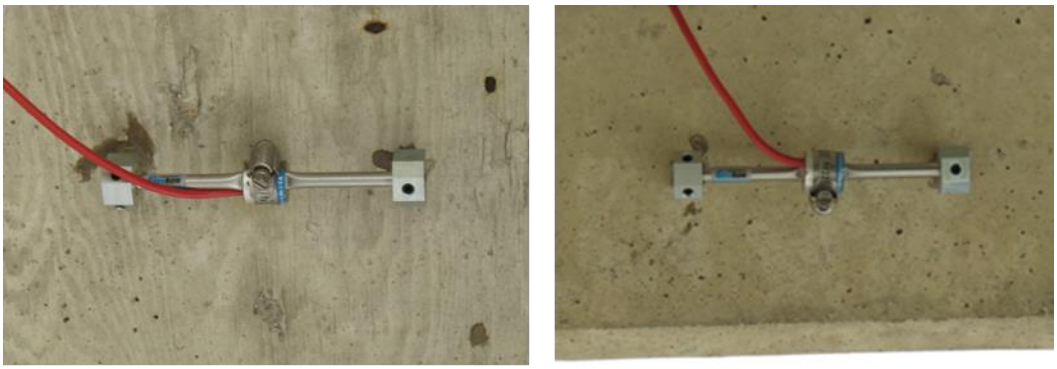

(a) Strain gage on the bottom surface of deck (b) Strain gage on girder

Figure 5.11. Installation of GEOKON 4000 beneath deck and on girder

Note that the sensors and wires received extra attention during the installation process because it would be very difficult to repair them once they were cast inside concrete. In this project, small holes were drilled through the decks at the locations near the sensors, which allowed all wires to be routed through the deck, spliced to create connections, and placed in a polyvinyl chloride (PVC) pipe under bridge, as shown in Figure 5.12.

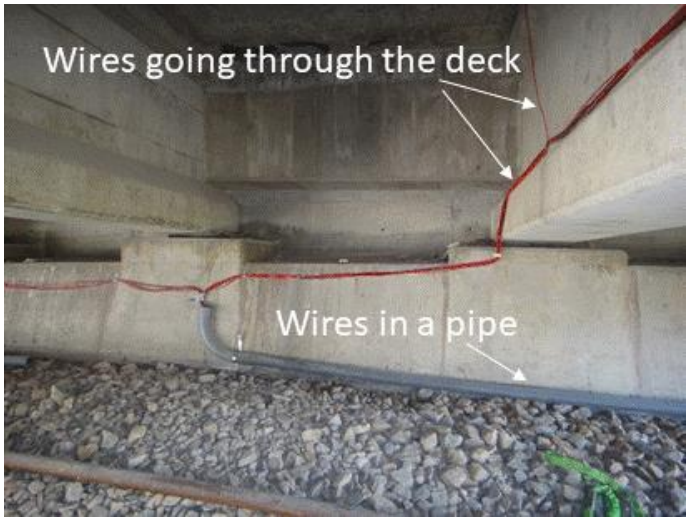

Figure 5.12. Wires in PVC pipe

The PVC pipes on the ground were extended to the area near the data logger, and the wires coming from the pipes were connected to the data acquisition system (DAS), as shown in Figure 5.13. To avoid entanglement of the wires, extra wires from all sensors were mounted to PVC pipe using cable zip ties. The Type T thermocouple (shown in Figure 5.13) was attached under the concrete deck above the DAS to record ambient temperature.

Figure 5.13. Wires to DAS

Data Acquisition System (DAS)

Figure 5.14 shows the DAS used in the US 20 over I-35 bridge project. It includes one Campbell CR1000 data logger, three AM16/32B-ST-SW multiplexers, one vibrating wire analyzer module (AVW200), one solar panel, and one battery used for data collection.

(a) Data logger (b) Solar panel

Figure 5.14. Data acquisition system

All the DAS components were stored in an alloy shield box that was fixed under the edge of the deck, but positioned above the ground for protection from animals, rain, wind, and other external disturbances. Power for the DAS was continuously supplied by an external 12 V battery source, which was charged by a solar panel. The solar panel was placed in an open area between the east- and westbound bridges. The CR1000 data logger was connected with both an AM16/32 multiplexer for moisture sensors, and an AVW200 analyzer, followed by two AM16/32 multiplexers for strain gages as shown in Figure 5.15. In this study, the moisture and strain sensor readings were recorded every 5 minutes, and the total sensor monitoring time was about one year.

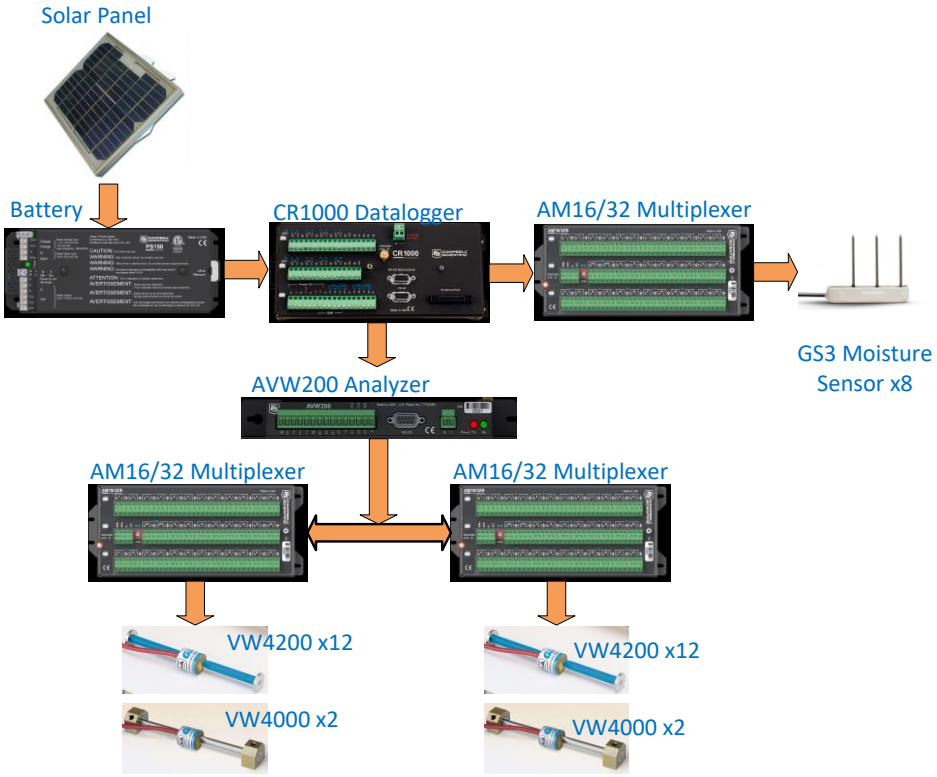

Figure 5.15. Moisture and strain monitoring system

5.3.2 Moisture Sensor Calibration

The GS3 moisture sensors had been calibrated in various media (including potting soil, perlite, and peat) by the manufacturer using a generic calibration equation with an accuracy of better than 5% volumetric water content (VWC) as seen below.

$$VWC(\frac{m^3}{m^3}) = 5.89 \text{ x } 10^{-6}\varepsilon^3 - 7.62 \text{ x } 10^{-4}\varepsilon^2 + 3.67 \text{ x } 10^{-2}\varepsilon - 7.53 \text{ x } 10^{-2} \quad (5)$$

Where, Ɛ is dielectric permittivity measured directly by the GS3 sensor. Using this equation, the VWC of a tested material can be computed from the Ɛ measured by the moisture sensor.

However, the default equation shown above is not valid for concrete substrate or cannot be directly used in this project because this VWC equation is not suitable for concrete. The relationship between the VWC and Ɛ in concrete had to be recalibrated for each concrete mix studied. The basic idea for this calibration was to measure the VWC and Ɛ with time in concrete under different given moisture conditions and then to regress the VWC- Ɛ trend line to obtain a new polynomial equation for the concrete mix that would be similar to the above default equation.

After the production of each mix, 17 bags of concrete with the same volume of 400 cm^3 and a 4×8 in. cylinder were cast. These 17 concrete bags were completely sealed, and the water content of the concrete in each bag was determined at a selected curing time. At the same time, a GS3 moisture sensor was inserted into the freshly cast concrete cylinder, and the cylinder, together with the moisture sensor, was sealed tightly with a plastic sheet. The sensor was then connected to the data logger, which recorded Ɛ as shown in Figure 5.16.

(a) Concrete in sealed bags (b) Concrete cylinder with moisture sensor

Figure 5.16. Concrete samples used for moisture sensor calibration

At a selected time interval, the water content in concrete (later converted to VWC) was determined by measuring the weight loss of concrete in each bag after microwave drying. At the same time, the permittivity (Ɛ) of the concrete was recorded from the moisture sensor that was inserted in the concrete cylinder. Generally, the time interval was small (one to two hours) before the concrete had aged for one day, but larger (three to four hours) after one day as the rate of moisture loss decreased. To simulate the conditions of field concrete under curing, the bags of the concrete samples were arranged to be used up in the same amount of time as the field concrete was cured under burlap. Next, the concrete cylinder was demolded on the same day as

the burlap was removed from the field concrete. The weight of the cylinder, together with the inserted moisture sensor, was measured daily until the concrete samples reached the age of 36 days. (This study found that concrete weight loss became negligible after 36 days and, therefore, the calibration stopped on day 36 for each mix.) Based on the test results, a VWC vs. Ɛ curve was plotted for each concrete mix studied. Using a polynomial curve fitting, an equation was generated to describe the relationship between VWC vs. Ɛ for each concrete mix. Figures 5.17 through 5.20 show the VWC - Ɛ curves and corresponding moisture sensor calibration equations for all four concrete mixes studied.

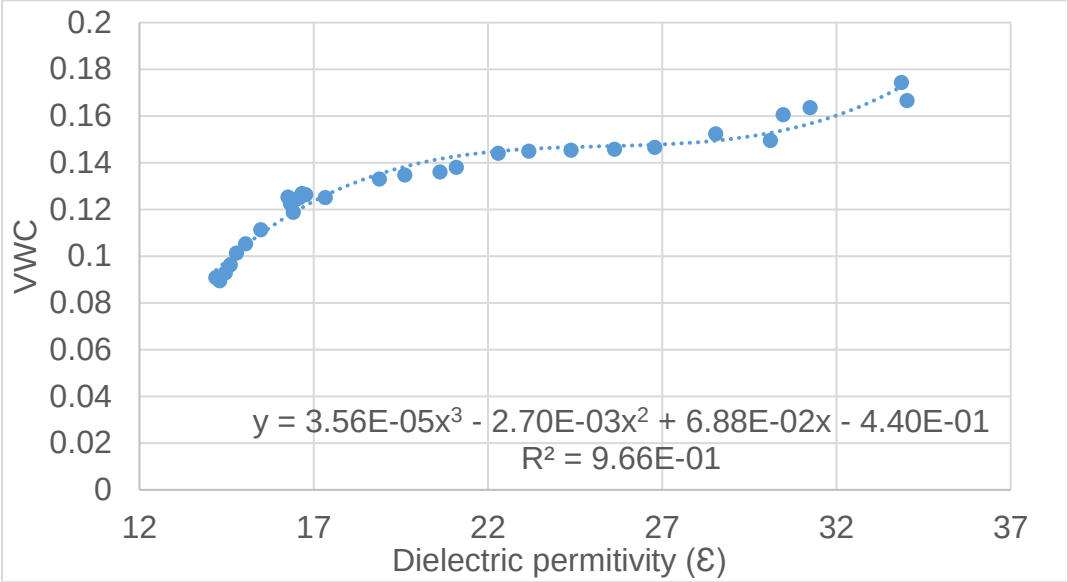

Figure 5.17. Calibrated VWC equation for Mix 6

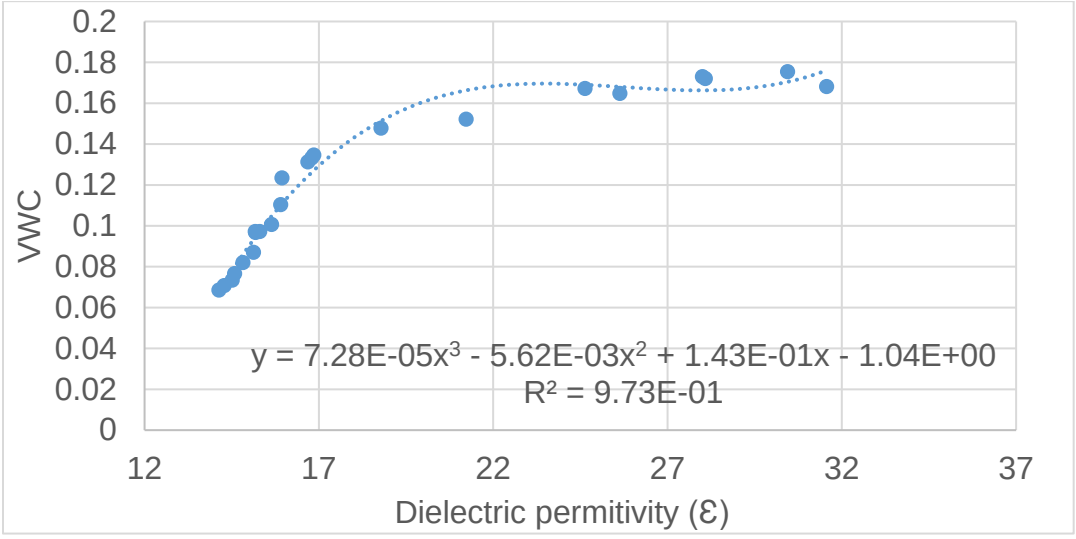

Figure 5.18. Calibrated VWC equation for modified Mix 6

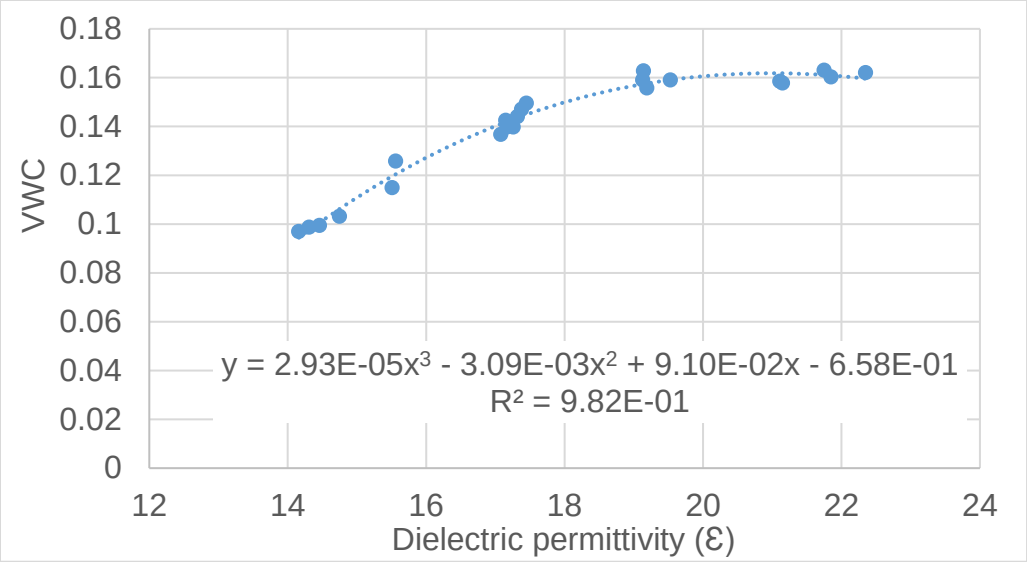

Figure 5.19. Calibrated VWC equation for Mix 8

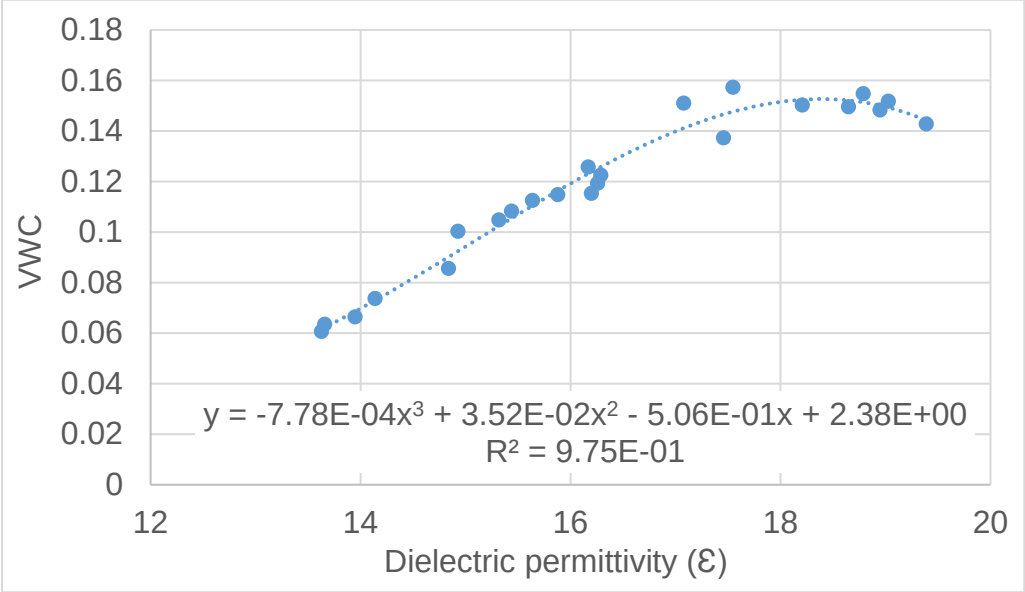

Figure 5.20. Calibrated VWC equation for modified Mix 8

Using these equations, the VWC of field concrete overlays made with different concrete mixes was computed, based on the Ɛ read directly from embedded sensors in the concrete.

5.3.3 Strain Measurements

According to the instruction manual for GEOKON vibrating wire strain gages, the equation for the true strain corrected for temperature could be as follows:

$$\mu = (R_1 - R_0)\, B + (T_1 - T_0)\,(C_1 - C_2) \qquad (6)$$

Where, μ is strain; R_0 is the initial reading and R_1 is the current reading of strain from the strain gage; B is the batch gage factor suppled with 0.975; T_0 is the initial temperature and T_1 is the current temperature; and C_1 is the coefficient expansion of steel and C_2 is the coefficient of expansion of concrete. It should be noted that the positive μ is tensile and the negative μ is compressive.

5.4 Field Construction and Sample Preparations

5.4.1 Construction Information

As indicated previously in Table 5.1, crack surveys, sensor installation, and overlay placement were conducted for different sections (stages and parts) of the bridge studied. The HPC mixes used in the field were Mix 6, Mix 6-SR1.0, Mix 8, and Mix 8-CM90. The proportions of the concrete mixes and their total shrinkage (as shown in Figure 3.14) are listed in Table 5.3.

Although the types of concrete materials were the same, the sources of cement and aggregate were different from those used in the laboratory investigation. For instance, the cement used in field investigation was from the Ash Grove Cement Company, while that used in the laboratory was from the Continental Cement Company.

Table 5.3. Field concrete mix proportions and their shrinkage

Mix	SR gal/yd^3	Type I Cement lb/yd^3	C-FA lb/yd^3	GGBFS (Gr 120) lb/yd^3	Limestone lb/yd^3	Sand lb/yd^3	Water lb/yd^3	w/b ratio	Total* shrinkage microstrain
6	-	825.4	-	-	1386.3	1365.6	269.9	0.33	920
6-SR1.0	1.0	825.4			1386.3	1365.6	269.9	0.33	590
8	-	367.9	133.8	167.2	1430.8	1404.9	267.6	0.40	880
8-CM90	-	342.1	124.4	155.5	1478.1	1451.4	248.8	0.40	530

* See Figure 3.14 for the total shrinkage values of the mixes.

Milling and sand blasting were carried out on the old bridge decks before overlay construction. A layer of grout was applied to the surfaces of the concrete substrates during overlay construction (Figure 5.21a). After fresh concrete was discharged from a mixing truck, it was spread on the deck by shoveling. External vibrators were used for consolidation. Then, a paver removed the extra concrete to ensure that the concrete overlay was leveled and had a uniform thickness, followed by finishing with a screed which further consolidated the concrete (Figure 5.21b).

(a) Grouting

(b) Spreading and initial vibration

(c) Leveling

(d) Finishing

Figure 5.21. Concrete overlay construction

The surface was textured by dragging a piece of burlap in the longitudinal direction. Water was sprayed onto the pavement surface after texturing, followed by the spraying of chemical components for curing purposes as shown in Figure 5.22.

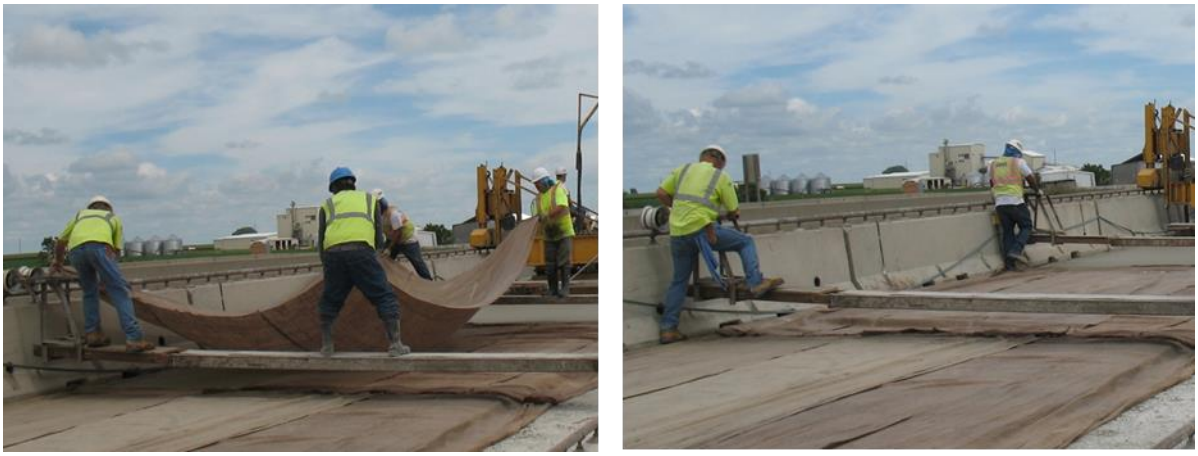

Figure 5.22. Curing method

However, both the paver and vibrator were potential threats to the sensors. The auger and vibration forces that the paver and vibrator produced during pavement construction could break either the sensors or the wires. Moreover, dropping a heavy mass of concrete could crush the sensors and tear the wires. Therefore, to protect the sensors as much as possible, fresh concrete was carefully pre-poured on the top of sensors to mitigate the forces from the paver, vibrator, and dropped concrete. Figure 5.23 shows the new overlays before opening to traffic on September 21, 2016.

(a) Westbound (b) Eastbound

Figure 5.23. New overlays before opening to traffic

5.4.2 Fresh Concrete Properties

Since the concretes cast in the field and laboratory were different (even for the same mix) due to technical and environmental conditions, the fresh properties of field concrete were tested on site including slump, unit weight, and air content, while the hardened properties were also characterized for the samples collected from the field. The properties of the field samples are discussed in this chapter.

The test methods for slump, unit weight, and air content were the same as those employed in the laboratory. The results are summarized in Table 5.4.

Table 5.4. Fresh concrete properties in the field

	Mix 6		Mix 6-SR 1.25		Mix 8		Mix 8-CM 90	
Property	**Lab**	**Field**	**Lab**	**Field**	**Lab**	**Field**	**Lab**	**Field**
Slump, in.	1.75	1.00	0.75	0.75	8.50	2.75	7.00	1.5
Unit weight, pcf	138.8	141.5	146.4	143.0	138.6	-	140.2	-
Air content, %	9.5	6.0	5.5	7.0	9.0	7.0	8.0	7.0

Unit weights of Mix 8 and Mix 8-CM90 were not tested in the field.

Table 5.4 shows that the fresh properties (e.g., slump, unit weight, and air content) of field concrete were somewhat different from those of laboratory concrete. This may be due to different mixing and environmental conditions. The large differences in slump between the field and laboratory concrete mixtures might be the result of different aggregate moisture conditions and potentially high slump loss under field environmental conditions.

5.4.3 Field Sample Preparation

For each field concrete mix, 20 4×8 in. cylinders, 3 3×3×11.25 in. prisms, and 1 12×6×2 in. mini slab were cast on site. Their purposes are stated in Table 5.5.

Table 5.5. Field samples and their uses

Sample type	Test	No.
Cylinder	Compressive strength	18
	CTE	2
Prism	Free drying shrinkage	3
Mini slab	Strain	1

All 20 cylinders were demolded after 1 day; 3 were cured on the field site for 28 days under the same environmental conditions as the overlay, and the remaining 17 cylinders were cured in the ISU Portland Cement Concrete Research Laboratory (at 25°C and 99% RH). The compressive strength of the laboratory-cured cylinders was tested at 1, 3, 7, 14, and 28 days, and the coefficients of thermal expansion (CTE) of the concrete mixes were tested at 7 and 28 days. The three field-cured cylinders were tested for compressive strength at 28 days as well. The prism samples cast at the field site were taken to the laboratory on the day after casting, and free drying shrinkage of the samples was measured according to ASTM C157.

To make a mini slab as shown in Figure 5.24, a GEOKON 4200 strain gage was installed in the middle of the slab formwork (also midway in the slab height) before concrete casting.

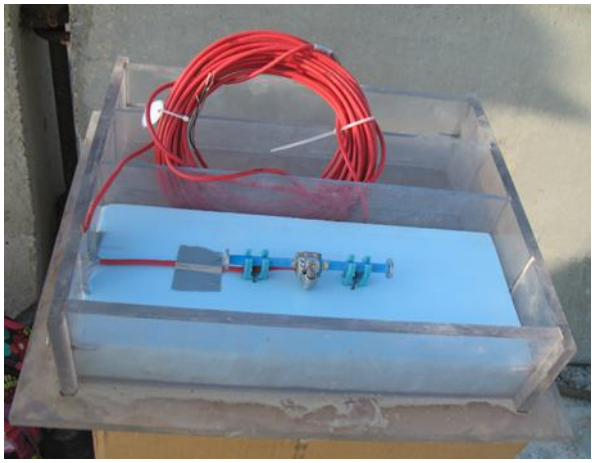

Figure 5.24. Formwork of a mini slab and strain gage location

After casting, the mini concrete slab was covered by a wet towel. The slab sample was placed under the bridge, and the wires of the strain gage sensor were connected to the data logger. One day after casting, the slab formwork was removed, and a concrete sealer applied on the bottom and side surfaces of the slab, leaving only the top surface open to the environment. The slab was then moved to an open area near the solar panel so that it would experience the same weather conditions as its corresponding concrete overlay. The strain measurement of each mini slab provided information on the difference between the restrained concrete (overlay) and the non-restrained concrete (mini slab) under the same environment.

Figure 5.25 illustrates the layout of mini slabs with wooden protection.

Figure 5.25. Mini slabs on the field site

The mini slabs made from four field concrete mixes were placed together on the plywood sheets that were supported by wooden stakes and their positions were reinforced using steel wires. The figure also shows how the wires from the strain gages of the mini slabs were tied together using duct tape and passed through a PVC pipe to connect to the data logger.

5.5 Field Sample Tests and Results

5.5.1 Compressive Strength

Compressive strengths of all field-cast concrete samples were tested. Figure 5.26 and Figure 5.27 present the results of the samples cast and cured in the field for one day, demolded, and cured under standard laboratory curing conditions until testing, as compared with the results of the corresponding laboratory-cast and laboratory-cured samples obtained in the laboratory investigation.

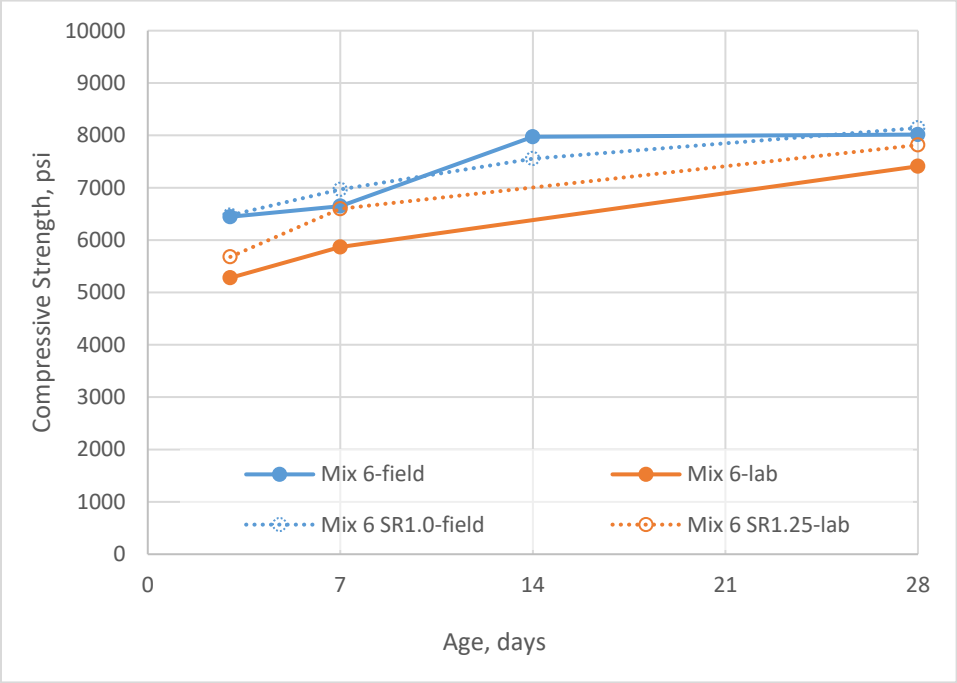

Figure 5.26. Compressive strength of laboratory- and field-cast samples (original and modified Mix 6)

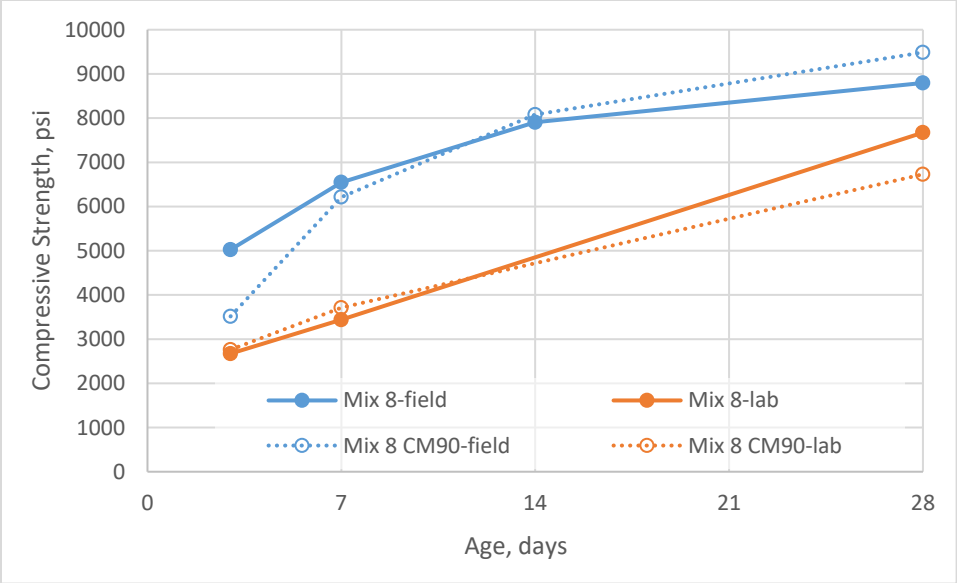

Figure 5.27. Compressive strength of laboratory- and field-cast samples (original and modified Mix 8)

It can be seen from the laboratory-cast sample results for Mix 6 that the 1.0 gal/yd^3 addition of SR did not affect the concrete compressive strength of field-cast samples. This is possibly because the original Mix 6 overlay was placed on July 22, 2016, when the weather was hot, while the Mix 6-1.0SR overlay was placed on August 29, 2016, when the weather was cooler. The one-day curing in the field weather conditions made the strength of these concrete mixes similar.

For Mix 8, the strengths of the field-cast Mix 8-CM90 and Mix 8-CM100 samples were all much higher than those of the corresponding laboratory-cast concrete samples. This might be due to the hotter environmental temperature in the field, especially the hotter ambient temperature in the first few days after the construction, which in turn accelerated both cement and pozzolanic reaction of slag and fly ash. Interestingly, it was noted that the 28-day strength of the field Mix 8-CM90 samples was slightly higher than that of the field Mix 8-CM100 samples. This might be also due to the hotter environmental temperature in the field when the Mix 8-CM90 overlay was constructed in a comparison with the environmental temperature in the field when the Mix 8-CM100 overlay was constructed.

In addition, a comparison of the effect of laboratory and field curing conditions on 28-day compressive strength is shown in Figure 5.28. The strength of cylinders in field curing varied slightly compared to those of laboratory curing, except for Mix 8-CM90. This may be attributed to the high rate of moisture loss in the field during its curing days. High temperature and wind speed could accelerate moisture loss in concrete.

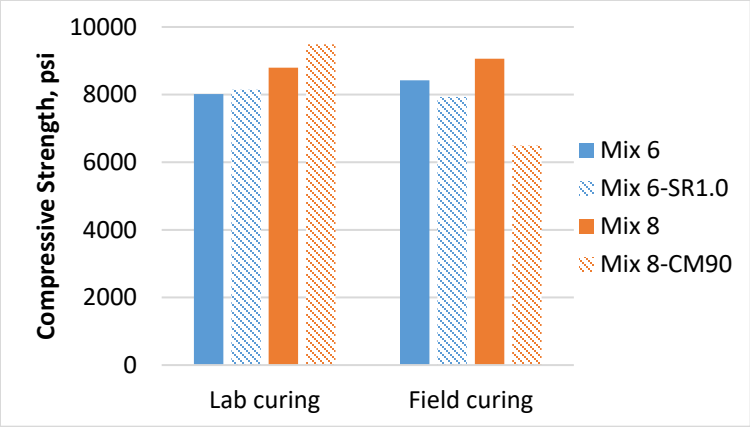

Note: Field samples were cast on different dates.

Figure 5.28. 28-day compressive strength for field-cast samples under laboratory and field curing conditions

5.5.2 Free Drying Shrinkage

Although it is known that SR addition and cementitious material reduction decrease concrete shrinkage, it is necessary to measure their effectiveness in reducing shrinkage of field concrete mixes. In this study, the free drying shrinkage of field concrete samples was measured and the results are shown in Figure 5.29.

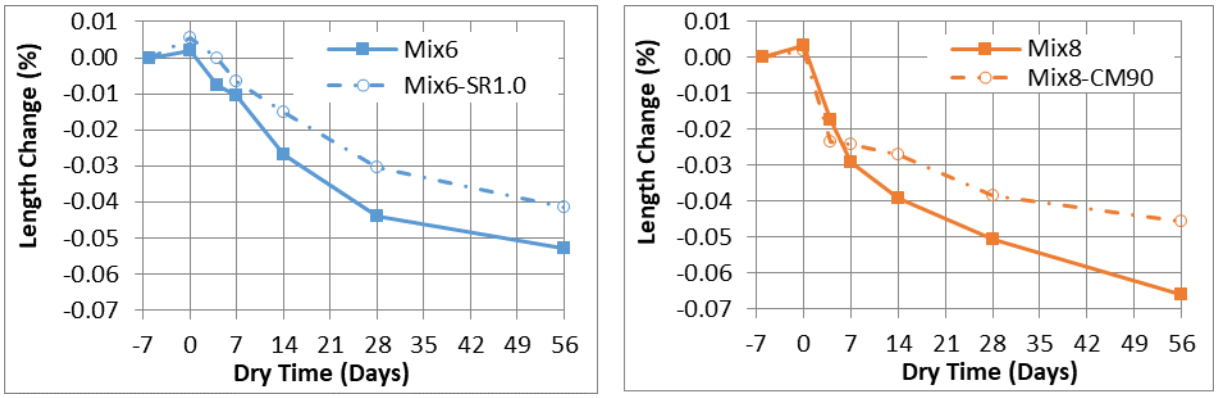

(a) Mix 6 (b) Mix 8

Figure 5.29. Free drying shrinkage of field concrete samples

Figure 5.29 illustrates that the 1.0 gal/yd^3 SR addition reduced the free drying shrinkage of Mix 6 by 20%, and the 10% cementitious material reduction decreased the free drying shrinkage of Mix 8 by approximately 30%. These results were similar to those observed from laboratory concrete samples.

5.5.3 Coefficient of Thermal Expansion (CTE)

Although most random cracks in bridge decks result from drying shrinkage due to its large surface area-to-volume ratio, a large percentage of cracks are actually due to thermal effects. Therefore, in the present study, CTE of field concrete mixes was evaluated to provide a better understanding of the strain and stress development in concrete decks in addition to the cause of drying shrinkage. The CTE measurements were conducted according to AASHTO TP60. The main apparatus used in the test consisted of a water bath, support frame, temperature measuring device, and linear variable differential transformer (LVDT) gage as shown in Figure 5.30.

Figure 5.30. Apparatus for CTE

In the test, a 4×7 in. concrete cylinder was saturated and maintained in water. The change in specimen length was monitored by the LVDT when the specimen temperature changed from 10°C to 50°C. The CTE results of four field concrete mixes are presented in Figure 5.31.

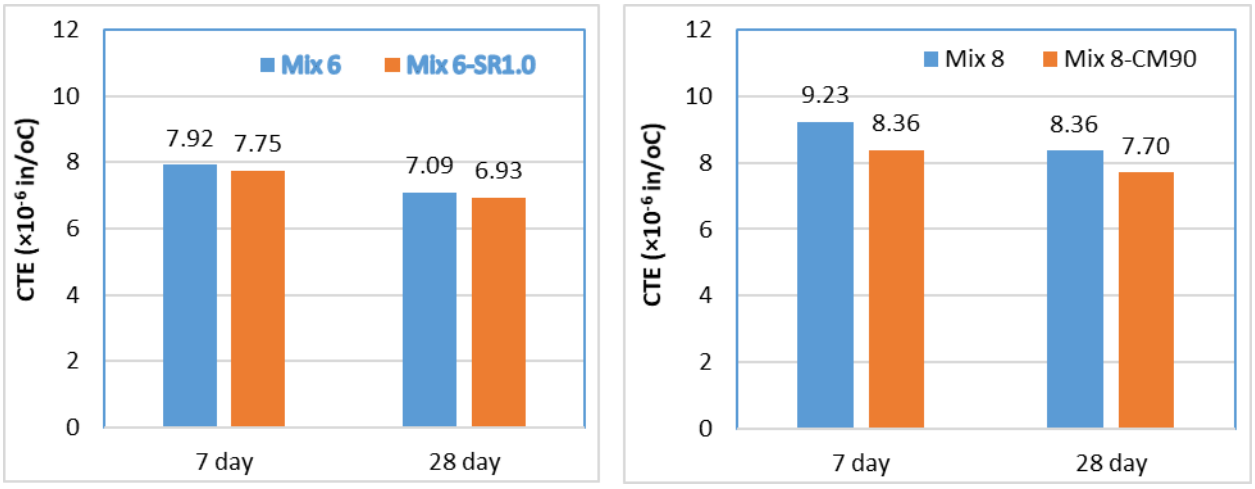

(a) Mix 6 (b) Mix 8

Figure 5.31. CTE results of field concrete mixes

The samples were field-cast, field-cured for 1 day and then demolded and cured in the standard laboratory curing conditions for the rest of days until testing. It can be seen from the figure that extended curing from 7 to 28 days slightly reduced CTE of both Mixes 6 and 8 (by 10% or less). A similar reduction trend for concrete made with limestone coarse aggregate was also found by other researchers (Berwanger and Sarkar 1976, Shin and Chung 2011, Yang and Sato 2002). In addition, Mix 8 series had noticeably higher CTE values than Mix 6 series. The major differences in these two mixes were the w/b ratios (0.33 for Mix 6 and 0.40 for Mix 8) and the cementitious materials (pure portland cement for Mix 6 but ternary cement for Mix 8). In addition, Mix 6 had 3% less aggregates than Mix 8.

Research has indicated that w/b ratio does not significantly affect CTE since water moves from one capillary void to another capillary void without causing thermal expansion of the paste (Choktaweekarn and Tangtermsirikul 2009). It was found that CTE is around 18 to 20×10^{-6}/°C for a cement paste with a w/b ratio of 0.4 to 0.6, and it is about 12×10^{-6}/°C for a mortar paste (FHWA 2016), much higher than the CTE of limestone aggregate (about 5×10^{-6}/°C) in the concrete. Shin and Chung (2013) studied 25 concrete mixes fabricated with various combinations of fly ashes (class C and F), slags (grade 100 and 120 GGBSF), and Portland cement (Type I), and they reported that all the CTE values of ternary mixtures were generally larger than that of the control mixture (100% Portland cement concrete). This is consistent with the present observation that the Mix 8 series had higher CTE values than the Mix 6 series. CTE of a cement paste largely depends on the bond strength between cementitious particles in the paste. Paste with GGBSF might have strong particle bonds, resulting in a low CTE. The CTE value of Mix 8-CM90 was lower than that of Mix 8 (or Mix8-CM100) because of lesser amounts of cementitious materials in Mix 8-CM90. Figure 5.31(a) shows that SR addition decreased the CTE of Mix 6 very slightly.

5.6 Field Sensor Monitoring and Data Analysis

The field sensor monitoring took place from July 22, 2016 to June 20, 2017, and the sensor data collection occurred monthly. Since the overlay construction for different stages and parts was carried out on different days from July to September 2016, the data collection periods for different concrete overlay mixes were not the same. The details on sensor performance and data analyses follow.

5.6.1 Field Ambient Temperature

Figure 5.32 illustrates the daily average ambient temperature profiles captured by the thermal couple on the bottom concrete surface of the bridge deck. A maximum temperature of 30.4°C was observed on Day 0 (June 22, 2016) and a minimum temperature of -17.6°C was observed on Day 150 (November 20, 2016) during the monitoring period. The maximum ambient temperature difference was 48.0°C in the monitoring period.

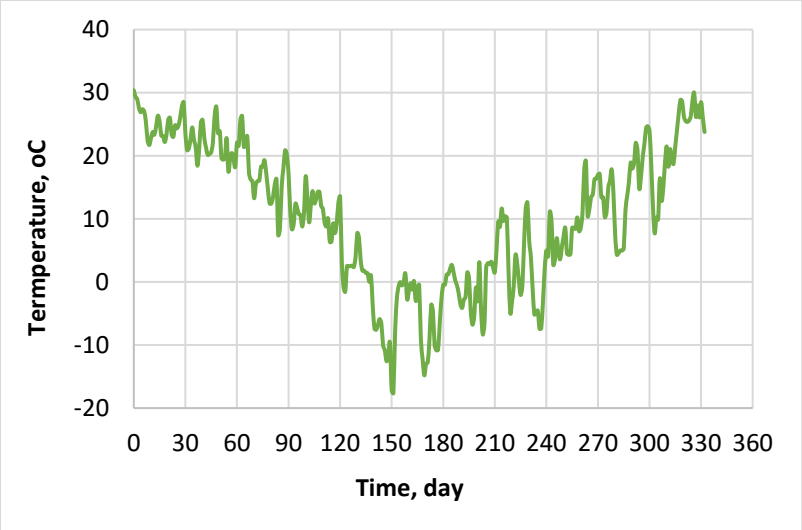

Day 0 was June 22, 2016, the day of the first overlay construction.

Figure 5.32. Ambient temperature of the field site

5.6.2 Moisture Content of Concrete Overlays

Eight GS3 digital moisture sensors (MS) were embedded in the dual bridge decks, and their locations were shown in Figure 5.9, where MS1, 3, 5, and 7 were 23 ft 8 in. and MS2, 4, 6, and 8 were 74 ft 7 in. from the abutment. All the moisture sensors functioned appropriately during the entire monitoring period. The VWC profiles captured by the moisture sensors are illustrated in Figures 5.33 and 5.34.

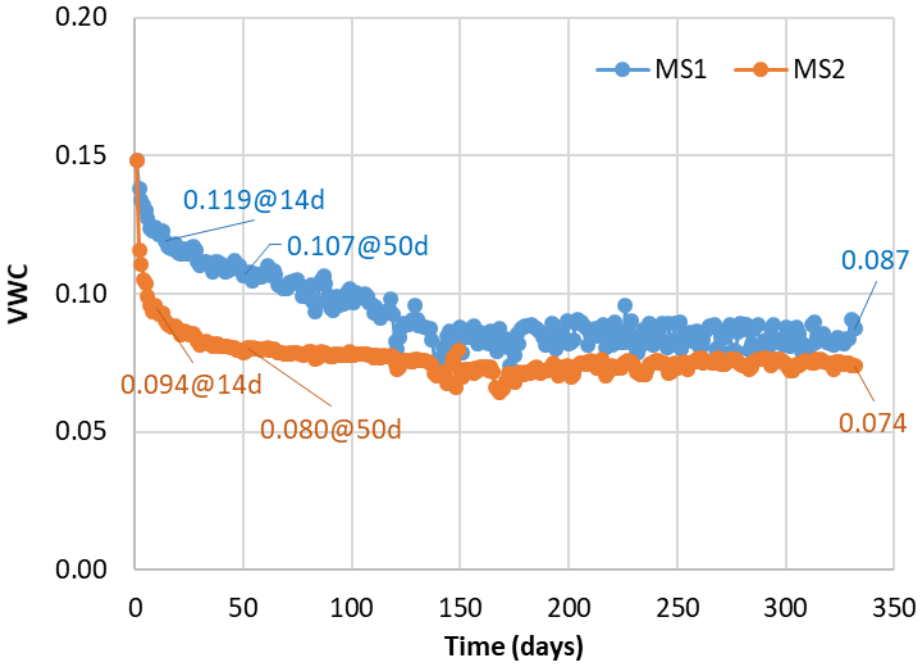

(a) Mix 6

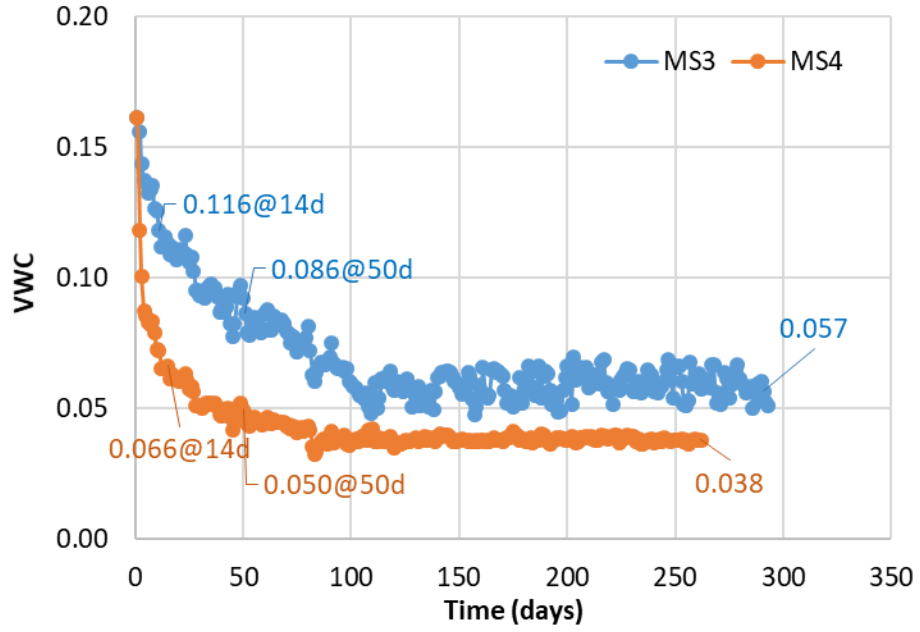

(b) Mix 6-SR1.0

MS1 and 3 were 23 ft 8 in. and MS 2 and 4 were 74 ft 7 in. from the abutment.

Figure 5.33. VWC measurements from Mix 6 series

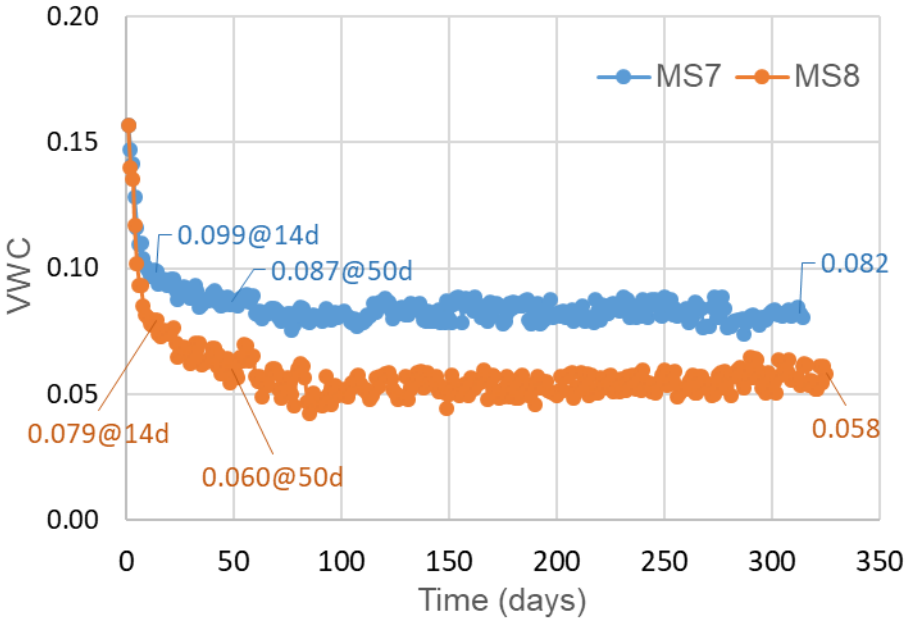

(a) Mix 8 (Mix 8-CM100)

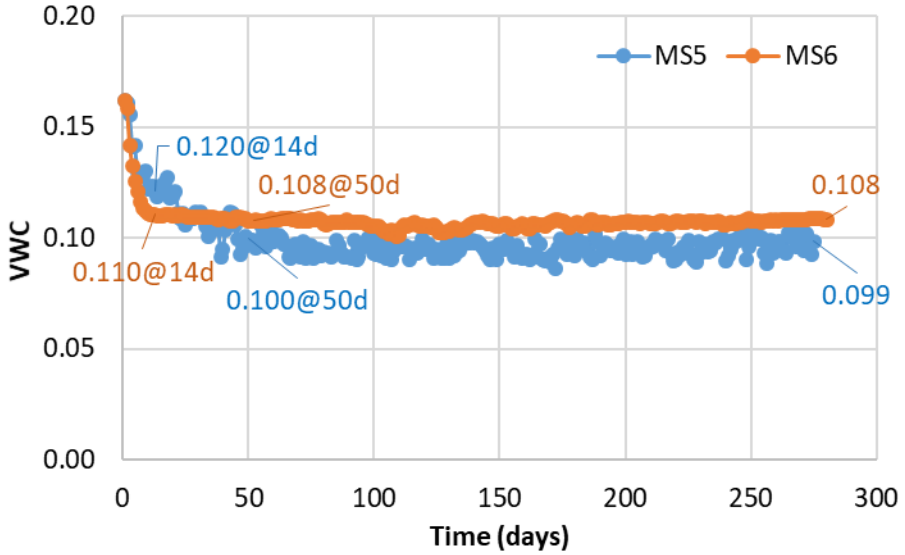

(b) Mix 8-CM90

MS5 and 7 were 23 ft 8 in. and MS 6 and 8 were 74 ft 7 in. from the abutment.

Figure 5.34. VWC measurements from Mix 8 series

The following observations can be made from these figures:

- The initial VWC was about 0.15 for Mix 6 and 0.16 for the rest of the mixes, which was the same as or almost the same as that calculated from their mix proportions.

- The VWC readings of the moisture sensors (MS1, 3, 5, and 7, in blue) at the locations 23 ft 8 in. from the joint (near the abutment) were generally higher than those of the moisture

sensors (MS2, 4, 6, and 8, in orange) at the locations 74 ft 7 in. from the joint/abutment, except for the sensors in Mix 8-CM90.

- For the Mix 6 series (Figure 5.33), the VWC readings of the moisture sensors (MS1 and 3, in blue) close to the joint near the abutment dropped slowly to a stable VWC; while the VWC readings of the moisture sensors (MS2 and 4, in orange) further away from the joint dropped rapidly to a stable VWC. This indicates that the joint probably allowed moisture to enter.

- Mix 6 reached a stable VWC at approximately 150 days after the overlay construction, the coldest day of that winter, and the stable VWC values of Mix 6 were 0.087 and 0.074 for MS1 and MS2, respectively. Mix 6-1.0SR reached a stable VWC at approximately 100 days after its overlay construction, and the stable VWC values of Mix 6-1.0SR were 0.057 and 0.038 for MS3 and MS4, respectively. The difference in VWC between Mix 6 and Mix 6-1.0SR could be partially attributed to the different overlay construction time (Mix 6 on 7/22/2016 (Day 0) and Mix 6-1.0SR on 8/29/2016 (Day 38)). The exposure to conditions at early ages could have a significant impact on moisture presence in the concrete.

- As shown in Figure 5.34, although it was placed only 8 days after Mix 6, Mix 8 (or Mix 8-CM100) reached a stable VWC in less than 100 days after its overlay construction, and the stable VWC values of Mix 8 were 0.082 and 0.058 for MS7 and MS8, respectively. Placed 32 days after Mix 8, Mix 8-CM90 displayed quite different moisture conditions, especially in the location away from the joint/abutment (MS6). MS6 readings (Figure 5.34b) show that the concrete had a very rapid moisture drop before 14 days, and reached a relatively high but stable VWC value (0.108) shortly thereafter. Such behavior might be related to the pore structure of the concrete, which needs further study. The relatively high VWC value might also be responsible for the reduced free drying shrinkage of the concrete.

Figures 5.33 and 5.34 illustrate that concrete at the location away from the abutment had a sharp moisture decrease in the first 14 days, which might have been heavily influenced by cement hydration. All VWC curves exhibited a fluctuating trend daily throughout the entire sensor monitoring period. This fluctuation was probably due to environmental moisture changes during day and night as well as weather changes.

5.6.3 Strains of Mini Slabs

Concrete in bridge elements (e.g., overlays/decks) is often under conditions of restraint, while the concrete mini slabs studied in this project were under an unrestrained condition. Four mini slab samples were prepared, one for each concrete mix, and their free shrinkage behavior was studied to further understand field concrete shrinkage behavior. As seen in Figure 5.24, the strain gages in the mini slabs were in the longitudinal direction. Figure 5.35 illustrates the microstrain monitored by the strain gages in the mini slabs.

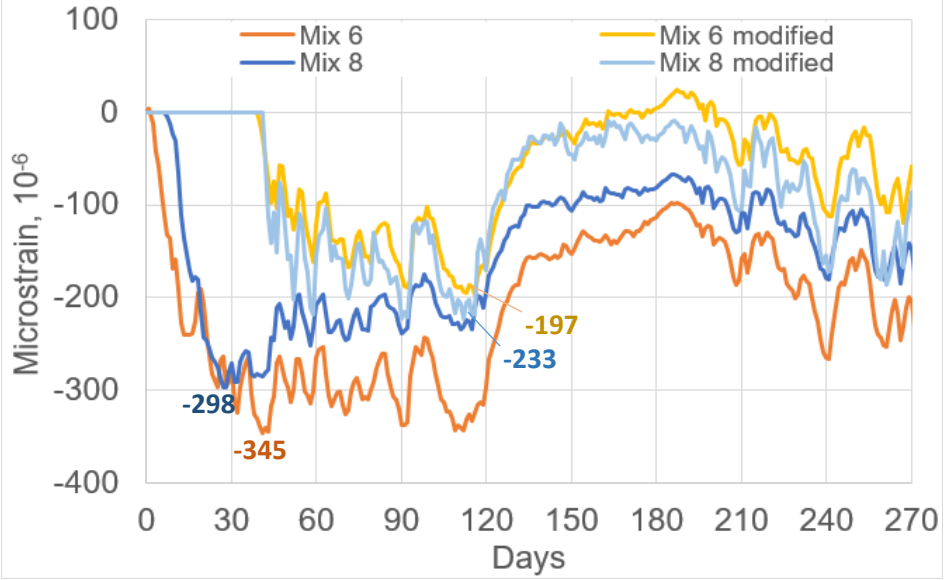

Figure 5.35. Microstrain for different mixes used in mini slabs

It was noted that the strains in mini slabs were mainly compression strains, and they were due to concrete shrinkage under an unrestrained condition. As the slabs had a very large surface to volume ratio and all surfaces were exposed to environmental stresses (under the bridge deck was a shaded area), summertime thermal expansion during the early ages of the slabs was much less than that of the concrete overlays and, therefore, free drying shrinkage was the dominant deformation behavior. During the winter time (around days 150 to 210), the mini slabs were subjected to freezing temperatures, they expanded, and the expansion offset the shrinkage, thus reducing the compressive strain. When the weather got warmer, expansion of the concrete slabs due to frost action disappeared, and compressive strain caused by continued drying shrinkage increased until the second summer.

Figure 5.35 indicates that the compressive strains caused by free shrinkage in mini slabs were in order, Mix 6 (highest), Mix 8, Mix 8-CM90, and Mix 6-1.0SR (lowest). The maximum strain values for Mix 6, Mix 8, Mix 8-CM90, and Mix 6-1.0SR were 345, 298, 233, and 197 microstrain, respectively. This order is consistent with the results of the crack survey conducted a year after the overlay construction. (As seen from Figure 5.6, five cracks were found on the overlay made with the original Mix 6 and two cracks on the overlay made with the original Mix 8. No cracks were found in the modified mixes.) The laboratory shrinkage test results presented in Figure 3.14 also show that the total shrinkage at the concrete age of 56 days is the highest for Mix 6, which was very closely followed by Mix 8. The total shrinkage values of Mix 6-1.0SR and Mix 8-CM90 were very close, and they were much lower than Mixes 6 and 8. This is consistent with results in Figure 5.35.

5.6.4 Strains of Bridge Overlays

As illustrated in Figure 5.9, four strain gages for each overlay mix studied were installed in the transverse direction (perpendicular to the traffic direction) of the bridge at a distance of 3 ft to 74

ft 7 in. from the abutment. One strain gage was installed in the longitudinal direction (parallel to the traffic direction) of the bridge at a distance of 74 ft 7 in. from the abutment. All strain gages worked during the entire monitoring period, except one on a girder that stopped providing readings during the monitoring period. Figures 5.36 and 5.37 show the strain values of all the overlay mixes studied. As the concrete in the bridge overlay was under a restrained condition, positive strain indicates that the concrete was in tension and negative strain indicates that the concrete was in compression.

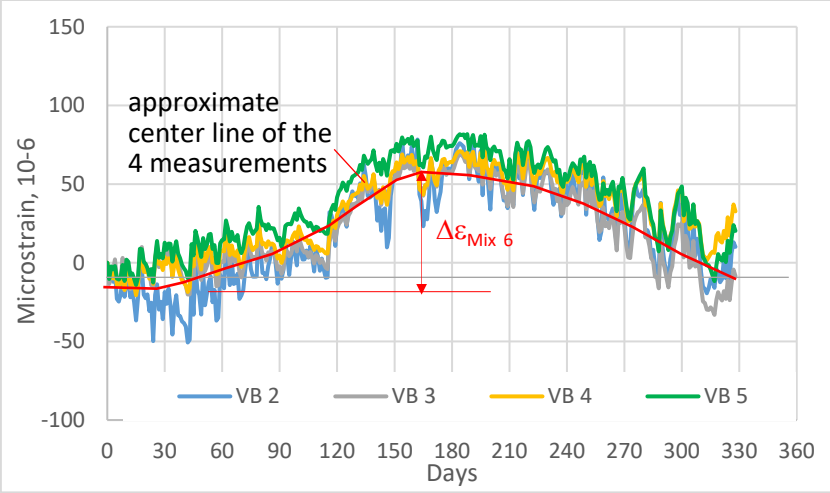

(a) Mix 6 (constructed on Day 0)

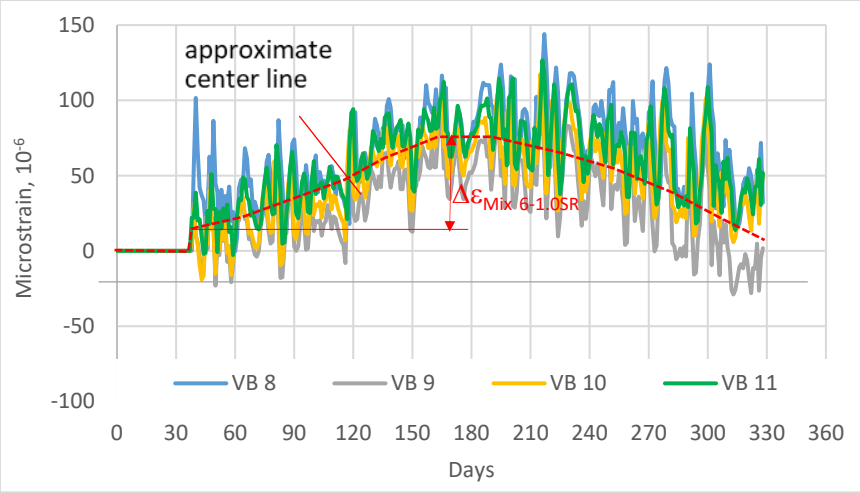

(b) Mix 6-1.0SR (constructed on Day 38)

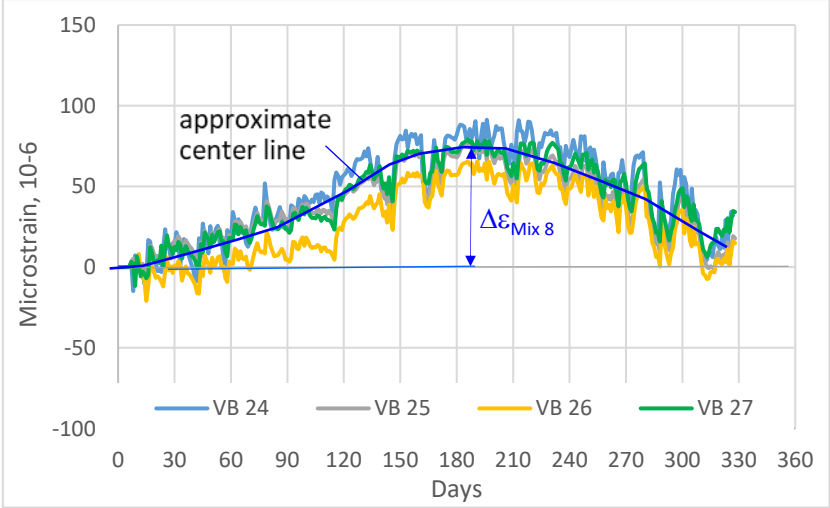

(c) Mix 8 (constructed on Day 6)

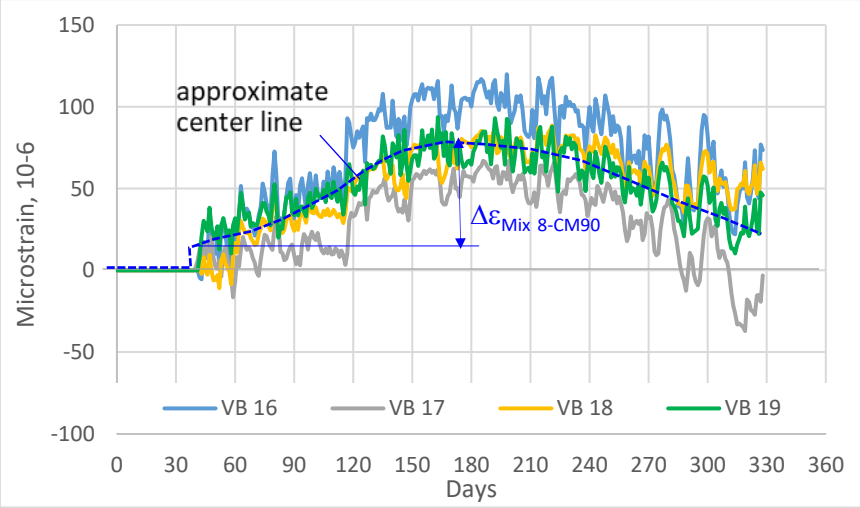

(d) Mix 8-CM90 (constructed on Day 40)

Figure 5.36. Strain gage readings at various locations of overlays in the transverse direction

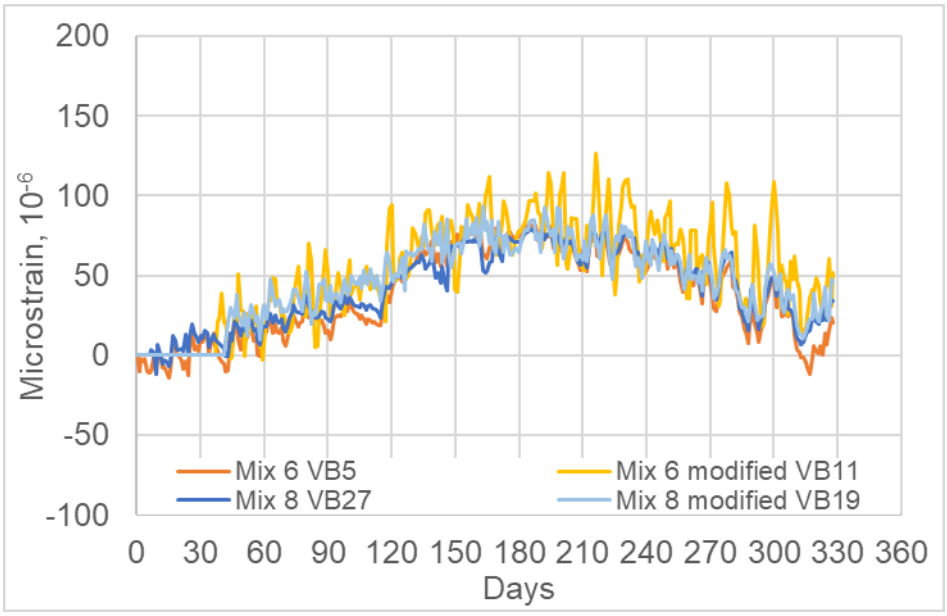

(a) Strain gages in transverse direction

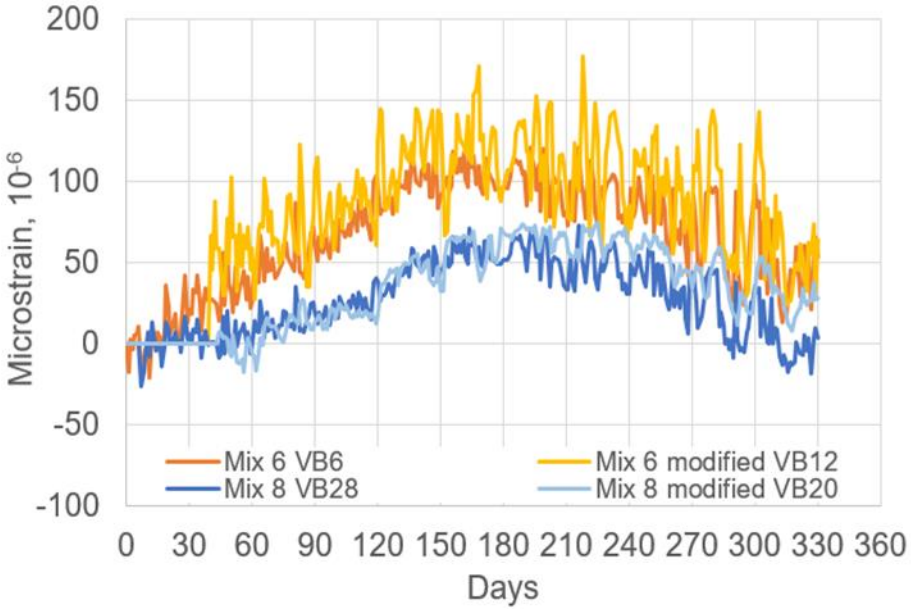

(b) Strain gages in longitudinal direction

Figure 5.37. Comparison of strains in different concrete mixes

It was noted that the strains measured by the embedded strain gages in the field concrete decks resulted from the combined effects of cementitious hydration (autogenous deformation), the exposed condition (drying/wetting and thermal expansion/contraction), mechanical loading (structural and traffic loads), and creep behavior. The bridge deck concrete was under a strained condition. The following observations can be made from Figures 5.36 and 5.37:

- The strain values ranged from -50 to +150 microstrain for all strain gages embedded in overlays. The value captured was similar to those in studies by Wells (2005), Asbahan

(2009), Qin (2011), and Nassiri (2011), who found typical strain values range from -150 to +150 microstrain in response to environmental loads.

- The shapes of all the strain curves were similar, and they were all opposite to the shape of the ambient temperature curve in Figure 5.32. For all mixes studied, the highest tensile strains (positive strains caused by shrinkage) occurred in the wintertime (around Day 180). Some compressive strains (negative strains caused by expansion) were seen in the summertime (around Day 0 and Day 330). This indicated that the thermal strain dominated the strain in the concrete. More compressive strains (exhibiting large values in a relatively long time) were seen in the overlay made with the original Mix 6, which had the highest cement content, or potentially the highest heat of cement hydration, and was constructed on the hottest day of the sensor monitoring period.

- The strain curves from the strain gage measurements all displayed fluctuations that corresponded to the daily temperature changes in the ambient temperature curve. However, researchers noticed that Mix 6-1.0SR had much larger daily strain fluctuations (in both transverse and longitudinal sensor readings) than the other mixes studied. It is not clear if this was related to the addition of SRA, and further study is needed.

- For sensors embedded in a given concrete mix in the bridge's transverse direction, strain readings were expected to be very similar or not significantly influenced by the sensor locations. The sensors in the transverse cross section were part of the concrete deck supported by the same girders, regardless of its distance from the abutment. However, Figure 5.36 shows some differences. For example, the strain readings of VB2-VB5 were not overlapped. For the overlays made with original mixes (Figures 5.36a and c, Mixes 6 and 8), the differences in the transverse strain readings among the sensors at different locations were quite small. These two overlays were constructed on June 22 and 28, 2016, respectively, when the ambient temperature was relatively high (> 25°C during the first 7 days). For the overlays made with modified mixes (Figures 5.36b and d, Mixes 6-1.0SR and 8-CM90), the differences in the transverse strain readings among the sensors at different locations appeared relatively large. These two overlays were constructed on August 29 and 31, 2016 respectively, when the ambient temperature was lower (mostly < 25°C during the first 7 days). This may imply that condition and concrete maturity at early age can significantly affect long-term strain behavior.

- To filter the effects of the variations in strain readings from transverse strain gages in different locations of a given mix, an approximate centerline was drawn for each concrete mix studied (as shown in Figure 5.36). By comparing the centerline curves, it appears that although the mini slab study showed that Mix 6 had the highest shrinkage among all mixes, the maximum tensile strain obtained from the average of 4 transverse strain gages (Figure 5.36a) appeared lower than that of Mix 6-1.0SR. This is possibly because Mix 6 had a negative (compressive) strain due to the concrete expansion caused by heat of hydration and hot weather at an early age, and the tensile strain generated by the shrinkage of the concrete due to drying and frost had to offset the compressive strain. As a result, the absolute strain difference ($\Delta\varepsilon$) for Mix 6 was the highest among all mixes studied. Mix 8 had the second

highest Δε, while Mix8-CM90 and Mix 6-1.0SR had similar Δε values. This trend is consistent with the order of strains of mini slabs.

- Figure 5.37 provides comparisons of strains in different concrete mixes at the locations 74 ft 7 in. from the abutment in both transverse and longitudinal directions. It can be seen from Figure 5.37(a) that in the transverse direction the strain behaviors of concrete made with different mixes were very similar. However, in the longitudinal direction (Figure 5.37b), the strains of concrete overlays made with Mixes 6 and 6-1.0SR were much larger than those of overlays made with Mixes 8 and 8-CM90 in the longitudinal direction, and they were also larger than the strains of the corresponding concrete mixes in the transverse direction. As mentioned previously, the field strains measured by strain gages resulted from the combined effects of cementitious hydration, exposure to environmental conditions, mechanical/traffic loads, and creep behavior. The combinations may be complex, and more stress analyses should be conducted to verify the potential for overlay cracking. In this study, only one set of strain gages was installed longitudinally and it would be desirable if more strain gages were installed in the longitudinal direction of each concrete mix.

5.6.5 Strains of the Bottoms of Decks and Girders

At the location 74 ft 7 in. from the west abutment, one strain gage was mounted on the bottom surface of the bridge deck with the overlay of Mix 6-1.0SR, and another was affixed on the bottom surface of the bridge deck with the overlay of Mix 8-CM90. Both of the sensors on the bottom surfaces of the decks were mounted in the transverse direction. In addition, one strain gage was mounted on the web of a girder under the deck with an overlay of Mix 6-1.0SR, and another gage was stationed on the web of a girder under the deck with overlay of Mix 8-CM90. Both the sensors on the girders were fixed in the longitudinal direction, along with the length of the girders. As those sensors were mounted on the unprotected deck and girder surfaces, they were exposed to a harsh environment. The sensor on the girder under the deck with the overlay of Mix 8-CM90 stopped providing readings during the bridge monitoring period. The results from the strain gages on the surface of bottoms of the bridge decks and girders are presented in Appendix B since the strain readings might not be reliable due to the effects of harsh weather conditions.

6. SUMMARY, CONCLUSIONS, AND RECOMMENDATIONS

6.1 Research Activities

This project consisted of two parts: a laboratory investigation and a field investigation. In the laboratory investigation, shrinkage behaviors of three different Iowa HPC mixes (Mix 6, Mix 8, and Mix 2) classified as having high, medium, and low shrinkage cracking potential in the Phase I study were modified using different shrinkage control methods. The modification methods involved use of differing amounts of SRA and SCA for Mix 6, CM reductions for Mix 8, and internal curing agents (LWFA and SAP) for Mix 2. The autogenous, free drying, and restrained shrinkage behaviors of both the original and modified mixes were evaluated. (Note: Since the concrete materials, including sources of cementitious materials and types/sources of aggregates, used in Phase II were different from those in Phase I, the shrinkage behavior of the original mixes also changed.) Based on the shrinkage test results, the optimal amounts of the modification agents were determined, and they were 1.25 gal/yd^3 of SRA for Mix 6, 90% CM reduction for Mix 8, and 34%LWFA for Mix 2. Then, the fresh concrete properties (such as slump, air content, and unit weight), the mechanical properties (such as compressive strength, elastic modulus, splitting tensile strength, surface resistivity, and creep behavior), and F-T durability were evaluated for both the original mixes (Mixes 6, 8, and 2) and modified mixes (Mixes 6-1.25SR, 8-CM90, and 2-34% LWFA).

The field investigation was conducted on the US 20 over I-35 dual bridge, where Mix 6 and Mix 6-1.0SRA (instead of Mix 6-1.25SR) as well as Mix 8 and Mix 8-90CM were placed side by side on the bridge overlays in the west- and eastbound sections, respectively. Quality control properties, construction conditions, and procedures used for the field project were recorded. Twenty-four strain gages and 8 moisture sensors were installed in the bridge's new concrete overlays. The moisture sensors were calibrated in the laboratory to coordinate with the field concrete moisture conditions. A thermocouple was placed under the bridge decks and it monitored the ambient temperature of the bridge. The sensor monitoring time was approximately one year. In addition, the mechanical and F-T durability properties of field-cast concrete samples were tested, and the results were compared with those of laboratory-cast concrete samples. Visual examinations were conducted on the concrete surfaces before, during, and one year after the overlay construction, and crack size and pattern were recorded.

6.2 Results and Observations from Laboratory Investigation

6.2.1 Shrinkage Behavior of HPC Mixes Studied

The autogenous, free drying, and restrained shrinkage behaviors were evaluated for both the original and modified mixes studied. Figure 6.1 summarizes the free shrinkage behavior of the concrete mixes modified with different amounts of SRA for Mix 6, cementitious material (CM) reductions for Mix 8, and LWFA as the IC agent for Mix 2.

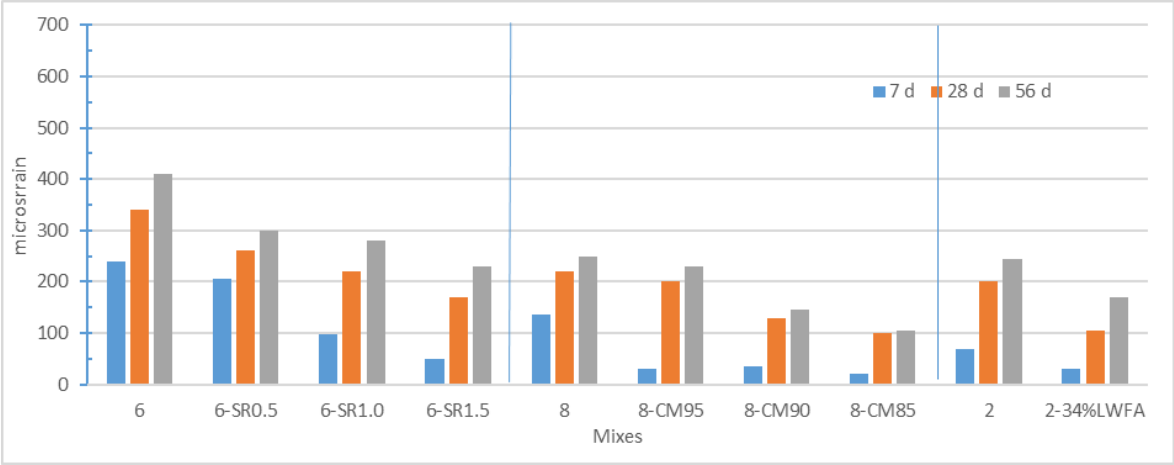

(a) Autogenous shrinkage

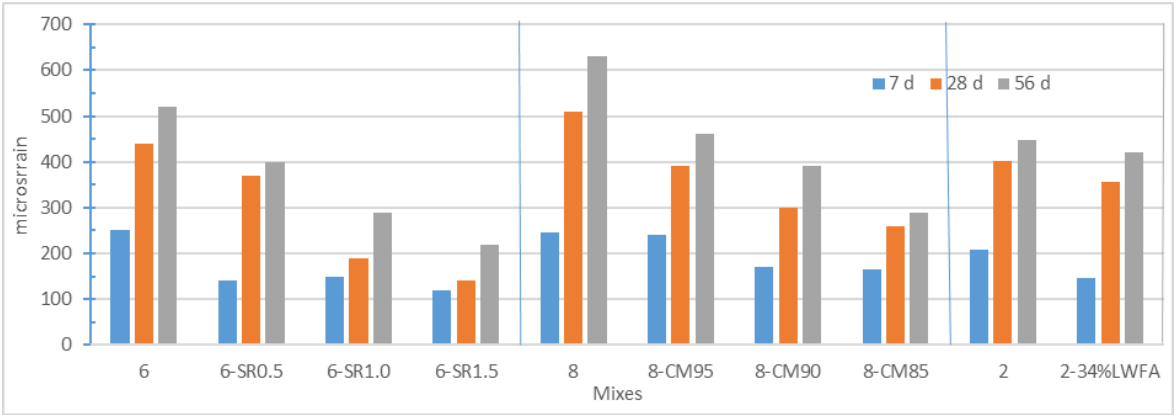

(b) Free drying shrinkage

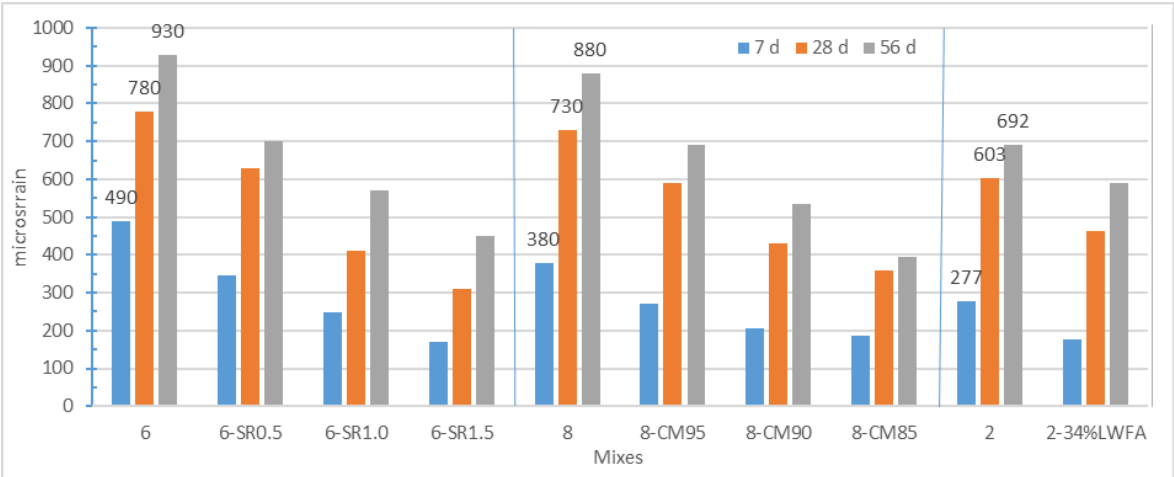

(c) Total shrinkage (autogenous + free drying shrinkage)

Figure 6.1. Shrinkage behaviors of different mixes at given ages

Use of SCA at the binder dosage of 2.5% to 7.5% did not effectively reduce the stress rate of Mix 6. The SRA and use of SAP did not provide consistent results in this study; therefore, those

shrinkage control methods were not studied in detail, and their results are not included in this section. Figure 6.2 summarizes the restrained ring shrinkage behavior of the concrete mixes.

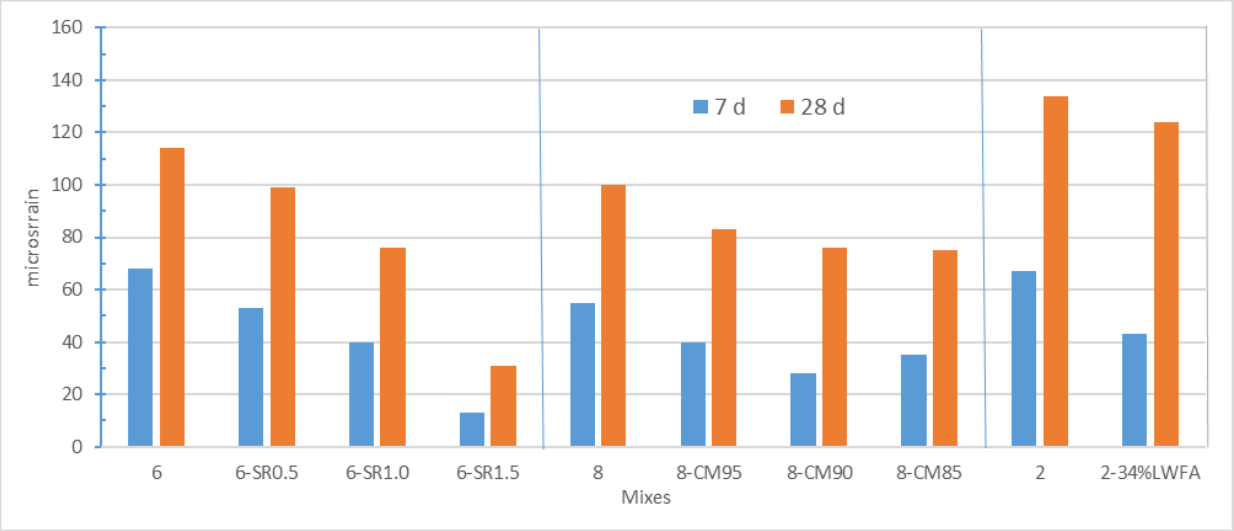

Figure 6.2. Restrained ring shrinkage behaviors of different mixes at given ages

The following observations can be made from these figures:

- The total shrinkage values (autogenous and free drying shrinkage) of the original mixes studied in Phase II ranged from high to low, Mix 6 > Mix 8 > Mix 2. This was similar to the observations from the Phase I study. Mix 6 (HPC-O, w/c = 0.33) had the highest autogenous shrinkage, Mix 8 (HPC-O-C20-S25, w/b ratio = 0.42) had the highest free drying shrinkage, and Mix 2 ((HPC-O-C20, w/b ratio = 0.42) had the highest ring shrinkage, especially at 28 days. (None of the ring samples made with these mixes cracked.)

- Increasing the amount of SR addition (from 0.5% to 1.5%) in Mix 6 noticeably reduced both autogenous and free drying shrinkage at all ages. Cementitious material reduction in Mix 8 from 5% to 15% decreased the shrinkage, especially the free drying shrinkage. Use of 34% LWFA replacement in Mix 2 significantly reduced autogenous shrinkage but only slightly decreased free drying shrinkage. Internal curing appeared to be more effective in reducing autogenous shrinkage of concrete.

6.2.2 Mechanical Properties of HPC Mixes Studied

The mechanical properties, including compressive strength, splitting tensile strength, elastic modulus, surface resistivity, and creep behavior, were evaluated for all original mixes (Mixes 6, 8, and 2) and selected modified mixes (Mixes 6-1.25SR, 8-CM90, and 2-34% LWFA). Figure 6.3 summarizes the strength and elastic modulus test results of these mixes, and Figure 6.4 summarizes the creep behavior of these mixes.

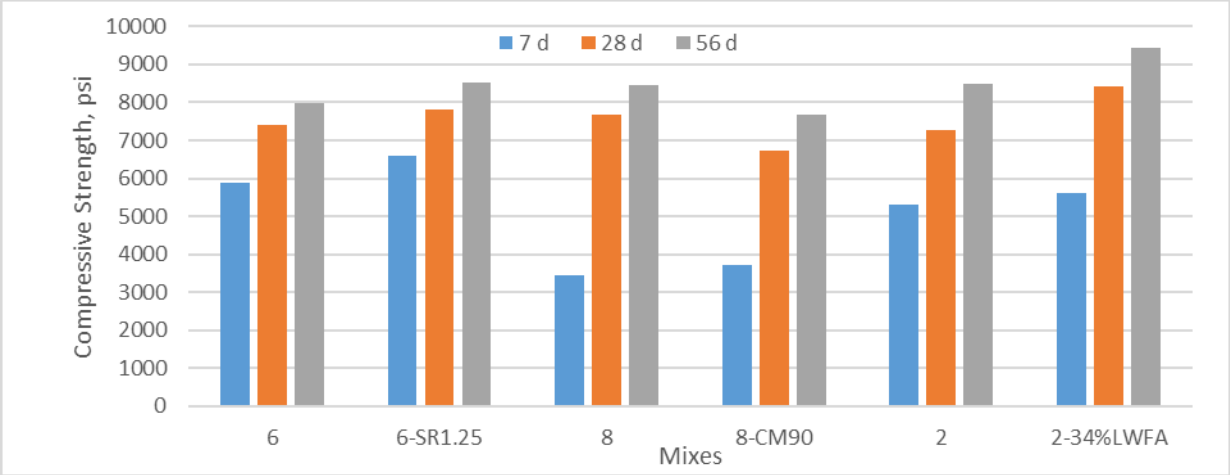

(a) Compressive strength

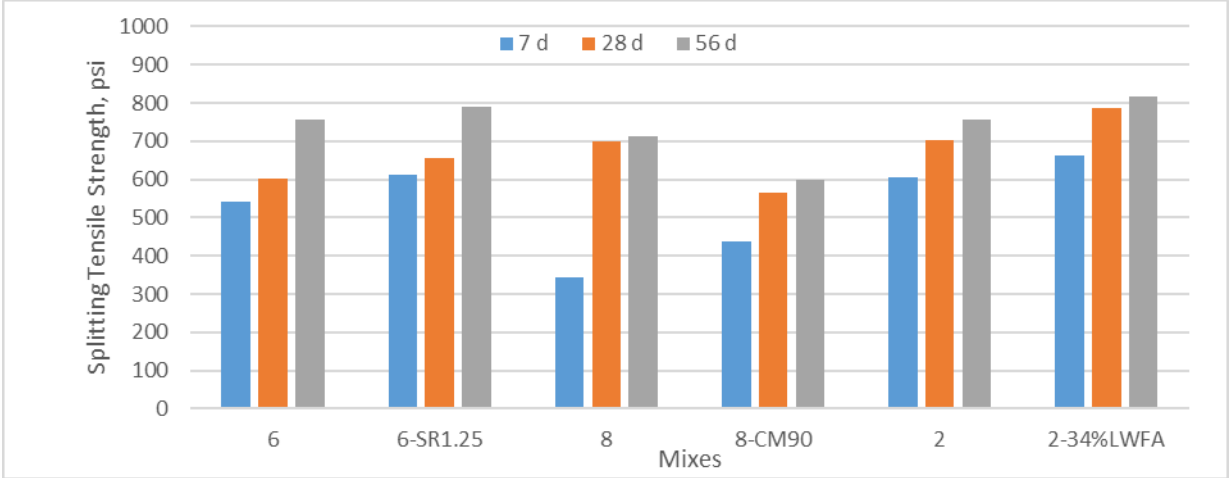

(b) Splitting tensile strength

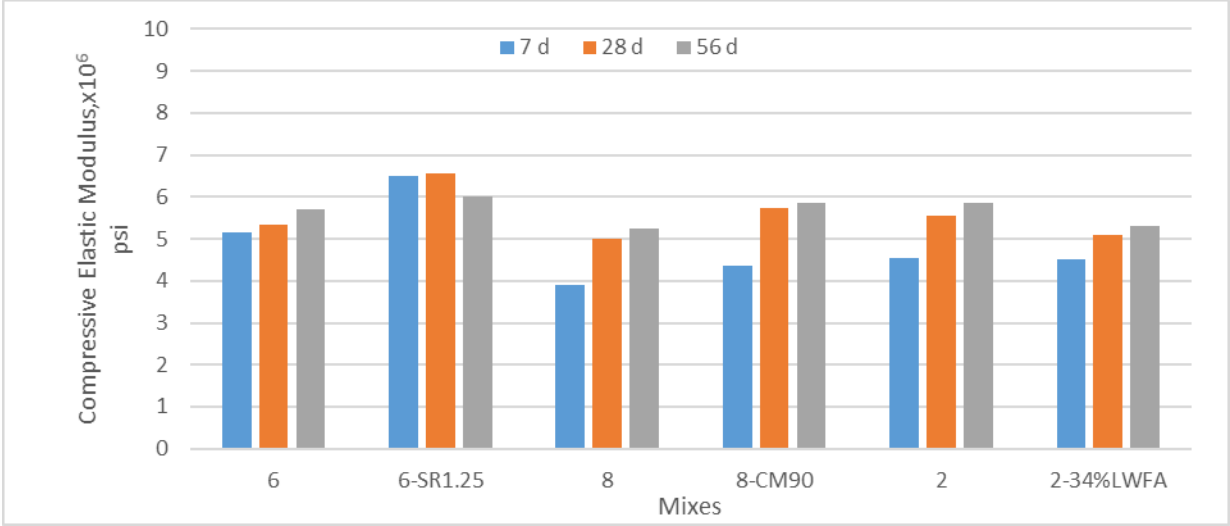

(c) Compressive elastic modulus

Figure 6.3. Strength and elastic modulus of selected mixes

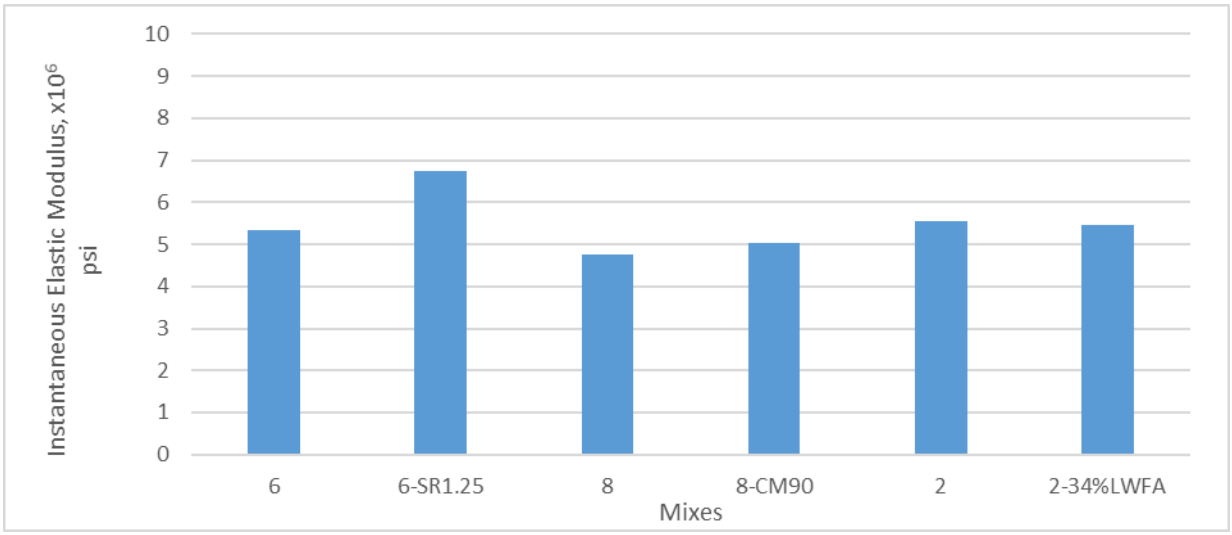

(a) Instantaneous elastic modulus

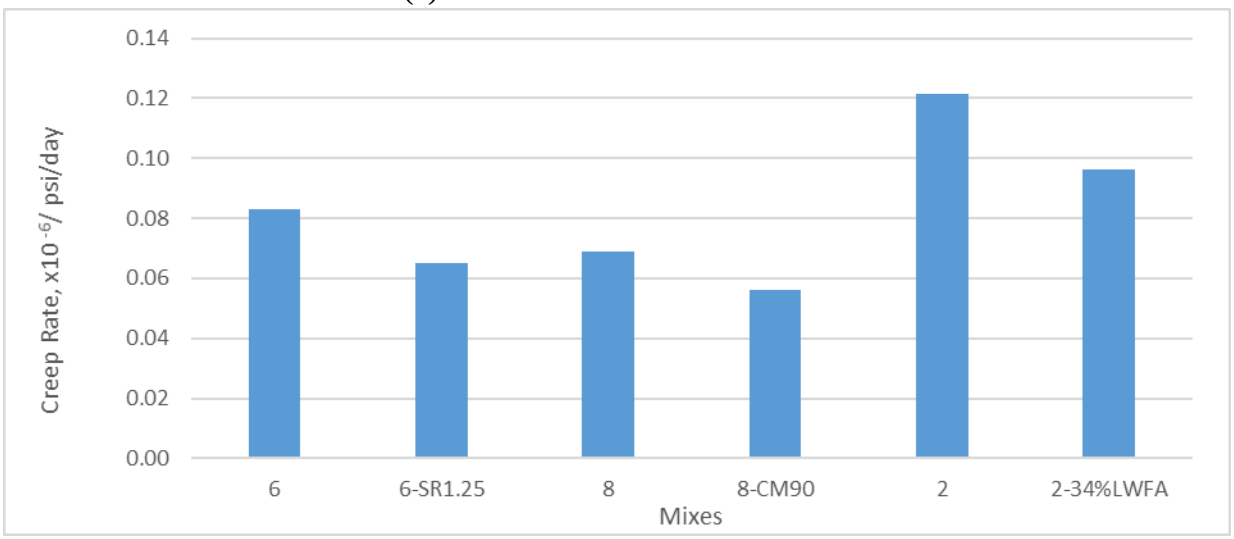

(b) Creep rate

Figure 6.4. Creep behavior of selected mixes

The following observations can be made from these figures:

- When compared with the corresponding original mixes, addition of SR in Mix 6 and use of LWFA in Mix 2 increased the concrete strength, while cementitious material reduction in Mix 8 decreased the concrete strength.

- Addition of SR in Mix 6 also increased the elastic modulus of the concrete, probably due to the increase in its strength. Cementitious material reduction in Mix 8 also increased the elastic modulus of the concrete, probably due to the increased aggregate content. However, use of LWFA to replace sand in Mix 2 reduced the elastic modulus of the concrete as the LWFA had lower elastic modulus than sand.

- There was a very good relationship between compressive and splitting tensile strength of the concrete mixes.

- The trend of the instantaneous elastic modulus measurements was similar to that of the compressive elastic modulus.

- All modified mixes had a lower creep rate than their original mixes, which might be mainly related to the increased strength of the mixes (Mixes 6-1.25SR and 2-34%LWFA) at the time of loading or increased aggregate content (Mix 8-CM90). Further study is needed to find out why Mix 2 and Mix 2-34% LWFA exhibited much higher creep rates than other mixes.

6.2.3 Durability-Related Properties of HPC Mixes Studied

The durability properties, including surface resistivity and F-T durability, were evaluated for all original mixes (Mixes 6, 8, and 2) and selected modified mixes (Mixes 6-1.25SR, 8-CM90, and 2-34% LWFA). Figure 6.5 summarizes the test results.

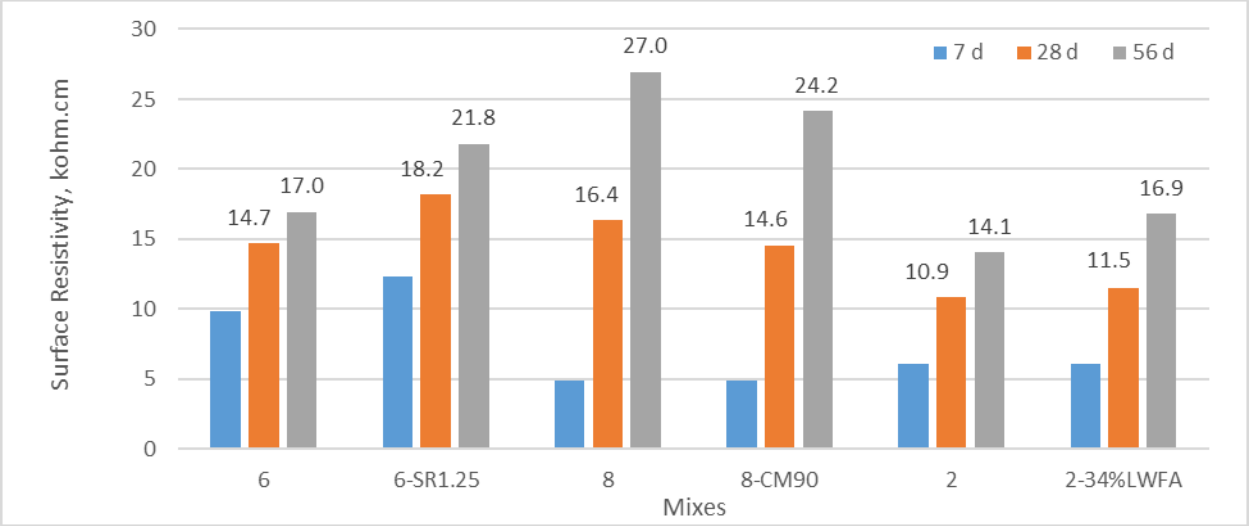

(a) Surface resistivity

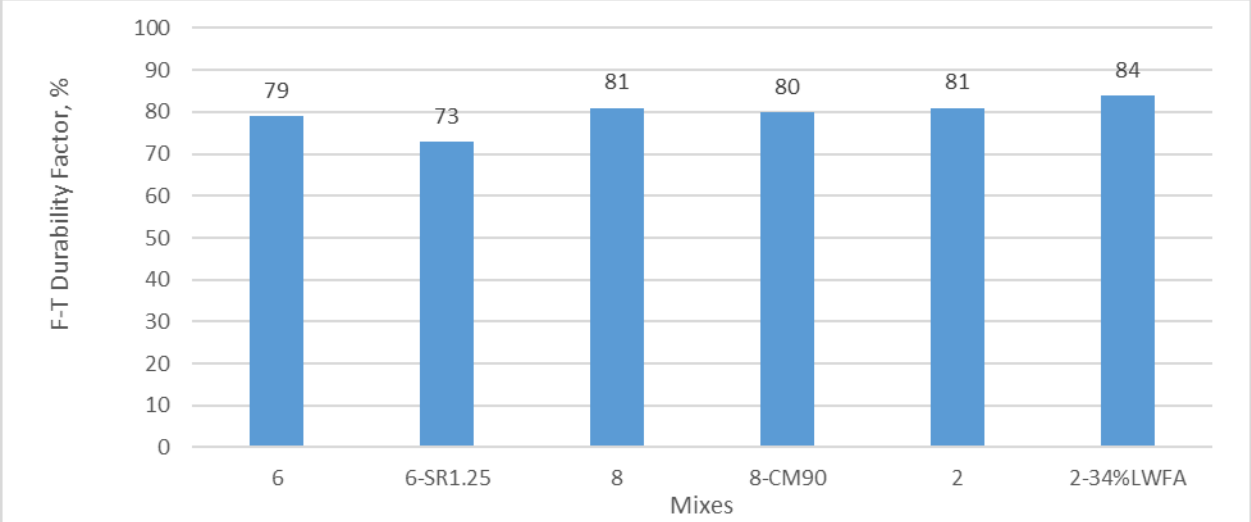

(b) F-T durability factor at 300 cycles

Figure 6.5. Durability properties of selected mixes

The following observations can be made from the figure:

- Most mixes studied had a surface resistivity value higher than 12 kΩ-cm after 28 days, indicating moderate permeability, except for Mix 2 (HPC-O-C20), which had a surface resistivity value higher than 12 kΩ-cm after 56 days. This could be due to the slow FA hydration.

- Among the mixes studied, Mix 2 (HPC-0-S20-C20) and Mix 2-CM90 had noticeably higher surface resistivity values than other mixes, which is likely related to the slag used in the mixes. (GGBSF is often effective in refining concrete pore structure.)

- Similar to the trend of strength improvement, when compared with the corresponding original mixes, addition of SRA in Mix 6 and use of LWFA in Mix 2 increased surface resistivity, while cementitious material reduction in Mix 8 generally reduced the surface resistivity of the concrete. (It has noted that although surface resistivity reflects impermeability of concrete, which is not necessarily related to concrete strength but more related to concrete pore structure, higher strength concrete often has higher surface resistivity due to low porosity and refined pore structure.)

- When compared with the corresponding original mixes, Mix 6-1.0SR reduced F-T durability slightly as reported by previous researchers. Mix 8-CM90 had F-T durability comparable to the original Mix 8. Mix 2-34%LWFA slightly improved the concrete F-T durability due to enhanced cement hydration. The differences in the DF values between the original and modified mixes were not significant.

6.3 Results and Observations from the Field Investigation

The field investigation was conducted on the US 20 over I-35 dual bridge. At the field site, Mix 6 and Mix 6-1.0SR (instead of Mix 6-1.25SR, as used in the extended laboratory investigation) were placed side by side as the new overlays on the westbound bridge and Mix 8 and Mix 8-90CM were placed side by side on the eastbound bridge. The original Mix 6 and Mix 8 were placed on July 22 and 28, 2016, respectively, and they were designated as Stage 1 construction (slower and slowest traffic lanes). The modified mixes, Mix 6-1.0SR and Mix 8-CM90, were placed on August 29 and 31, 2016, respectively, and they were designated as Stage 2 construction (fastest traffic lanes).

6.3.1 Properties of Field Samples

For each field concrete mix, 20 cylinders, 3 prisms, and 1 mini slab were cast on site. After being demolded after 1 day, 3 cylinders were cured on the field site, and 17 cylinders were cured in the ISU Portland Cement Concrete Research Laboratory (at 25°C and 99% RH). Compressive strength of the field-cast, laboratory-cured cylinders was tested at 1, 3, 7, 14, and 28 days, and the CTE of the cylinders was tested at 7 and 28 days. The 3 field-cured cylinders were also tested for compressive strength at 28 days. Table 6.1 summarizes the compressive strength, free drying shrinkage, and CTE test results of laboratory and/or field samples at 28 days.

Table 6.1. Comparisons of properties of field and laboratory samples

Mix	28-day compressive strength, psi		
	Lab-cast and lab-cured samples (lab investigation)	Field-cast and lab-cured samples	Field-cast and field-cured samples
6	7410	8016	8422
6-1.0 or 1.25SR	7817 (1.25SR)	8143 (1.0SR)	7931 (1.0SR)
8	7672	8795	9059
8-CM90	6729	9486	6490
Mix	**28-day free drying shrinkage, microstrain**		**28-day CTE, $\times 10^{-6}$/°C**
	Lab-cast and lab-cured samples (lab investigation)	**Field-cast and field-cured samples**	**Field-cast and lab-cured samples**
6	440	440	7.09
6-1.0 or 1.25SR	187 (1.25SR)	302 (1.0SR)	6.93 (1.0SR)
8	510	502	8.36
8-CM90	300	390	7.70

Note: Laboratory-cast samples had the same types of concrete materials and mix proportions but different sources of concrete materials from the field-cast samples. Field samples were cast on different dates. Field-cast, laboratory-cured samples were those cured in the field in molds for 1 day and then brought to the ISU Portland Cement Concrete Research Laboratory for standard curing until testing. Field-cured samples were those cured in field for 28 days before testing.

The following observations can be made based on the results shown in the table:

- Mix 6-1.0SR samples that were cast and cured in the field for 28 days had lower (rather than higher) strength than the original Mix 6 samples that were cast and cured in the field for 28 days. This differed from the results of the laboratory-cast and laboratory-cured samples in the laboratory investigation. Mix 8-CM90 samples that were cast and cured in the field for 28 days had much lower (rather than slightly lower) strength than the original Mix 8 samples that were cast and cured in the field for 28 days. (The strength reduction was 28% for field-cast and field-cured samples and 12% for laboratory-cast and laboratory-cured samples.) These differences were strongly attributed to the field curing conditions for the concrete samples. The overlays made with the original mixes (Mix 6 and Mix 8) were placed in hotter weather conditions than the modified mixes (Mix 6-1.0SR and Mix 8-CM90).

- There were some differences in 28-day compressive strength between the laboratory-cast and laboratory-cured samples in the laboratory investigation and the field-cast and laboratory-cured samples in the field investigation. These differences were attributed mainly to the different material sources and the casting and first-day curing conditions.

- The field Mix 6-1.0SR and Mix 8-CM90 samples were cast and cured in the field for 1 day and then brought to the ISU Portland Cement Concrete Research Laboratory, where they were demolded, and cured in the standard laboratory curing condition for 6 more days. These modified mix samples had lower free drying shrinkage values than the original Mix 6 and

Mix 8 field samples that were cast and subjected to the same curing and drying conditions. This trend is similar to what was observed from the results of the laboratory-cast and laboratory-cured samples in the laboratory investigation. However, the degrees of shrinkage reduction for the Mix 6-1.0SR and Mix 8-CM90 field samples were lower than the degrees of shrinkage reduction of the laboratory-cast and laboratory-cured samples. Further examination is necessary to explain the test results.

- Based on the 28-day test results of the field-cast and laboratory-cured samples, Mixes 8 and 8-CM90 had noticeably higher CTE values than Mixes 6 and 6-1.0SR, probably due to the slag replacement in the Mix 8 series. Mix 6-1.0SR had a similar (slightly lower) CTE value to Mix 6. Mix 8-CM90 had an 8% lower CTE value than Mix 8.

6.3.2 Results from Field Crack Surveys

Visual inspections were performed on the surface of the bridge decks before, after, and one year after the new overlay construction. The following results were found:

- Before overlay construction, map cracks, longitudinal cracks, and potholes were found on the deck surface in Stage 1, and longitudinal cracks, transverse cracks, spalling, and joint deterioration were observed on the deck surface in Stage 2.

- No cracks were found on any of the new overlays before the bridge was opened to traffic.

- One year after the new overlays began service, several cracks were found on the overlays made with the original Mix 6, and a couple of cracks appeared on the overlay made with the original Mix 8. The crack widths ranged from 0.3 mm to 1 mm.

- Figure 6.6 shows the comparison of crack types and locations found before and after overlay construction. It was not clear if any cracks on the new overlays were related to the cracks in the old bridge decks, since some cracks might not be well identified on milled concrete surfaces.

- No cracks were found on the overlays made with the modified mixes (Mix 6-1.0SR and Mix 8-CM90).

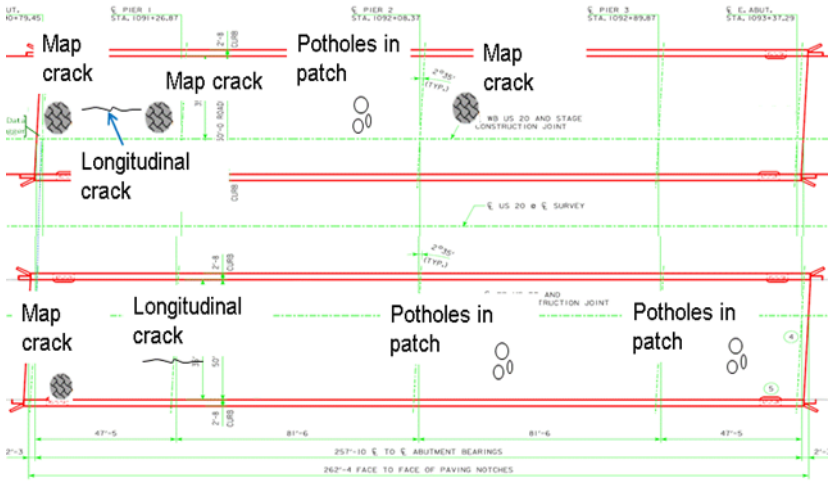

(a) Cracks found in Stage 1 milled decks just before overlay construction

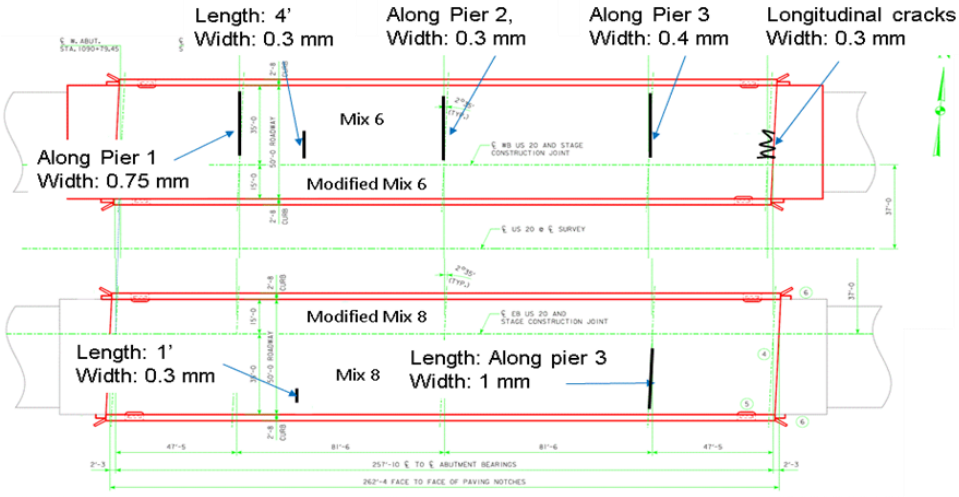

(b) Cracks found in Stage 1 overlays one year after the construction

Figure 6.6. Comparison of crack types and locations found before and after overlay construction

6.3.3 Results from Field Sensor Monitoring

Three types of sensor monitoring were conducted in this field investigation: (1) moisture sensor monitoring in bridge overlays, (2) free shrinkage strain monitoring in unrestrained mini slabs, and (3) restrained strain monitoring in bridge overlays. Figure 6.7 summarizes the results from the moisture sensor readings. Table 6.2 lists maximum compressive strain values of all mini slabs studied. Figures 5.36 and 5.37 illustrated the strains monitored in the bridge overlays studied.

Table 6.2. Maximum compressive strain in mini slabs

Mix	Maximum compressive strain
6	344
6-1.0 or 1.25SR	197
8	298
8-CM90	233

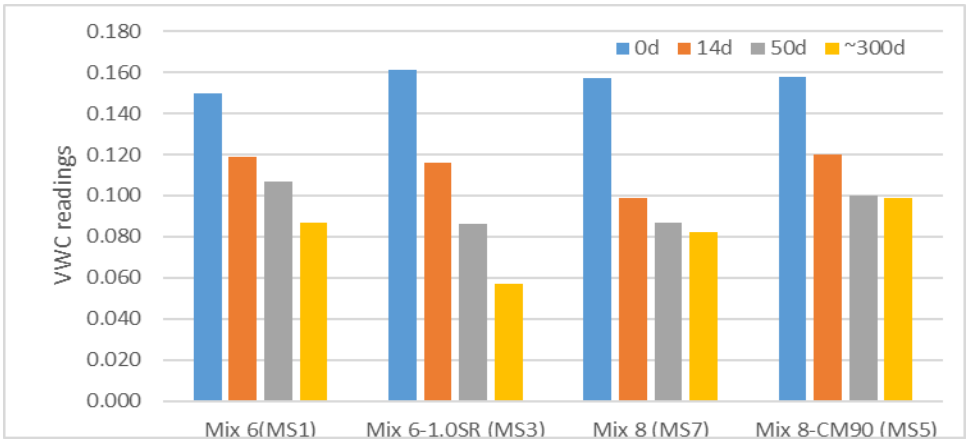

(a) Sensor location: 23 ft 8 in. from the abutment

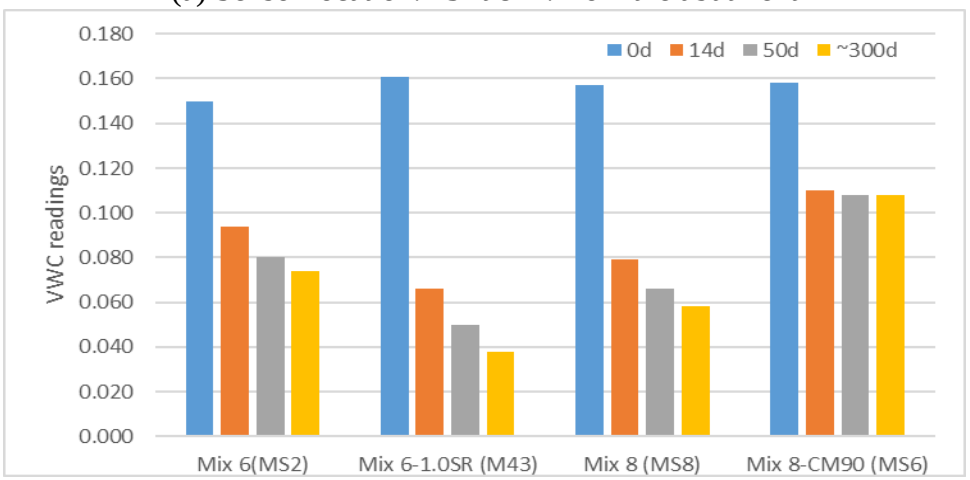

(b) Sensor location: 74 ft 7 in. from the abutment

Figure 6.7. Comparison of moisture sensor readings on different days

The following observations emerged from the field sensor monitoring:

- Moisture sensors generally did a good job in capturing the moisture conditions for the overlays studied. The moisture content in all overlay concrete mixes dropped rapidly in the first 14 days, largely due to cement hydration, and gradually stabilized. At a given time after the overlay construction, the moisture content in the concrete near the abutment/joint was noticeably higher and took a little longer to become stable. Meanwhile, the moisture content

in concrete further away from the abutment/joint was lower and became stable relatively quickly.

- The stable moisture content (~300 days in Figure 6.7) was the highest for Mix 8-CM90, which might be associated with the pore structure of the concrete, and the lowest for Mix 6-1.0SR, which might be a function of the SRA used.

- Maximum free shrinkage strain readings (caused by drying and thermal changes) in the mini slabs made with Mix 6, Mix 8, Mix 8-CM90, and Mix 6-1.0SR were 345, 298, 233, and 197 microstrain, respectively. This order is consistent with the results of the crack survey conducted a year after the overlay construction. (Figures 5.6 and 6.6 showed that five cracks were found on the overlay made with the original Mix 6 and two cracks appeared on the overlay made with the original Mix 8. No cracks were found in the modified mixes.)

- The strains measured by the embedded strain gages in the field concrete overlays resulted from the combined effects of cementitious hydration (autogenous deformation), the exposed conditions (drying/wetting and thermal expansion/contraction), mechanical loading (structural and traffic loads), and creep behavior. The overall shapes of all the strain curves were similar, and they were all opposite to the overall shape of the ambient temperature curve in Figure 5.32. This indicated that thermal strain dominated the strain presence in the concrete.

- For a given concrete mix, there were slight variations in strain readings from the gages installed in the transverse direction of the bridge at locations at different distances from the abutment/joint. At the locations 74 ft 7 in. from the abutment, there were also only small variations in the strain readings from the gages in the transverse direction of the bridge decks made with different concrete mixes. However, at the same locations, strains in the longitudinal direction of concrete overlays made with Mixes 6 and 6-1.0SR were much larger than those of longitudinal overlays made with Mixes 8 and 8-CM90. They were also larger than the strains of the corresponding concrete mixes in the transverse direction. More detailed stress analyses should be conducted to help explain the field concrete strain data and to verify the overlay cracking potential.

6.4 Major Findings

The following major conclusions can be drawn from this project.

6.4.1 Effects of Shrinkage Control Methods on Concrete Properties

Effects on Shrinkage

- Addition of 1.0 or 1.25 gal/yd^3 of SRA in Mix 6 reduced 28-day autogenous shrinkage by approximately 30%, 28-day free drying shrinkage over 50%, and the stress rate of restrained ring shrinkage by 60%.

- The 10% cementitious material reduction in Mix 8 decreased 28-day autogenous shrinkage and free drying shrinkage by approximately 40% and the stress rate of restrained ring shrinkage by 13%.

- Use of 34% LWFA as an IC material to replace fine aggregate in Mix 2 reduced 28-day autogenous shrinkage by 47.5%, 28-day free drying shrinkage by only 11%, and the stress rate of restrained ring shrinkage by only 1.3%.

Effects on Mechanical Properties

- Addition of 1.0 or 1.25 gal/yd^3 of SRA in Mix 6 increased 28-day compressive strength by approximately 5%, splitting tensile strength about 9%, and compressive elastic modulus by around 22%. It decreased the concrete creep rate by almost 22%.

- The 10% cementitious material reduction in Mix 8 decreased 28-day compressive strength by approximately 12% and splitting tensile strength about 19% but increased compressive elastic modulus by around 15% and creep rate by almost 18%.

- Use of 34% LWFA as an IC material to replace fine aggregate in Mix 2 increased 28-day compressive strength by approximately 15% and splitting tensile strength about 12% but decreased compressive elastic modulus by around 8% and creep rate by almost 21%.

Effects on Durability

- Addition of 1.0 or 1.25 gal/yd^3 of SRA in Mix 6 increased concrete surface resistivity by approximately 24% but decreased the concrete F-T durability factor by almost 8%.

- The 10% cementitious material reduction in Mix 8 decreased concrete surface resistivity by approximately 11% but had little effect on the concrete F-T durability factor.

- Use of 34% LWFA as an IC material to replace fine aggregate in Mix 2 increased concrete surface resistivity by about 5% and the F-T durability factor by nearly 4%.

6.4.2 Field Performance of Concrete Overlays with and without Shrinkage Control

- Cracks were observed on the overlays made with both original HPC mixes (five cracks for Mix 6 and two cracks for Mix 8) after the repaired bridge had been opened to traffic for about one year.

- No cracks were found on the overlays made with the modified mixes (Mix 6-1.0SR and Mix 8-CM90) after the repaired bridge had been opened to traffic for about one year.

- There are some differences in compressive strength between the laboratory-cast, laboratory-cured samples and the field-cast, laboratory-cured samples for a given mix. The results suggested that the environmental conditions of the casting day and the first few days of curing play an important role in development of the concrete properties.

6.4.3 Field Sensor Monitoring

Moisture Content

- Moisture sensors generally did a good job of capturing the major changes in the moisture conditions of the overlays studied. The concrete moisture content decreased rapidly at an early age (before 14 days), mainly due to cement hydration, and then gradually became stable.

- The moisture profiles varied noticeably among different concrete mixes that were placed at different dates.

- For the same mix, the concrete near the abutment/joint had higher moisture content and took a little longer to become stable than the same concrete farther away from the abutment.

Strain in Mini Slabs

- The strain measurements of the mini slabs provided valuable information on concrete strain under an unrestrained condition, free of mechanical/traffic loading. The measurements showed that the maximum strain was the highest and second highest in the mini slabs made with Mix 6 and Mix 8, respectively, which might be responsible for the cracks observed on the corresponding overlays one year after the overlay construction.

Strain in Overlays

- Strains monitored from concrete overlays in the transverse direction appeared not to vary significantly from the concrete mixes.

- Strains monitored from concrete overlays in the longitudinal direction made with Mixes 6 and 6-1.0SR were similar, and they were much higher than the strains monitored from concrete overlays made with Mixes 8 and 8-CM90, which were also similar to each other.

- Strains monitored by the embedded strain gages in the field concrete overlays resulted from the combined effects of cementitious hydration (autogenous deformation), the exposed conditions (drying/wetting and thermal expansion/contraction), mechanical loading (structural and traffic loads), and creep behavior. Comprehensive combinations of these effects might have made the strain readings more complex.

Ambient Temperature

- Having the year-round ambient temperature monitored by a thermocouple provided vital information for concrete strain analysis in this project.

- The overall shapes of all the strain curves of the concrete overlays studied were similar, and they were all opposite to the overall shape of the ambient temperature curve. This implies that thermal strain dominated the total strain in the concrete, while autogenous and drying shrinkage strains were superimposed on it.

6.5 Recommendations

The following proposed recommendations are based on the project observations and discussions.

6.5.1 Recommendations for Research Implementation

- Addition of 1.0/1.25 gal/yd^3 SRA in Mix 6 demonstrated many positive effects on concrete shrinkage control and mechanical property improvements, except for the slight reduction in F-T durability. This shrinkage control method could reduce the concrete ring shrinkage stress rate by 60%, which is highly effective. Its use is recommended for shrinkage reduction and prevention of premature concrete distress in Iowa bridge decks/overlays.

- The 10% cementitious material reduction in Mix 8 decreased autogenous and free drying shrinkage significantly, but the stress rate of restrained ring shrinkage was reduced by only 13%. This shrinkage control method also resulted in noticeable reductions in concrete strength, elastic modulus, creep rate, and surface resistivity, which might impair the concrete serviceability, and, therefore, it should be employed very cautiously.

- Use of LWFA as an IC material in Mix 2 effectively reduced the concrete autogenous shrinkage (47.5%) but only slightly reduced free drying shrinkage (11%) and yielded little reduction in the ring shrinkage stress rate (1.3%). This shrinkage control method also helped improve concrete strength, surface resistivity, and F-T durability slightly, except for the reduction in elastic modulus and creep rate. It can be considered for use in concrete mixes

with moderate free drying shrinkage potential and/or concrete with high autogenous shrinkage potential (low w/b ratio concrete).

6.5.2 Recommendations for Further Research

- In this study, the field investigation was performed on the use of SRA and CM for shrinkage control. Use of LWFA in Mix 2 was studied in the laboratory investigation but not in the field investigation. A future field investigation may be conducted to verify the effectiveness of LWFA used as an IC agent in various HPC mixes (e.g., HPC-O, O-S20-C20, and O-C20 mixes).

- Concrete shrinkage behavior and crack resistance are closely related to concrete pore structure and degree of hydration. Moisture content in field concrete is also strongly associated with concrete pore structure. Further study is necessary to find out how SRA addition influences cement hydration and pore structure, and the results would offer added understanding of the moisture sensor readings obtained from this study.

- Strains monitored by gages within the field concrete overlays resulted from the combined effects of cementitious hydration (autogenous deformation), the exposed conditions (drying/wetting and thermal expansion/contraction), mechanical loading (structural and traffic loads), and creep behavior. To fully understand these effects, a comprehensive stress analysis could be conducted on bridge structures using applications of various HPC overlay mixes.

- In this project, sensor monitoring was conducted for only one year, and an extended monitoring time (up to three or five years) may be beneficial to identify the potential concrete cracks in the later stages. In this project, sensor data were downloaded manually on site. In the future, the data transmitted via the internet could be downloaded either at home or at an office.

REFERENCES

Ardani, A. and J. Tanesi. 2012. *Surface Resistivity Test Evaluation as an Indicator of the Chloride Permeability of Concrete*. Tech Brief. FHWA-HRT-13-024. Turner-Fairbank Highway Research Center, McLean, VA.

Asbahan, R. E. 2009. Effects of the built-in construction gradient and environmental conditions on jointed plain concrete pavements. PhD dissertation. University of Pittsburgh, Pittsburg, PA.

Babcock, A. and P. Taylor. 2015. *Impacts of Internal Curing on Concrete Properties*. National Concrete Pavement Technology Center, Iowa State University, Ames, IA.

Bae, J., N. S. Berke, R. J. Hoopes, and J. Malone. 2002. Freezing and Thawing Resistance of Concretes with Shrinkage-Reducing Admixtures. Proceedings of the International RILEM Workshop on Frost Resistance of Concrete, pp. 327–333.

Bentz, D. P. 2006. Influence of Shrinkage-Reducing Admixtures on Early-Age Properties of Cement Pastes. *Journal of Advanced Concrete Technology*, Vol. 4, No. 3, pp. 423–429.

Bentz, D. P., M. R. Geiker, and K. K. Hansen. 2001. Shrinkage-Reducing Admixtures and Early-Age Desiccation in Cement Pastes and Mortars. *Cement and Concrete Research*, Vol. 31, No. 7, pp. 1075–1085.

Berwanger, C. and A. F. Sarkar. 1976. Thermal Expansion of Concrete and Reinforced Concrete. *Journal of the American Concrete Institute*, Vol. 73, No. 11, pp. 618–621.

Brooks, J. J. and M. A. M. Johari. 2001. Effect of Metakaolin on Creep and Shrinkage of Concrete. *Cement and Concrete Composites*, Vol. 23, No. 6, pp. 495–502.

Camiletti, J., A. M. Soliman, and M. L. Nehdi. 2013. Effects of Nano- and Micro-Limestone Addition on Early Age Properties of Ultra-High-Performance Concrete. *Materials and Structures*, Vol. 46, No. 6, pp. 881–898.

Castrodale, R. W. 2015. Internal Curing with Lightweight Aggregate for Transportation Structures and Pavements. 2015 Virginia Concrete Conference, March 5, Richmond, VA.

Chen, D., C. Liu, and C. Qian. 2011. Study on Shrinkage and Cracking Performance of SAP-Modified Concrete. *Materials Science Forum*, Vols. 675-677, pp. 697–700.

Chen, W. and H. J .H. Brouwers. 2012. Hydration of Mineral Shrinkage-Compensating Admixture for Concrete: An Experimental and Numerical Study. *Construction and Building Materials*, Vol. 26, No. 1, pp. 670–676.

Choktaweekarn, P. and S. Tangtermsirikul. 2009. A Model for Predicting the Coefficient of Thermal Expansion of Cementitious Paste. *ScienceAsia*, Vol. 35, pp. 57–63.

Collepardi, M., A. Borsoi, S. Collepardi, J. J. O. Olagot, and R. Troli. 2005. Effects of Shrinkage-Reducing Admixture in Shrinkage Compensating Concrete under Non-Wet Curing Conditions. *Cement and Concrete Composites*, Volume 27, Issue 6, pp. 704–708.

FHWA. 2016. *Portland Cement Concrete Pavements Research*. Federal Highway Administration Office of Research and Technology, Washington, DC. https://www.fhwa.dot.gov/publications/research/infrastructure/pavements/pccp/thermal.cfm.

Folliard, K. J. and N. S. Berke. 1997. Properties of High-Performance Concrete Containing Shrinkage-Reducing Admixture. *Cement and Concrete Research*, Vol. 27, No. 9, pp. 1357–1364.

Friedemann, K., F. Stallmach, and J. Karger. 2006. NMR Diffusion and Relaxation Studies during Cement Hydration—A Non-Destructive Approach for Clarification of the Mechanism of Internal Post Curing of Cementitious Materials. *Cement and Concrete Research*, Vol. 36, No. 5, pp. 817–826.

Fulton, F.S. 1986. *Fulton's Concrete Technology*. Sixth Edition. Portland Cement Institute, Midrand, South Africa.

Geiker, M. R., D. P. Bentz, and O. M. Jensen. 2004. Mitigating autogenous shrinkage by internal curing, In *High-Performance Structural Lightweight Concrete,* ACI Special Publication 218. American Concrete Institute, Farmington Hills, MI.

Gettu, R., J. Roncero, and M. A. Martin. 2002. Study of the Behavior of Concrete with Shrinkage-Reducing Admixtures Subjected to Long-Term Drying. In *Concrete: Material Science to Application,* ACI SP 206-10. American Concrete Institute, Farmington Hills, MI.

Guthrie, W. S., J. Yaede, and A. Bitnoff. 2014. *Comparison of Conventional and Internally Internal Cured Concrete Bridge Decks in Utah: Mountain View Corridor Project*. Utah Department of Transportation, Salt Lake City, UT.

Jensen, O. M. and P. F. Hansen. 2002. Water-Entrained Cement-Based Materials: II. Experimental Observations. *Cement and Concrete Research*, Vol. 32, No. 6, pp. 973–978.

Jianyong, L. and Y. Yan. 2001. A Study on Creep and Shrinkage of High-Performance Concrete. *Cement and Concrete Research*, Vol. 31, No. 8, pp. 1203–1206.

Jones, W. A., M. W. House, and W. J. Weiss. 2014. *Internal Curing of High-Performance Concrete Using Lightweight Aggregate and Other Techniques*. CDOT-2014-3. Colorado Department of Transportation, Denver, CO.

Kang, S., S. Hong, and J. Moon. 2018. Importance of Monovalent Ions on Water Retention Capacity of Superabsorbent Polymer in Cement-based Solutions. *Cement and Concrete Composites*, Vol. 88, pp. 64–72.

Kovler, K. and O. M. Jensen. 2007. *Internal Curing of Concrete*. RILEM TC 196-ICC: State of the Art Report 41. RILEM Publications, Paris, France.

Kong, X., Z. Zhang, and Z. Lu. 2015. Effect of Pre-Soaked Superabsorbent Polymer on Shrinkage of High-Strength Concrete. *Materials and Structures*, Vol. 48, No. 9, pp. 2741–2758.

Liu, J., C. Shi, X. Ma, H. K. Khayat, J. Zhang, and D. Wang. 2017. An Overview on the Effect of Internal Curing on Shrinkage of High-Performance Cement-Based Materials. *Construction and Building Materials*, Vol. 146, pp. 702–712.

Maltese, C., C. Pistolesi, A. Lolli, A. Bravo, T. Cerulli, and D. Salvioni. 2005. Combined Effect of Expansive and Shrinkage-Reducing Admixtures to Obtain Stable and Durable Mortars. *Cement and Concrete Research*, Vol. 35, No. 12, pp. 2244–2251.

Mechtcherine, V. and H.-W. Reinhardt. 2012. *Application of Super Absorbent Polymers (SAP) in Concrete Construction*. RILEM TC 225-SAP: State of the Art Report. Springer Netherlands.

Miyazawa, S., A. Hiroshima, K. Koibuchi, and T. Ohtomo. 2008. Influence of Cement Type on Restraint Stress in Concrete at Early Ages. In *Shrinkage, and Durability Mechanics of Concrete Structures*, Vol. 1, pp. 373–379. Two Volume Set: Proceedings of the Eighth International Conference on Creep, Shrinkage and Durability of Concrete and Concrete Structures, September 30–October 2, Ise-Shima, Japan.

Mo, L., M. Deng, and M. Tang. 2010. Effects of Calcination Condition on Expansion Property of MgO-Type Expansive Agent Used in Cement-Based Materials. *Cement and Concrete Research*, Vol. 40, pp. 437–446.

Mo, L., M. Deng, M. Tang, and A. Al-Tabbaa. 2014. MgO Expansive Cement and Concrete in China: Past, Present and Future. *Cement and Concrete Research*, Vol. 57, pp. 1–12.

Nair, H., C. Ozyildirim, and M. Sprinkel. 2016. *Reducing Cracks in Concrete Bridge Decks Using Shrinkage-Reducing Admixture*. VTRC 16-R13. Virginia Department of Transportation, Richmond, VA.

Nakarai, K. and T. Ishida. 2008. Numerical Evaluation of Influence of Pozzolanic Materials on Shrinkage Base on Moisture State and Pore Structure. In *Creep, Shrinkage, and Durability Mechanics of Concrete Structures*, Vol. 1, pp. 153–159. Two Volume Set: Proceedings of the Eighth International Conference on Creep, Shrinkage and Durability of Concrete and Concrete Structures, September 30–October 2, Ise-Shima, Japan.

Nassiri, S. 2011. Establishing permanent curl/warp temperature gradient in jointed plain concrete pavements. PhD dissertation. University of Pittsburgh, Pittsburgh, PA.

Pang, L., S. Ruan, and Y. Cai. 2011. Effects of Internal Curing by Super Absorbent Polymer on Shrinkage of Concrete. *Key Engineering Materials*, Vol. 477, pp. 200–204.

Pourjavadi, A., S. M. Fakoorpoor, P. Hosseini, and A. Khaloo. 2013. Interactions between Superabsorbent Polymers and Cement-Based Composites Incorporating Colloidal Silica Nanoparticles. *Cement and Concrete Composites*, Vol. 37, pp. 196–204.

Qin, Y. 2011. Numerical study on the curling and warping of hardened rigid pavement slabs. PhD dissertation. Michigan Technological University, Houghton, MI.

Ribeiro, A. B., A. Goncalves, and A. Carrajola. 2006. Effect of Shrinkage-Reducing Admixtures on the Pore Structure Properties of Mortars. *Materials and Structures*, Vol. 39, No. 2, pp. 179–187.

Saliba, J., E. Rozière, F. Grondin, and A. Loukili. 2011. Influence of Shrinkage-Reducing Admixtures on Plastic and Long-Term Shrinkage. *Cement and Concrete Composites*, Vol. 33, No. 2, pp. 209–217.

Satio, M, M. Kawamura, and S. Arakawa. 1991. Role of Aggregate in the Shrinkage of Ordinary Portland and Expansive Cement Concrete. *Cement and Concrete Composites*, Vol. 13, No. 2, pp. 115–121.

Schröfl, C., V. Mechtcherine, and M. Gorges. 2012. Relation between the Molecular Structure and the Efficiency of Superabsorbent Polymers (SAP) as Concrete Admixture to Mitigate Autogenous Shrinkage. *Cement and Concrete Research*, Vol. 42, No. 6, pp. 865–873.

Sensale, G. R. and A. F. Goncalvas. 2014. Effects of Fine LWA and SAP as Internal Water Curing Agents. *International Journal of Concrete Structures and Materials*, Vol. 8, No. 3, pp. 229–238.

Shen, D., X. Wang, D. Cheng, J. Zhang, and G. Jiang. 2016. Effect of Internal Curing with Super Absorbent Polymers on Autogenous Shrinkage of Concrete at Early Age. *Construction and Building Materials*, Vol. 106, pp. 512–522.

Shin, A. and Y. Chung. 2013. Coefficient of Thermal Expansion for Concrete Containing Fly Ash and Slag. Third International Conference on Sustainable Construction Materials and Technology, August 18-21, Kyoto, Japan.

Shin, H. and Y. Chung. 2011. *Determination of Coefficient of Thermal Expansion Effects on Louisiana's PCC Pavement Design*. Louisiana Department of Transportation and Development, Baton Rouge, LA.

Tadros, M. K., N. Al-Omaishi, S. J. Seguirant, and J. G. Gallt. 2003. *NCHRP Report 496: Prestress Losses in Pretensioned High-Strength Concrete Bridge Girders*. National Cooperative Highway Research Program, Washington, DC.

Tazawa, E. and S. Miyazawa. 1997. Influence of Constituents and Composition on Autogenous Shrinkage of Cementitious Materials. *Magazine of Concrete Research*, Vol. 49, No. 178, pp. 15–22. https://www.icevirtuallibrary.com/doi/abs/10.1680/macr.1997.49.178.15.

Treesuwan, S. and K. Maleesee. 2017. Effects of Shrinkage Reducing Agent and Expansive Additive on Mortar Properties. *Advances in Materials Science and Engineering*, Volume 2017, No. 2, pp. 1–11.

Wang, K., S. Schlorholtz, S. Sritharan, H. Seneviratne, X. Wang, and Q. Hou. 2013. *Investigation into Shrinkage of High-Performance Concrete Used for Iowa Bridge Decks and Overlays*. Institute for Transportation, Iowa State University. Ames, IA.

Wang, Q., Z. Ren, and Z. Zhang. 2011. Study on the Delayed Ettringite Formation in Massive Shrinkage Compensating Concrete with U-Type Expansive Agent. *Key Engineering Materials*, Vol. 477, pp. 340–347.

Weiss J. 2016a. *Internal Curing for Concrete Pavements*. Tech Brief FHWA-HIF-16-006. Federal Highway Administration, Washington, DC.

Weiss, J. 2016b. Internal Curing. Prepared for the National Concrete Consortium Webinar Series. March 23. National Concrete Pavement Technology Center, Iowa State University, Ames, IA. https://intrans.iastate.edu/app/uploads/sites/7/2018/08/160323-InternalCuringWebinar.pdf.

Weiss W. J. and L. Montanari. 2017. *Guide Specification for Internally Curing Concrete*. National Concrete Pavement Technology Center, Iowa State University, Ames, IA.

Weiss, W. J., W. Yang, and S. P. Shah. 1998. Shrinkage Cracking of Restrained Concrete Slabs. *Journal of Engineering Mechanics*, Vol. 124, No. 7, pp. 765–774.

Weiss, W. J., B. B. Borischevsky, and S. P. Shah. 1999. The Influence of a Shrinkage-Reducing Admixture on the Early-Age Behavior of High-Performance Concrete. 5th Int. Sym. on the Utilization of High-Strength/High-Performance Conc., Sandefjord, Norway, Vol. 2, pp. 1418–1428.

Wells, S. A. 2005. Early Age Response of Jointed Plain Concrete Pavements to Environmental Loads. MS thesis. University of Pittsburgh, Pittsburgh, PA.

Whiting, D. A., R. Detwiler, and E. S. Lagergren. 2000. Cracking Tendency and Drying Shrinkage of Silica Fume Concrete for Bridge Applications. *ACI Materials Journal*, Vol. 97, No. 1, pp. 71–77.

Yang, Y. and R. Sato. 2002. A New Approach for Evaluation of Autogenous Shrinkage of High-Strength Concrete under Heat of Hydration. *Proceedings of the Third International Research Seminar on Self-Desiccation in Concrete*. Lund, Sweden. pp. 51–65.

Yoo, D. Y., N. Banthia, and Y. S. Yoon. 2015. Effectiveness of Shrinkage-Reducing Admixture in Reducing Autogenous Shrinkage Stress of Ultra-High-Performance Fiber-Reinforced Concrete. *Cement and Concrete Composites*, Vol. 64, pp. 27–36.

Yurdakul, E., P. C. Taylor, H. Ceylan, and F. Bektas. 2013. Effect of Paste-to-Voids Volume Ratio on the Performance of Concrete Mixtures. *Journal of Materials in Civil Engineering*, Vol. 25, No. 12, pp. 1840–1851.

APPENDIX A: SHRINKAGE TEST RESULTS OF CONCRETE (MIX 2) HAVING SUPERABSORPTENCE POLYMER (SAP) AS AN INTERNAL CURING AGENT

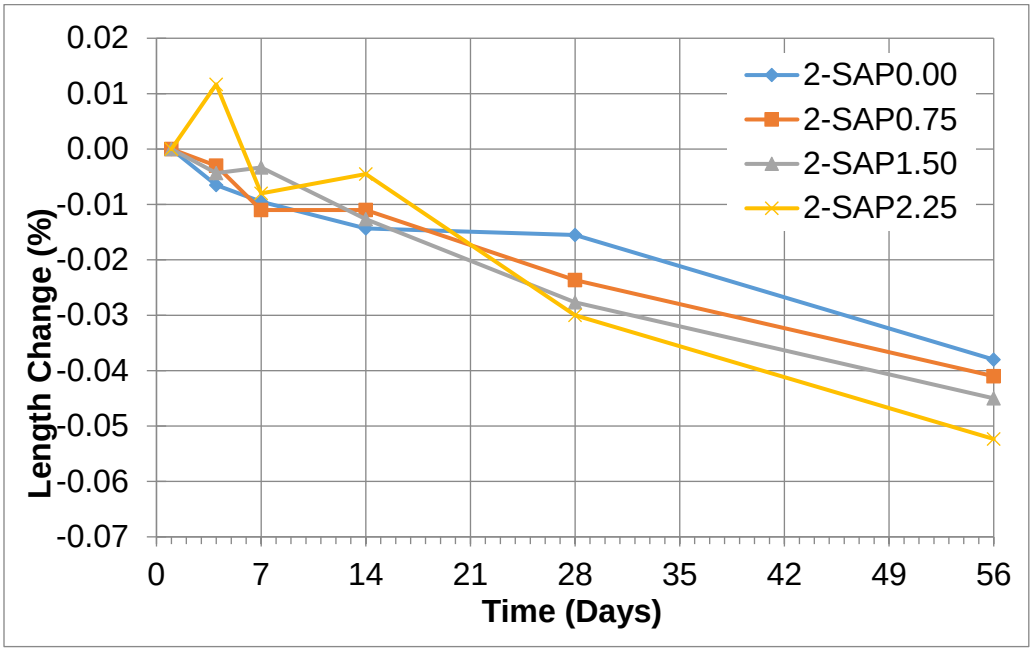

(a) Autogenous shrinkage

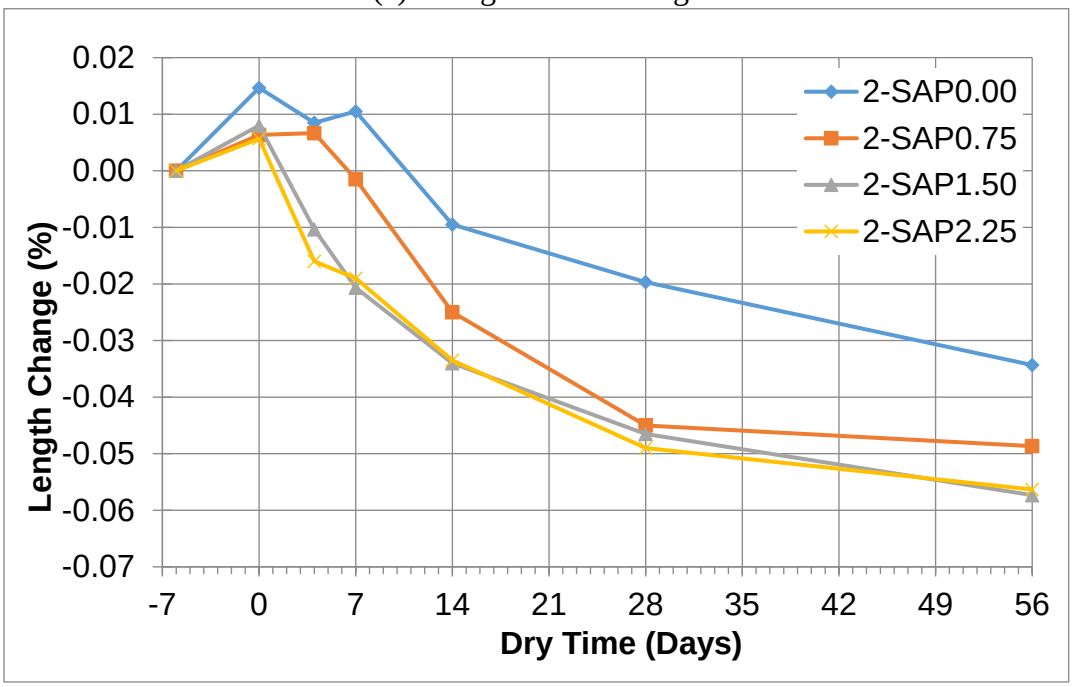

(b) Free drying shrinkage

Figure A.1. First trial on SAP for Mix 2 (presoaked with additional water)

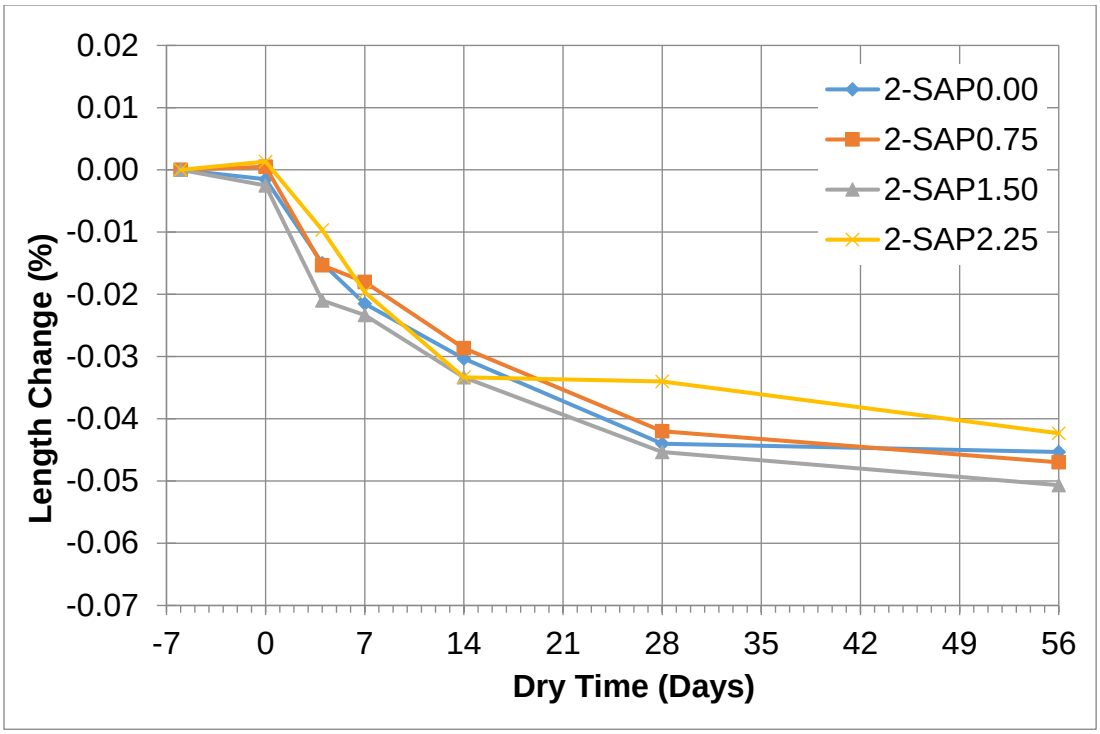

Figure A.2. Second trial on SAP for Mix 2 (without presoak) (free drying shrinkage)

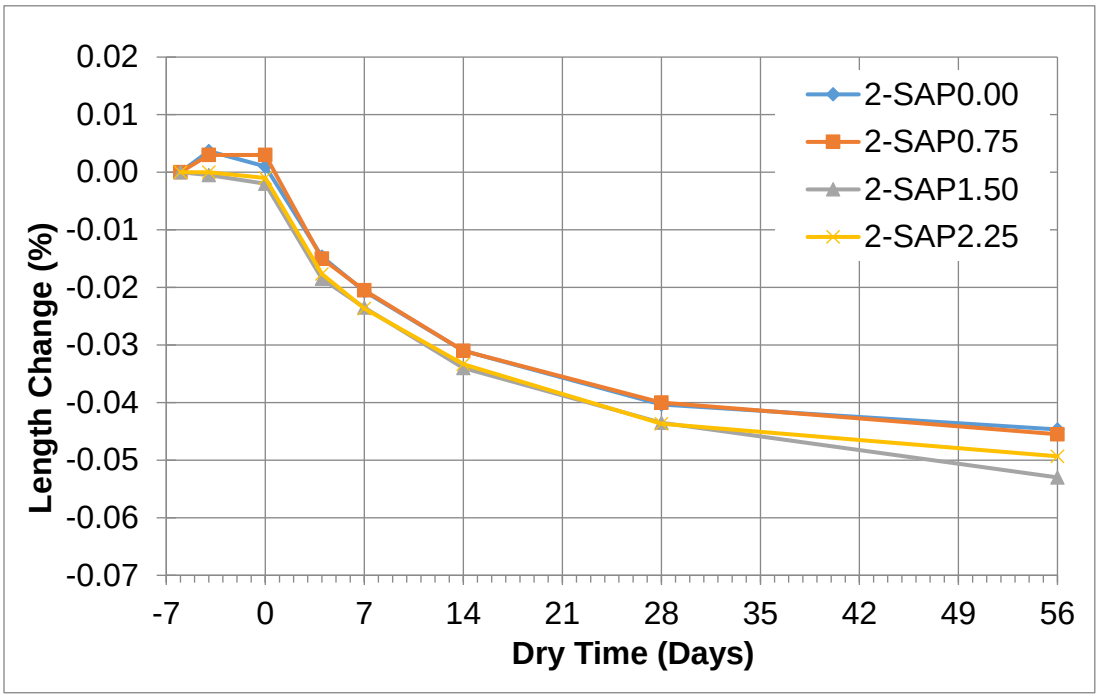

Figure A.3. Third trial on SAP for Mix 2 (presoaked with mixing water) (free drying shrinkage)

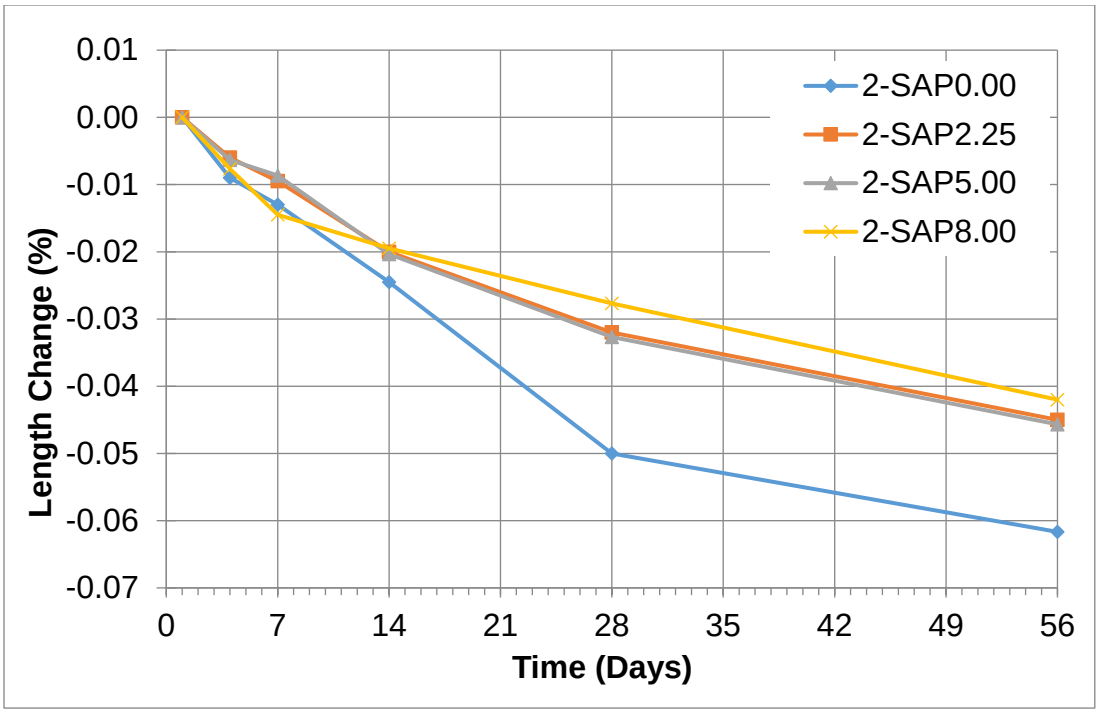

(a) Autogenous shrinkage

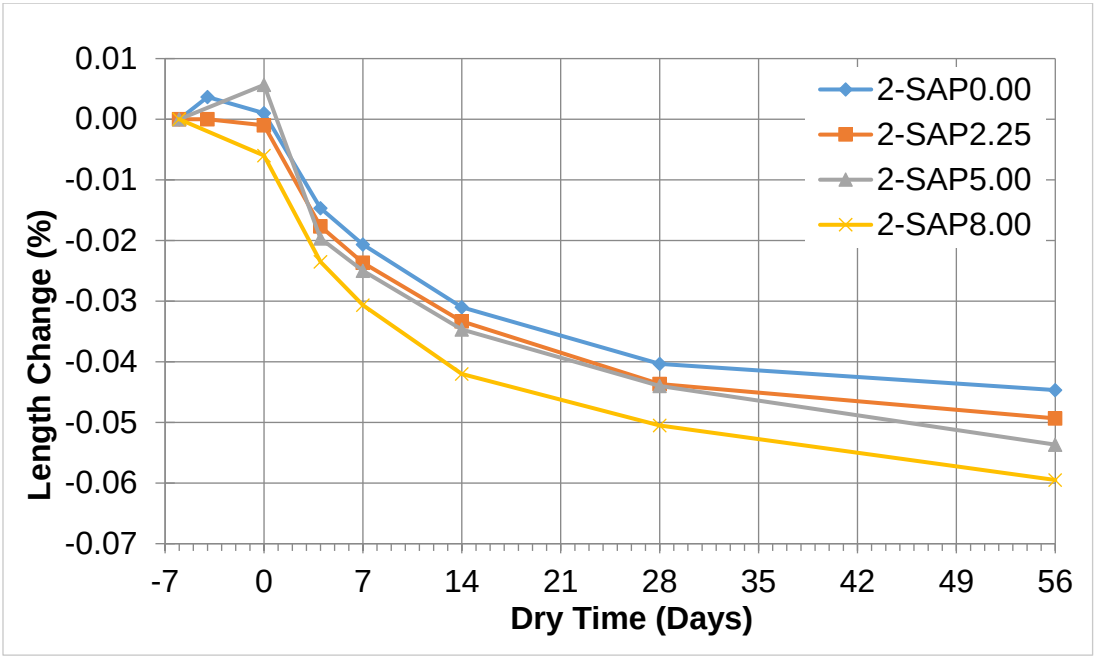

(b) Free drying shrinkage

Figure A.4. Fourth trial on increased SAP dosage for Mix 2 (presoaked with mixing water)

APPENDIX B: STRAIN MEASUREMENT OF GAUGES ON THE TOP/BOTTOM SURFACES OF DECKS AND WEBS OF GIRDERS

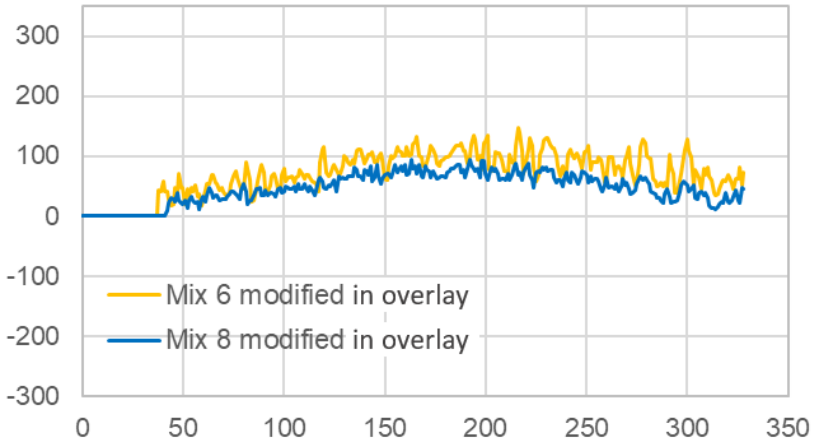

Figure B.1. Strain readings of gages in concrete overlays

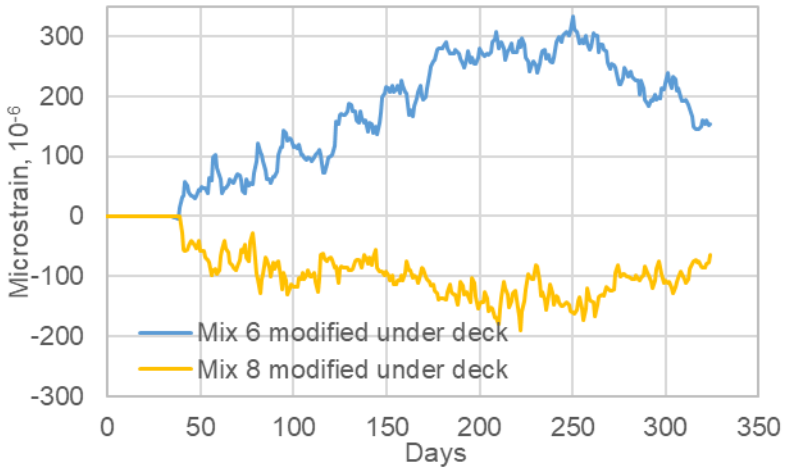

Figure B.2. Strain readings of gages on the bottom surfaces of concrete decks

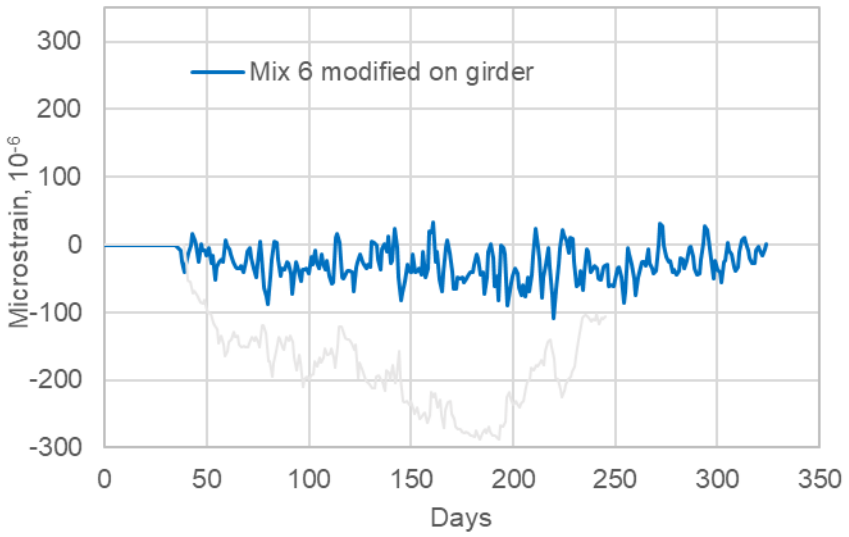

Figure B.3. Strain readings of gages on the web of concrete girder (strain gage for Mix 8 modified broken during the sensor monitoring)

THE INSTITUTE FOR TRANSPORTATION IS THE FOCAL POINT FOR TRANSPORTATION AT IOWA STATE UNIVERSITY.

InTrans centers and programs perform transportation research and provide technology transfer services for government agencies and private companies;

InTrans manages its own education program for transportation students and provides K-12 resources; and

InTrans conducts local, regional, and national transportation services and continuing education programs.

IOWA STATE UNIVERSITY

Visit www.InTrans.iastate.edu for color pdfs of this and other research reports.